Femtosecond Broadbandfluorescence Upconversion

D I S S E R T A T I O N

zur Erlangung des akademischen Grades
doctor rerum naturalium
(dr. rer. nat.)
im Fach Mathematik

eingereicht an der
Mathematisch-Naturwissenschaftlichen Fakultät I
Humboldt-Universität zu Berlin

von
Herrn Dipl.-Chem. Hans Roland Schanz
geboren am 15.06.1971 in Freiburg i. Br.

Präsident der Humboldt-Universität zu Berlin:
Prof. Dr. Jürgen Mlynek

Dekan der Mathematisch-Naturwissenschaftlichen Fakultät I:
Prof. Dr. Bernhard Ronacher

Gutachter:

1. Prof. Dr. Nilolaus P. Ernsting
2. Priv.-Doz. Dr. Jürgen Bendig
3. Prof. Dr. Ludger Wöste

eingereicht am: 22. Februar 2002
Tag der mündlichen Prüfung: 28. Mai 2002

"A decent chemist is twenty times more useful than any poet." interrupted Bazarov. — "Oh, indeed!" remarked Pavel Petrovich, and as if he was falling asleep he slightly raised his eyebrows. (*Fathers and Sons*, Turgenev)

Zusammenfassung

Im Rahmen dieser Arbeit wird der Aufbau einer neuartigen Anlage zur breitbandigen Messung zeitaufgelöster Fluoreszenzspektren durch Summenfrequenzbildung ("Fluorescence Upconversion") beschrieben. Breitbandig heißt hier, daß der spektrale Bereich von 425 bis 610 nm ($\Delta\tilde{\nu}=7200$ cm^{-1}) in einem einzigen Messgang erfaßt wird. Die Zeitauflösung der Messung liegt nach Dispersionskorrektur bei 100 fs. Die Erfüllung der geometrischen und optischen Randbedingungen ("Phase matching") für die Summenfrequenzbildung über einen so breiten spektralen Bereich wurde durch die Wahl eines dünnen, niederdispersiven, nichtlinearen Kristalls (KDP, 100 μm) und eines infraroten Torpulses ermöglicht.

Erste Messungen wurden an einem System durchgeführt, dessen Fluoreszenzverhalten aus der Literatur sehr gut bekannt ist, Coumarin 153 in Acetonitril. Aus der dynamischen Stokes-Verschiebung wurde die Solvations-Korrelations-Funktion für Acetonitril bestimmt. Die aus der Literatur bekannten Werte wurden reproduziert. Daraus wurde geschlossen, daß mit der Apparatur zuverlässig gemessen werden kann.

Als zweites System wurde 4-Dimethylamino-4'-cyanostilben (DCS) in Acetonitril untersucht. Aus der Literatur ist es bekannt für duale Fluoreszenz: unmittelbar nach der Anregung des Moleküls wächst eine Fluoreszenzbande an und schwindet wieder, während gleichzeitig zur ersten rotverschoben eine neue Bande anwächst. Mit Messungen der zeitaufgelösten Fluoreszenz bei verschiedenen Schichtdicken und der zeitaufgelösten Absorption sowie quantenmechanischen Rechnungen konnte dieses Phänomen auf eine starke Absorptionsbande im ersten elektronisch angeregten Zustand zurückgeführt werden. DCS besitzt also nur scheinbar duale Fluoreszenz. Bei genügend geringer Schichtdicke ist es möglich das wahre Emissionsverhalten zu beobachten, nämlich eine von der Lösungsmittel-Antwort bestimmte dynamische Rotverschiebung.

Abstract

In this work a new experimental design is presented that allows upconversion of a fluorescence band in a broad range of 7200 cm^{-1} without readjusting optical elements, thus allowing measurements with a single pump-gate scan. This broad phase matching could be achieved by utilizing a thin, nonlinear optical crystal (KDP, 100 μm) and an infrared gate wavelength. The setup provides a time-resolution of 100 fs.

First measurements were performed on a system which emission behaviour is best described in literature, the laser dye coumarin 153 (c153)in acetonitrile. From dynamical Stokes-shift the solvation correlation function of acetonitrile could obtained. Data known from literature was reproduced. From this it was concluded that with this new setup measurements can be performed reliably.

The second system investigated was 4-dimethylamino-4'-cyanostilbene (dcs) in acetonitrile. In literature it was discussed in terms of dual fluorescence: immediately after excitation of the dye an emission band rises in the blue and decays while synchronously a second band rises at longer wavelengths. By measuring time-resolved fluorescence at different sample thickness, time-resolved absorption as well as quantum mechanical calculations dual emission could be excluded, instead a new explanation was found. A strong transition from the S$_1$ state to higher states overlaps with the transient emission signal. The optical density of this transition scales with concentration, thickness of the sample and intensity of the pump-pulse. If the optical density is high then re-absorption gives the impression of dual emission; but if the it is kept low the true spectral behaviour of DCS is revealed: pure solvation dynamics.

Contents

Chapter 1

Introduction

Femtosecond-resolved fluorescence spectroscopy

Transient fluorescence spectroscopy is a powerful tool for the study of various aspects of intra- and intermolecular dynamics in liquids such as vibrational cooling or solvation dynamics [1]. Beyond researching chemical and physical problems it allows real-time investigation of important biological processes in which photons are involved such as the process of vision or photosynthesis. In the pico- to nanosecond region various techniques can be utilized to time-resolve fluorescence, e.g. streak-camera, time correlated single photon counting or the liquid Kerr-shutter [2]. They all offer the possibility of measuring the full fluorescence spectrum at a time t giving useful information like the time-dependent signal-intensity, peak position, bandwidth and skewness.

In the sub-picosecond region, however, the only technique well established is fluorescence upconversion [3] that allows time-resolution below 100 fs [4, 5]. After ultrafast excitation of the sample the emitted light is collected and focused onto a non-linear crystal where it is mixed with a second pulse, the gate pulse, to generate sum frequency radiation. Since the mixing takes place only during the presence of the second laser pulse, this provides time-resolution comparable to the laser pulse-width. The process of sum frequency generation requires compliance with optical and geometrical conditions, phase matching, which is usually met for one single wavelength only. The measurement of another transient, at neighbouring wavelength, would require optical readjustment. Therefore time-resolved spectra have to be reconstructed from several transient traces recorded at different wavelengths [6, 7]. This procedure is not only very time-consuming, but also fluctuations of the laser intensity can lead to wrong results. Only a limited number of points, for example one every 5 or 10 nm, is recorded. This is why band-shape analysis is difficult and often restricted to the two most reliable parameters,

the signal intensity and the peak frequency, while bandwidth and symmetry are not so well determined and their change with time is usually ignored.

Naturally the scientific community started looking for ways of measuring the entire emission band with femtosecond resolution. Such a broadband approach is, for example, pump supercontinuum probe-spectroscopy for measuring transient absorption which consists of three components: bleach, excited state absorption and stimulated emission [8, 9]. In some cases the latter is spectrally isolated and can be converted in the time-resolved spontaneous emission numerically. Another broadband approach utilizes the transient birefringence induced in a nonlinear medium by an intense laser pulse, the optical Kerr effect. Kanematsu and co-workers used as nonlinear medium glass of low nuclear and high electronic response [10]. Here temporal resolution should be limited by the duration of the laser-pulse. One inherent problem of this method is the large background signal. The reason is that thin film polarizers, required after the sample, allow an extinction ratio of 10^{-3}-10^{-4} only. The gated section of the fluorescence spectrum must be measured on a background of the time-integrated photon leakage through the crossed polarizers. Therefore the optical Kerr shutter is only suitable for molecules with a short fluorescence life time.

Motivation and Goal

Now consider a system that shows no isolated stimulated emission but a long fluorescence lifetime, in which case neither transient absorption nor Kerr-shutter measurements would be appropriate. So with an improved time-gated upconversion setup, is it possible to measure the evolving fluorescence spectrum simultaneously across its entire width? From this starting point, the goal of the project can be specified more precisely with the following tasks:

1. to understand the conditions under which phase matching is met for the whole fluorescence band;

2. to realize a setup for broadband fluorescence upconversion with which the whole femtosecond-evolution in the spectral region between 400 and 600nm can be measured in single pump-gate scan;

3. to measure the time-resolved emission of the laser dye coumarin 153 in acetonitrile, to compare the results to the literature, and to prove that this technique works reliably.

Chapter 2

Background

2.1 Optical considerations

2.1.1 Absorption and emission

Consider an isolated atom having two electronic states: the ground state S_g and the excited state S_e separated by the energy gap ΔE_{eg} (see Figure 2.1, page 6). This gap can be associated with the transition frequency ν or the wavenumber $\tilde{\nu}$ using the relation

$$\Delta E_{eg} = E_e - E_g = h\nu = hc\tilde{\nu} \tag{2.1}$$

where h is the Planck constant in J·s and c is the speed of light in cm/s. If radiation with the wavenumber $\tilde{\nu}$ interacts with the molecule three processes can occur (see Figure 2.1): absorption, in which the molecule absorbs a quantum of the energy $hc\tilde{\nu}$ and is excited from g to e. Spontaneous emission, in which a quantum is irradiated spontaneously from an excited molecule in the state S_e returning to S_g. And stimulated emission, in which a photon $hc\tilde{\nu}$ forces an excited molecule to return to the ground-state and to release a second photon of the energy $hc\tilde{\nu}$ [11]. We should mention that through this thesis we work in the SI-system of units in the sense that we adopt the rationalized system with 4 basic quantities.

Einstein coefficients and transition lines

The rate of change of population N_e of the state S_e due to induced absorption is given by
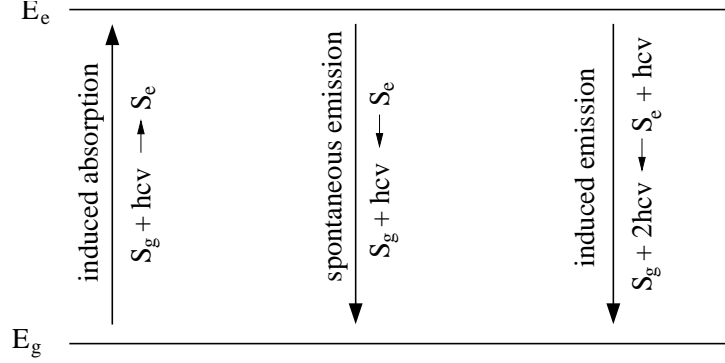
$$\frac{dN_e}{dt} = N_g B_{ge} \rho(\tilde{\nu}) \tag{2.2}$$

Figure 2.1: Absorption and emission processes between the two states S_e and S_g.

where B_{ge} is a so-called Einstein coefficient and $\rho(\tilde{\nu})$ is the energy density per volume and per wavenumber interval as derived by Planck for the radiation of a black body

$$\rho(\tilde{\nu}) = \frac{8\pi hc\tilde{\nu}^3}{\exp(hc\tilde{\nu}/kT) - 1}. \tag{2.3}$$

Similarly, induced emission changes the population N_e by

$$\frac{\mathrm{d}N_g}{\mathrm{d}t} = -N_e B_{eg} \rho(\tilde{\nu}) \tag{2.4}$$

where B_{eg} is the Einstein coefficient for this process and is equal to B_{ge}. For spontaneous emission

$$\frac{\mathrm{d}N_e}{\mathrm{d}t} = -N_g A_{eg} \tag{2.5}$$

where A_{eg} is another Einstein coefficient and the absence of $\rho(\tilde{\nu})$ indicates a spontaneous process. In the presence of radiation of wavenumber $\tilde{\nu}$ all three processes occur at the same time and the populations will reach an dynamic equilibrium

$$\frac{\mathrm{d}N_e}{\mathrm{d}t} = (N_g - N_e) B_{ge} \rho(\tilde{\nu}) - N_e A_{eg} = 0. \tag{2.6}$$

If the populations are equilibrated then they are related through the Boltzmann distribution , by

$$\frac{N_e}{N_g} = \frac{g_e}{g_e} \exp\left(-\frac{\Delta E}{kT}\right). \tag{2.7}$$

In case of equal degeneracies g_e and g_g, putting this relationship and the expression $\rho(\tilde{\nu})$ (equation 2.3) into the overall equilibrium rate equation 2.6

results in a basic relationship between the Einstein coefficients

$$A_{eg} = 8\pi hc\tilde{\nu}^3 B_{eg}. \tag{2.8}$$

The Einstein coefficients are related to the electronic wave functions ψ_g and ψ_e of the combining states through the transmission moment $\vec{R}_{eg}$, a vector quantity given by

$$\vec{R}_{eg} = \int \psi_e^* \vec{\mu} \psi_g \ d\tau \tag{2.9}$$

for interaction with the electric component of the radiation. Here $\vec{\mu}$ is the electric dipole moment operator

$$\vec{\mu} = \sum_i q_i \vec{r}_i \tag{2.10}$$

where q_i and $\vec{r}_i$ are the charge and the position vector of the ith particle (electron or nucleus). The transition moment can be thought of as oscillating electric dipole moment due to the transition. The square of the magnitude of $\vec{R}_{eg}$ is the transition probability and is related to the Einstein coefficient B_{ge} by

$$B_{eg} = \frac{8\pi^3}{4\pi\varepsilon_0 3h^2} |\vec{R}_{eg}|^2. \tag{2.11}$$

Another measure that is related to transition probability and Einstein coefficient is the oscillator strength f_{eg}. This dimensionless quantity is usually viewed as a correct measure of the intensity and it is given by [11, 12]

$$\begin{aligned} f_{eg} &= \frac{4\varepsilon_0 m_e c^2 h}{e^2} \tilde{\nu} \ B_{eg} \\ &= \frac{8}{3} \frac{m_e c^2 \pi^2}{e^2 h} \tilde{\nu} \ |\vec{R}_{eg}|^2. \end{aligned} \tag{2.12}$$

It should be noted that according to eq 2.12 the oscillator strength decreases if the transition shifts to the red even if the transition probability stays the same.

Band shapes

The considerations made before are only valid for atomic systems with two sharp levels in which each electronic transition results in a single narrow line placed in the spectrum at wavenumber $\tilde{\nu}$. The experiment concerns polyatomic molecules and every electronic transition is coupled to a set of

vibrational transitions. This results in a broadening of the narrow line over a spectral region.

To discuss this topic the vibrational wave functions ϕ_i and ϕ_j have to be introduced in addition to the electronic wave functions ψ_g and ψ_e which were discussed up to now. The indices i and j refer to vibrational levels in the ground and excited state. The transition moment of the vibronic transition $R_{ej,gi}$ can be defined in analogy to eq 2.9 as

$$\vec{R}_{ej,gi} = \int \psi_e^* \phi_j^* \vec{\mu} \psi_g \phi_i \ \mathrm{d}\tau. \tag{2.13}$$

In the case of a polyatomic molecule the number of allowed vibronic transitions may be quite high and, either with limited resolution or by solvent broadening (see below), a continuous band shape is produced. The quasi-continuous distribution of oscillators can be defined similarly to eq 2.12 by

$$f_{eg}(\tilde{\nu}) = f_{ej,gi} = \frac{8}{3} \frac{m_e c^2 \pi^2}{e^2 h} \ \tilde{\nu} |\vec{R}_{ej,gi}(\tilde{\nu})|^2. \tag{2.14}$$

In the isolated molecule, $|\vec{R}_{ej,gi}(\tilde{\nu})|^2$ is a spectrum of many discrete vibronic lines. In a solvent it becomes continuous, and

$$\int f_{eg}(\tilde{\nu}) \ \mathrm{d}\tilde{\nu} = f_{eg}. \tag{2.15}$$

This distributed oscillator strength function can be obtained from the electronic spectra in the condensed phase, for example. The relation to an absorption or stimulated emission band associated to a single transition $g{\rightarrow}e$ or $e{\rightarrow}g$ is given by

$$f_{eg}(\tilde{\nu}) = \frac{4\varepsilon_0 m_e c^2 \ln 10}{N_A e^2} \ \varepsilon(\tilde{\nu}). \tag{2.16}$$

$\varepsilon(\tilde{\nu})$ is the decadic molar absorption coefficient known from the Lambert-Beer law that defines absorbance A as the product of the absorption coefficient $\varepsilon(\tilde{\nu})$ and the length of the cell l and the concentration of the absorbing material c_m in the liquid phase

$$A = \varepsilon(\tilde{\nu})c_m l. \tag{2.17}$$

Next we turn to the spontaneous emission spectrum. It can be described with a distribution function $\Phi(\tilde{\nu})$, whose differential $\Phi(\tilde{\nu})\mathrm{d}\tilde{\nu}$ represents the fraction of fluorescence quanta detected between $\tilde{\nu}$ and $\tilde{\nu}+\mathrm{d}\tilde{\nu}$. According to this definition $\Phi(\tilde{\nu})$ is related to full fluorescence intensity and normalized:

$$\int_0^\infty \Phi(\tilde{\nu})\mathrm{d}\tilde{\nu} = 1. \tag{2.18}$$

Förster derived an equation relating the emission quantum distribution and the oscillator strength $f_{eg}(\tilde{\nu})$ [13]:

$$f_{ge}(\tilde{\nu}) = \frac{3m_e c^2}{8\pi^2 n e^2 \tau_e} \frac{\Phi(\tilde{\nu})}{\tilde{\nu}^2} \qquad (2.19)$$

where τ_e is the natural fluorescence life time.

Conversion between wavelength and wavenumber

Until now we discussed the fluorescence quantum distribution as function of the wavenumber $\tilde{\nu}$ measured in cm^{-1}. This is reasonable since the wavenumber scales with energy. But usually fluorescence spectra are recorded using a grating spectrometer. Hence, they are a function of wavelength measured typically in nm [2]. The spectrum is

$$\Phi(\lambda) = \frac{d\Phi}{d\lambda} \qquad (2.20)$$

where the overall integral is unity

$$\int_0^\infty \Phi(\lambda) d\lambda = 1. \qquad (2.21)$$

Conversion of the abscissa from nm to cm^{-1} is easily done by

$$\tilde{\nu} = 10^7/\lambda. \qquad (2.22)$$

And the relation between $\Phi(\lambda)$ and $\Phi(\tilde{\nu})$ can be shown to be

$$\Phi(\tilde{\nu}) = \frac{d\Phi}{d\tilde{\nu}} = \frac{d\Phi}{d\lambda}\frac{d\lambda}{d\tilde{\nu}} = \frac{10^7}{\tilde{\nu}^2}\Phi(\lambda). \qquad (2.23)$$

Conclusions for analysis of spectral dynamics

The considerations above allow us to make three important conclusions for the treatment and analysis of optical spectra:

1. Consider now spectra as function of wavenumber. According to equations 2.16 and 2.19 spectra of spontaneous emission (distribution of fluorescence quanta) can be converted into spectra of stimulated emission by division by $\tilde{\nu}^2$.

2. The oscillator strength (eq 2.14) is not the appropriate measure for the investigation of spectral dynamics. Even if there are no changes in the electronic and vibrational character of a molecule, a shift of the band due to environmental changes would necessarily result in a change of band shape. The spontaneous emission and the stimulated absorption/emission spectra have to be divided by $\tilde{\nu}^3$ and $\tilde{\nu}$, respectively, in order to obtain the distribution $|\vec{R}_{ej,gi}(\tilde{\nu})|^2$. The latter reflects the true spectral character of a molecule: the transition probability [13, 14].

3. Fluorescence quantum distributions recorded as quanta per nanometer have to be divided by $\tilde{\nu}^5$ to be converted into the measure of interest, i.e. transition probabilities as a function of energy.

2.1.2 Linear and nonlinear optics

Light

Light can be described as a plane electromagnetic wave with a wavelength λ and a circular frequency ω. The speed of light is

$$c = \frac{\lambda \cdot \omega}{2\pi}. \tag{2.24}$$

The speed of light depends as well on the frequency ω as on the medium it passes. In vacuum the speed of light is independent on the frequency. The index of refraction is defined as the ratio between the speed of light in vacuum and in a medium, c_0 and $c(\omega)$ respectively.

$$n(\omega) = \frac{c_0}{c(\omega)}. \tag{2.25}$$

The unit vector $\vec{s}$ points in the direction where the wave travels. The wave vector is defined as

$$\vec{k} = \frac{n \cdot \omega}{c_0} \cdot \vec{s} \tag{2.26}$$

The electromagnetic field E oscillates in a plane perpendicular to $\vec{s}$.

$$\vec{E} = \vec{E_0} \cdot \cos[\omega t - \vec{k}\vec{z}] \tag{2.27}$$

Anisotropy

The dielectric permittivity or constant ε relates the direction and the strength of an electric field $\vec{E}$ to the dielectric displacement $\vec{D}$ it causes. In isotropic

media the direction of the electric field and of the driven charge is the same. Here the dielectric constant ε is scalar [15].

$$\vec{D} = \varepsilon \cdot \vec{E} \tag{2.28}$$

In anisotropic media $\vec{D}$ and $\vec{E}$ are in general not parallel. The relation between the electric field and the moved charge may be transformed to

$$\begin{vmatrix} D_x \\ D_y \\ D_z \end{vmatrix} = \begin{vmatrix} \varepsilon_x & 0 & 0 \\ 0 & \varepsilon_y & 0 \\ 0 & 0 & \varepsilon_z \end{vmatrix} \begin{vmatrix} E_x \\ E_y \\ E_z \end{vmatrix} \tag{2.29}$$

where x, y and z refer to the principle dielectric axes.

If an electric field $\vec{E}$ is applied to a medium then the stored electric power density w_{el} is given in the cgs-system by

$$w_{el} = \frac{1}{2} \vec{D} \cdot \vec{E} = \frac{1}{2} \frac{\vec{D}^2}{\varepsilon}. \tag{2.30}$$

Since $\varepsilon_i = n_i^2$ this equation can be rewritten in a normalized form giving the index ellipsoid or indicatrix.

$$2w_{el} = \frac{D_1^2}{\varepsilon_1} + \frac{D_2^2}{\varepsilon_2} + \frac{D_3^2}{\varepsilon_3} \Rightarrow 1 = \frac{x^2}{n_1^2} + \frac{y^2}{n_2^2} + \frac{z^2}{n_3^2} \tag{2.31}$$
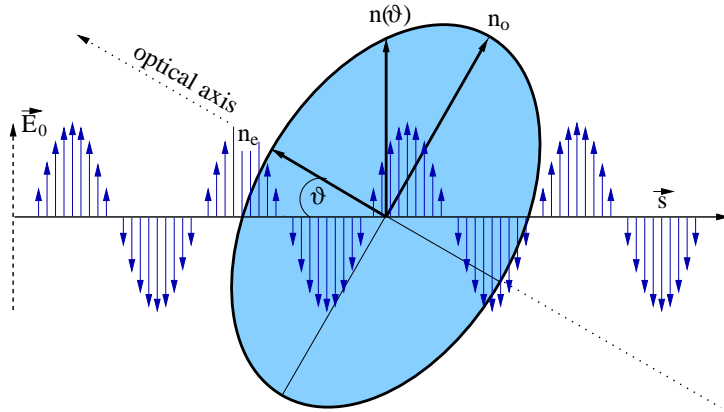

Figure 2.2: The indicatrix is an ellipsoid representing the birefringence of a crystal. The light travels in direction $\vec{s}$. The electric field oscillates along $\vec{E_0}$ and experiences the index of refraction $n(\theta)$.

The second part of this equation represents an ellipsoid with the semi-axes n_x, n_y and n_z. If the indices of refraction are all equal then the indicatrix describes a spheroid corresponding to an isotropic crystal. If all indices of refraction differ from each other the crystal is called biaxial. We will restrict our considerations to the practical case of an uniaxial crystal where $n_x = n_y \neq n_z$. The two equal indices of refraction, n_x and n_y, are called ordinary (n_o); the single different one is called extraordinary (n_e).

Light traversing an anisotropic crystal experiences different indices of refraction depending on the orientation of the crystal. This phenomenon is called birefringence. It can be utilized to tune the index of refraction by rotating the crystal around one of the two ordinary axes. The electric field $\vec{E}$ experiences an index of refraction $n_o < n(\theta) < n_e$, where θ is the angle between the n_e and $\vec{E}_0$ (see Figure 2.2).

$$n(\theta) = \frac{n_e n_o}{\sqrt{n_o^2 \sin^2 \theta + n_e^2 \cos^2 \theta}} \qquad (2.32)$$

One can consider a second wave traveling in the same direction $\vec{s}$, but linearly polarized perpendicular to $\vec{E}_0$ or the picture plane in Figure 2.2. The electric field of this second wave will always experience n_o, independent of the angel θ.

Nonlinear Optics

Nonlinear optics play an important role in the setup described in this thesis: the generation of the pump pulse (794 $\to$ 397 nm), the gate pulse (794 $\to$ 1300 nm) as well as the upconversion process itself.

The linear dependence of the polarization $\vec{P}$ on the applied field $\vec{E}$ is only valid if the field is weak [16]. As $\vec{E}$ increases nonlinear terms have to be considered.

$$\vec{P} = \varepsilon_0 \left[\chi^{(1)} \vec{E} + \chi^{(2)} \vec{E}^2 + \chi^{(3)} \vec{E}^3 + \ldots \right] \qquad (2.33)$$

Here $\chi^{(n)}$ is the nth order susceptibility. Because the equation $\chi^{(n)} \gg \chi^{(n+1)}$ is always valid for our experiments, the following calculations will be restricted to the first nonlinear term

$$\vec{P}_{nl} = \varepsilon_0 \chi^{(2)} \vec{E}^2 \qquad (2.34)$$

where $\vec{E}$ describes an electric field wave.

$$\vec{E}_i(z, t) = \vec{E}_i^0 \cos[\omega_i t + \vec{k}_i \vec{z}] \qquad (2.35)$$

susceptibility	effect
$\chi^{(1)}$	linear dispersion
	absorption
$\chi^{(2)}$	second harmonic generation
	sum and difference frequency generation
$\chi^{(3)}$	four wave mixing
	stimulated Raman scattering
	optical Kerr effect
	self phase modulation
	transient absorption
	stimulated emission

Table 2.1: Important non-linear effects

If the two waves $\vec{E}_1$ and $\vec{E}_2$ are traveling through a nonlinear crystal they interact and generate the nonlinear polarization

$$\begin{aligned}
\vec{P}_{nl} &= \varepsilon_0 \chi^{(2)} \vec{E}_1 \vec{E}_2 \\
&= \varepsilon_0 \chi^{(2)} [\vec{E}_1^2 \cos^2(\omega_1 t + \vec{k}_1 \vec{z}) + \vec{E}_2^2 \cos^2(\omega_2 t + \vec{k}_2 \vec{z}) \\
&+ 2\vec{E}_1 \vec{E}_2 \cos(\omega_1 t + \vec{k}_1 \vec{z}) \cos(\omega_2 t + \vec{k}_2 \vec{z})]
\end{aligned} \tag{2.36}$$

Applying the trigonometric relations $\cos^2 \alpha = (1 - \cos 2\alpha)/2$ and $\cos \alpha \cos \beta = [\cos(\alpha + \beta) + \cos(\alpha - \beta)]/2$ four new frequencies appear in the nonlinear polarization, giving four possibilities of frequency conversion:

$$\begin{aligned}
\vec{P}_{2\omega_1} &= \varepsilon_0 \chi^{(2)} \vec{E}_1^2 \cos[2(\omega_1 t + \vec{k}_1 \vec{z})] \\
\vec{P}_{2\omega_2} &= \varepsilon_0 \chi^{(2)} \vec{E}_2^2 \cos[2(\omega_2 t + \vec{k}_2 \vec{z})] \\
\vec{P}_{\omega_1 + \omega_2} &= 2\varepsilon_0 \chi^{(2)} \vec{E}_1^2 \vec{E}_2^2 \cos[(\omega_1 + \omega_2)t + (\vec{k}_1 + \vec{k}_2)\vec{z}] \\
\vec{P}_{\omega_1 - \omega_2} &= 2\varepsilon_0 \chi^{(2)} \vec{E}_1^2 \vec{E}_2^2 \cos[(\omega_1 - \omega_2)t + (\vec{k}_1 - \vec{k}_2)\vec{z}]
\end{aligned} \tag{2.37}$$

The polarizations $\vec{P}_{2\omega_1}$ and $\vec{P}_{2\omega_2}$ are source terms for second harmonic generation (SHG) of each input frequency. The third term $\vec{P}_{\omega_1 + \omega_2}$ results in sum frequency generation (SFG) and $\vec{P}_{\omega_1 - \omega_2}$ in difference frequency generation (DFG).

Sum Frequency Generation

Two photons of the frequencies ω_1 and ω_2 interact in a nonlinear crystal to create a new photon of the frequency ω_3. There are two laws that have to

be obeyed, the energy conservation

$$\omega_3 = \omega_2 + \omega_1 \tag{2.38}$$

and the momentum conservation[1]

$$\vec{k}_3 = \vec{k}_2 + \vec{k}_1. \tag{2.39}$$

Phase Matching

The parameter

$$\begin{aligned} \Delta \vec{k} &= \vec{k}_3 - \vec{k}_2 - \vec{k}_1 \\ &= \frac{n_3}{\lambda_3} - \frac{n_2}{\lambda_2} - \frac{n_1}{\lambda_1} \end{aligned} \tag{2.40}$$

is termed the phase mismatch. To maximize the efficiency of a three frequency interaction Δk has to be set to zero. This can be done by using the birefringence of an uniaxial crystal. As explained above the index of refraction in the extraordinary plane of an anisotropic crystal can be changed by rotation of the crystal. Another possibility to tune the indices of refraction is to change the temperature of the crystal.

Another degree of freedom is the angle between the two parent waves, $\alpha = \measuredangle(\vec{k}_1, \vec{k}_2)$. In the collinear case α is zero. In the non-collinear case the $\vec{k}$ components are obtained from the cosine law.

$$\vec{k}_3^2 = \vec{k}_2^2 + \vec{k}_1^2 - 2\vec{k}_1\vec{k}_2 \cos(\pi - \alpha) \tag{2.41}$$

One characteristic of a three frequency interaction is that two waves are polarized in the same plane while the third wave is polarized in a plane perpendicularly to the other two. If the two original waves ω_1 and ω_2 have the same polarization direction this kind of phase matching is called *type I* and the phase matching condition is written:

$$\vec{k}_1^o + \vec{k}_2^o = \vec{k}_3^e(\theta). \tag{2.42}$$

If the two parent waves are polarized in perpendicular planes it is called *type II* phase matching

$$\vec{k}_1^o + \vec{k}_2^e(\theta) = \vec{k}_3^e(\theta) \tag{2.43}$$

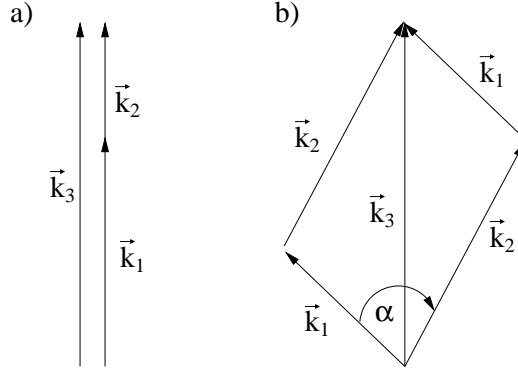[1]$p = \hbar k$ and $E = \hbar \omega$

14

Figure 2.3: Collinear (a) and non-collinear (b) sum frequency generation.

Conversion efficiency

For the construction of a broadband fluorescence upconversion setup it is important to find an appropriate nonlinear crystal, i.e. to be able to calculate conversion efficiencies. This is the ratio of P_3 and P_1, the powers of the original wave 1 and the upconverted wave 3, respectively. In the plane-wave fixed-field approximation in the SI system [17] the conversion efficiency can be calculated with

$$\frac{P_3}{P_1} = \frac{8\pi^2 d_{\text{eff}}^2 L^2 P_2}{\varepsilon_0 c n_1 n_2 n_3 \lambda_3^2 A} \text{sinc}^2(|\Delta k| L/2) \tag{2.44}$$

where

$$\text{sinc } x = \frac{\sin x}{x}.$$

Here L(m) is the length of the crystal, λ(m) the wavelength of the generated electric field, $\varepsilon_0 = 8.854 \times 10^{-12}$(As/Vm) the dielectricity constant, A(m^2) the cross-sectional area of the laser beam, $c = 3 \times 10^8$(m/s) the speed of light, n_i the dimensionless refractive indices and P_2(W) the power of the gating pulse. d_{eff}(m/V) is the effective nonlinearity of the crystal. The Sellmaier equations describing n and d_{eff} for two nonlinear crystals which were used in our setup are given on page 35.

Equation 2.44 shows that the conversion efficiency can be improved by increasing the gating pulse energy P_2 or – even more efficiently – the crystal length L. The drawback of increasing the crystal thickness is that at the same time the acceptance bandwidth decreases. This latter aspect is illustrated in Figure 2.4 where the conversion efficiency is calculated for the nonlinear optical crystal β-barium borate (BBO), a gate pulse centred at λ_2=800 nm, a phase matching angle of θ=50°, and for three different thicknesses L: 1000,
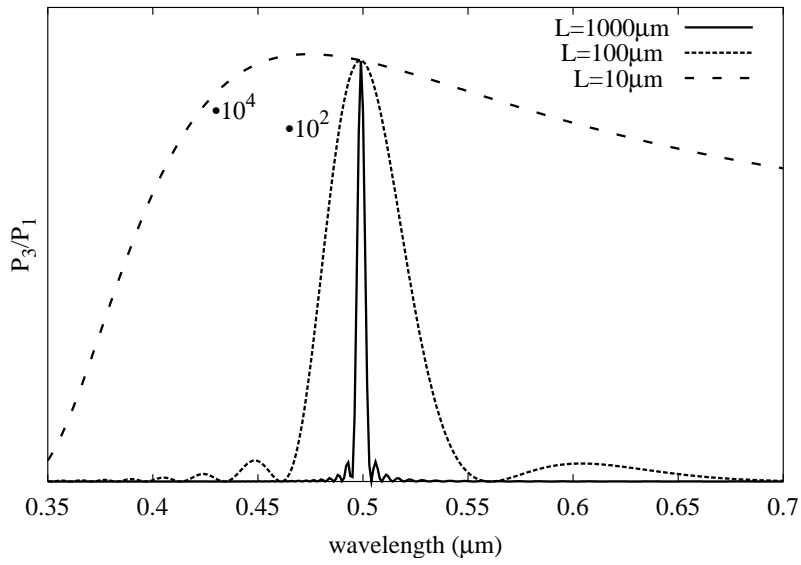
Figure 2.4: The conversion efficiencies P_3/P_1 (eq 2.44) for type II fluorescence upcoversion using a gate pulse at λ_2=800 nm and BBO as nonlinear crystal. The acceptance bandwidth increases as the thickness of the crystal L decreases, but the loss of conversion efficiency scales with L^2.

100 and 10 μm. One incoming field, P_1, is fluorescence equally distributed over the spectral region from 350 to 700 nm. Figure 2.4 reveals one strategy for the design of a broadband-fluorescence upconversion setup: decreasing the thickness of the crystal and compensating the loss of conversion efficiency with higher powers of the gating pulse. This strategy may succeed in the future, but for now we are limited with regard to gate pulse power P_2, and the detection sensitivity requires a certain minimum thickness of the crystal.

Nonlinear Phase Modulation and Continuum Generation

In the transparent region of many materials, the refractive index depends nonlinearly on the propagating field $\vec{E}$ [18]. This dependence can be expressed by

$$n(t) = n_0 + 2n_2\langle\vec{E}^2(t)\rangle. \tag{2.45}$$

The quantity n_2 is called nonlinear index coefficient and describes the strength of the coupling between the electric field and the refractive index. It can be shown that it is related to the third order susceptibility:

$$n_2 = \frac{3\chi^{(3)}}{8n_0}. \tag{2.46}$$

The intensity dependence of n implies a refractive index varying in time and space as an intense pulse propagates through the medium. The temporal variation results in spectral broadening. In the case of high power, a transform-limited femtosecond pulse at 800 nm can broaden from the ultraviolet to the infrared. Therefore this spectrally broadened pulse is called a white light continuum. As the electronic distortion response time is ca. 10^{-16}s the pulse does not broaden in time [19]. This is why continuum generation is a convenient method for the preparation of white femtosecond probe pulses for transient absorption measurements [20].

2.2 Dynamics

2.2.1 Solvation

Solvation is the arrangement of solvent molecules around a dissolved particle, the solute. The conformation depends on solute-solvent-interactions. Let the charge distribution of each particle be expanded in multipoles. For uncharged particles at the lowest order we have the electrostatic interactions between permanent and induced dipole moments of solvent and solute [14, 21].
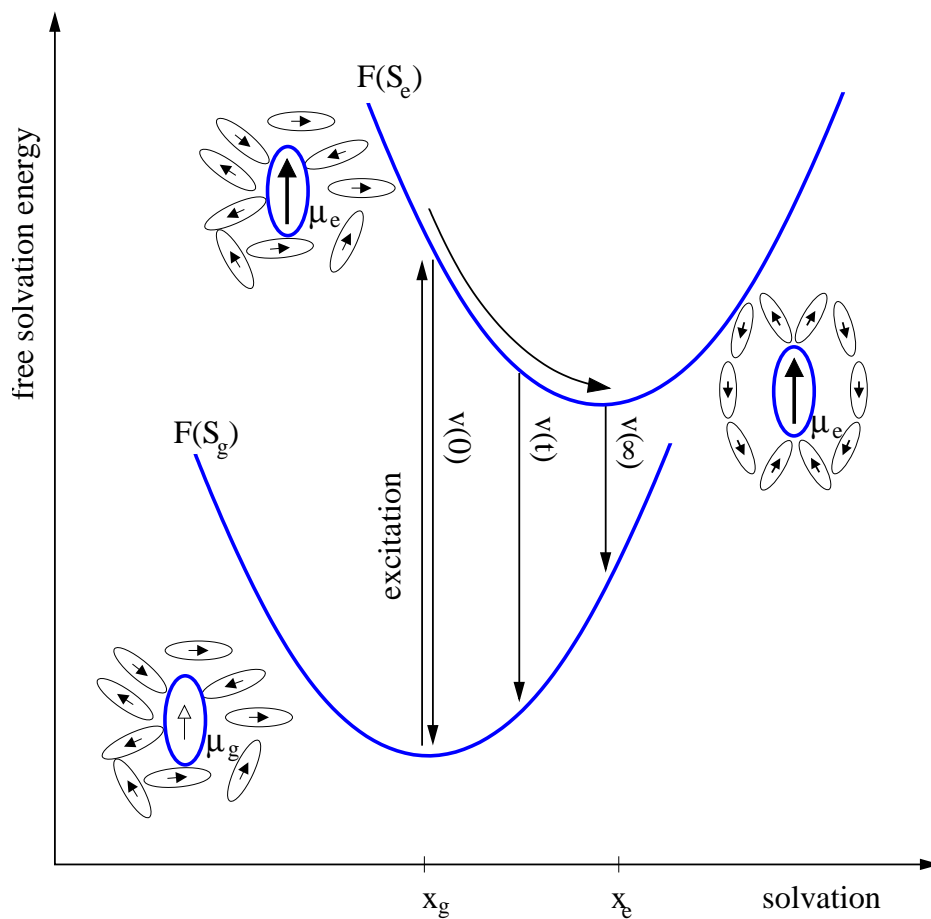
Figure 2.5: The solvation potentials along the solvation coordinate in the ground and excited state, S_g and S_e, respectively can be described in the linear response approximation by two parabolas of the same curvature with minima at x_g and x_e. Upon excitation of the solute molecule its dipole moment changes from μ_g to μ_e. The reorientation of the solvent molecules in the field of the excited state dipole μ_e can be traced by measuring the peak of the emission band $\tilde{\nu}(t)$ [7].

We restrict ourselves to the simple case of an uncharged dipolar solute in an aprotic dipolar solvent. A solvent meeting these requirements is for example acetonitrile. Here solvation can be described in the following fashion. The solute generates an electric field due to its ground state dipole moment μ_g. In the equilibrium the solvent molecules are orientated in the field of the solute according to some thermal distribution. On optical excitation from electronic ground state $g \rightarrow e$ the solute changes its dipole moment instantaneously. During this excitation the solvent shell is kept "frozen" in the equilibrated ground state configuration, as required by the Franck-Condon principle. After excitation the polar solvent molecules start to reorientate in the field of the excited state dipole moment μ_e. The relaxation is mainly due to dipole-dipole interactions and therefore it is accompanied by rotational motion.

This rotational motion of solvent molecules occurs on a femtosecond time scale and can be monitored by measuring time resolved fluorescence. A red shift of the emission band can be observed, which gives the solvation relaxation function [7, 22]

$$S(t) = \frac{\tilde{\nu}(t) - \tilde{\nu}(\infty)}{\tilde{\nu}(0) - \tilde{\nu}(\infty)}, \tag{2.47}$$

where $\tilde{\nu}$ is the peak frequency of the emission band. If there is little internal vibrational excitation of the solute after the transition, the time dependence of $\tilde{\nu}(t)$ arises mainly from the time-dependent solvation energy. The normalized solvation correlation function is then independent of the solute. It depends only on the dielectric properties of the solvent [23, 24, 25, 26]. For non-equilibrium phenomena the solvent is most often modeled as a dielectric continuum. In this treatment the solvent is modeled as a structureless fluid with a frequency-dependent dielectric constant, $\varepsilon(\omega)$. In experiments which access only the low frequency part, like dielectric relaxation measured by microwaves < 120 GHz, $\varepsilon(\omega)$ is expressed in the Debye form

$$\varepsilon(\omega) = \varepsilon_\infty + \frac{\varepsilon_0 - \varepsilon_\infty}{1 + i\omega\tau_D}, \tag{2.48}$$

where ε_∞ and ε_0 are the high-frequency and zero-frequency dielectric constants, respectively; τ_D is the Debye relaxation time representing orientational relaxation. The solvation correlation function can be obtained by Laplace transform of the appropriate functional of $\varepsilon(\omega)$ [27]. Better results can be obtained with a semi-empirical approach using $\varepsilon(\omega)$ from microwave and far-infrared spectra of pure solvents. This has been verified by Marcus in the case of water [28] while Ernsting and coworkers have shown perfect
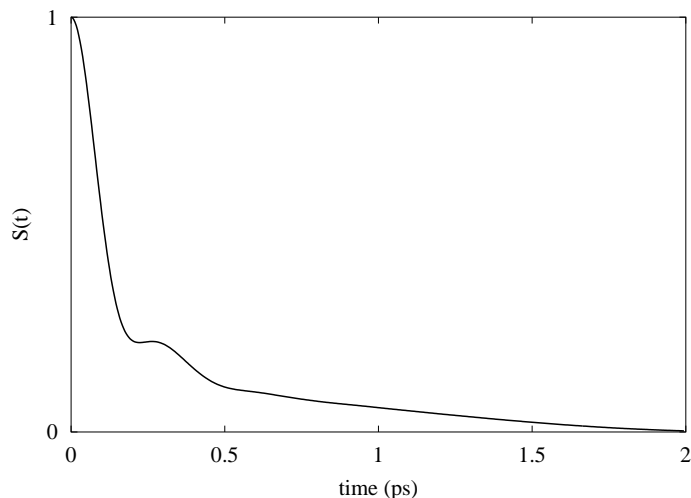
Figure 2.6: Solvation correlation function of acetonitrile at 22°C: a fast Gaussian component, a solvent oscillation at 0.3 ps followed by a slow exponential component [29].

agreement between experiment and theory for acetonitrile with amino-nitro-fluorene as solvation probe (see Figure 2.6) [29].

$S(t)$ can be well represented by a Gaussian plus a multi-exponential function:

$$S(t) = a_1 \exp\{-0.5(t/\tau_1)^2\} + \sum_{i>1} a_i \exp(-t/\tau_i) \quad \text{with} \quad \sum_i a_i = 1. \quad (2.49)$$

Here the Gaussian reflects an inertial motion of the "free streaming" solvent molecules. Before excitation of the solute, the solvent molecules move with random rotational velocities having an equilibrium Maxwell-Boltzmann distribution, which is independent of intermolecular interactions. After excitation the difference of the solvation potential between the electronic ground state and excited state, may be presumed to act on the distribution. The initial response then leads to a Gaussian energy relaxation. The exponential components can be assigned to relaxation of the solvent molecules by rotational diffusion. Equation 2.49 does not describe the hump at 300 fs shown in Figure 2.6 which represents underdamped solvent oscillation [22, 24].

2.2.2 Evolution of the band-shape

Analysis of time- and frequency resolved fluorescence measurements provides information in addition to the dynamic Stokes shift since the band-shape is

also characterized by spectral width $\Gamma(t)$ and asymmetry $\gamma(t)$ [30]. It is still under debate how these observables depend on solvation dynamics. Especially because solvation dynamics is traditionally discussed in the framework of the linear response approximation [6, 7, 22], where it is assumed that the change of the polarizability of the solute upon excitation can be neglected and that the solvation free energy curves for both ground and excited state are parabolas of the same curvature. Therefore the shape of the emission band should not change during solvation dynamics at all unless intramolecular reactions take place on the same time scale. Furthermore steady state absorption and emission spectra should be related by mirror symmetry. Slight deviations from both are usually met. On the other hand the linear response approach predicts solvation response functions that are in good agreement with the experiment; therefore it was supposed to be suitable for the description of solvation dynamics.

Thermal relaxation

One concept explaining the evolution of the band shape completely without solvation dynamics is that of thermal relaxation. By optical excitation vibrational excess energy is deposited inside a polyatomic solute. In a first ultrafast step (< 50 fs) this excess energy is distributed over several modes of low frequency of the molecule [23], which is then characterized by a temperature higher than that of the surrounding solvent. The hot molecule cools by collisional interaction with solvent molecules. This heat transfer occurs on a time scale between 5 and 50 ps depending on the specific solvent, specific solute-solvent interactions and the excess energy [31]. Now as the shape of the spectrum depends on temperature the change of shape can reflect the cooling of the solute [32].

Spectral diffusion of a hole

One model for broadening – that is consistent with the linear response approximation and incorporates the solvation correlation function – considers spectral diffusion of a hole burnt in the ground state equilibrium distribution and transfered to the excited state potential surface ('particle') [33, 34, 35]. Around time zero the emission spectrum should reflect the intramolecular Franck-Condon progression with each transition having the width of the pump pulse. As spectral diffusion proceeds each vibronic transition line broadens until their envelope achieves finally the width of the steady state spectrum. Figure 2.7 depicts a simulation of the evolution and shows how the extent of this effect depends on the Franck-Condon pattern. In the left
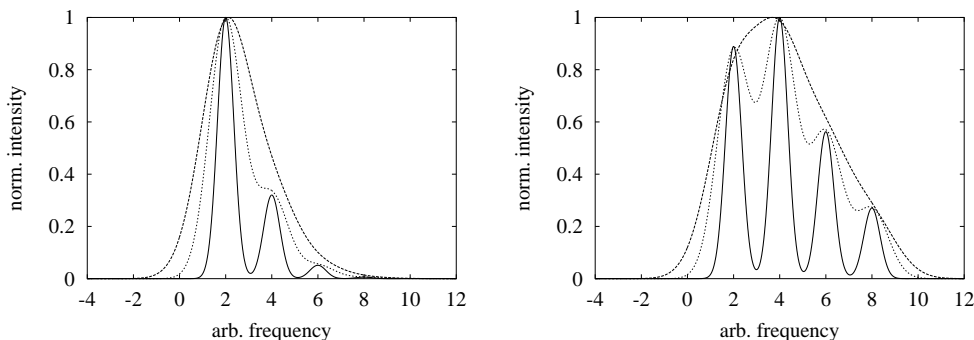
Figure 2.7: Simulation of time-resolved emission spectra of two different model solutes illustrates broadening due to spectral diffusion of a particle: from the Franck-Condon spectrum convoluted with the pulse-shape to the final shape. (Spectral drift has been ignored here.)

panel the pattern is dominated by a single transition line and the envelope broadens by a factor of three. In the right panel we see a pattern of three strong vibronic transitions, here the envelope broadens by only ten percent. However, the relation between the width $\Gamma(t)$ and the solvation correlation function $S(t)$ was derived to be

$$\Gamma(t) = \sqrt{A - B \cdot S(t)^2}. \tag{2.50}$$

Here A and B reflect the squares of widths of the equilibrated band, the pump and the probe pulse, respectively [34, 36]. The qualitative validity of this equation was shown for dye molecules at low temperatures, e.g. retinal in ethanol at 247 K [33] and rhodamine 6G in ethanol at temperatures below 150 K [36]. Nishiyama and Okada measured the spectral shift and broadening of HITC in ethanol at different temperatures. At 190 K both processes occurred on the same time scale while at room temperature the shift was much faster than the broadening [37].

Nonlinear response

Transient broadening or narrowing on a solvation time scale can be understood phenomenologically if one assumes solvation potential surfaces of different curvatures in the ground and excited state. This was proposed first by Kakitani and Mataga [38]. The authors predicted the curvature of the solvent free energy curve to be steeper for a charged solute than for a neutral solute due to dielectric saturation of the first solvent shell. This approach

was supported by molecular dynamics computer calculations of Carter and Hynes [39]. The authors also derived another relation between the square of the width and the solvation correlation function

$$\Gamma(t) = \sqrt{A - B \cdot S(t)}. \tag{2.51}$$

Matyushov derived the same relation for chromophores in polar solvents; here the change of the polarizability of the solute upon excitation was taken into account and results in nonlinear solvent response [40].

A direct relation between the time dependent width and the spectral shift, such as

$$\Gamma(t) = A + B \cdot S(t), \tag{2.52}$$

could not be derived so far but – even more interesting – it was already observed in experiments on DCM in ethylene glycol by Glasbeek and co-workers [41]. The authors made simulations using a nonlinear response approach in which anharmonicities of the solvation potentials were taken into account. One of their interesting results is that the sign of the anharmonicity term governs the direction of this evolution, whether the emission spectrum broadens or narrows.

However, none of the equations 2.50-2.52 can be considered established. One reason is the lack of reliable data; only few experimentalists were able to achieve necessary time-resolution and at the same time to extract $\Gamma(t)$ from reconstructed spectra. Another reason is that the few results which are available at present do not permit, as yet, to establish a unique characteristic behaviour. Mokhtari *et. al.* found solvation dynamics of nile blue and oxazine 1 in methanol accompanied by line narrowing [5]; narrowing was also observed by van der Meulen *et. al.* in the case of DCM in ethylene glycol [41]. Smith *et. al.* observed broadening in the case of LDS-750 in aniline [42]. Bingemann and Ernsting found narrowing followed by broadening in the case of DASPI in methanol [8] while Maroncelli *et. al.* observed broadening followed by narrowing in the cases of coumarin 102 in N-methylpropionamide [6] and coumarin 153 in DMSO [23]. Although these evolutions of the width are different they have one thing in common: they all show biexponential behaviour with one time constant less than a picosecond and the other of the order of tens of picoseconds. It seems reasonable to assume that the small time constant is somehow related to solvation dynamics – as suggested by several theories – and the larger time constant to thermalization of the solute [23]. In conclusion at this stage, it appears that new experimental approaches are needed to characterize the evolution of spectral width in the case of solvation.

2.2.3 The time-zero spectrum

The spectrum at time infinity can be considered identical with the stationary fluorescence spectrum if the fluorescence life time is in the nanosecond range. But an important problem associated with experimental determination of $S(t)$ is the difficulty to determine the peak position of the time-zero spectrum, $\tilde{\nu}(0)$. The time-zero spectrum is the hypothetical spectrum that would be observed for a solute that has completely relaxed vibrationally but before any relaxation of the solvent has occurred. This requires that intramolecular relaxation of Franck-Condon-active modes occur on a sub 100 fs timescale, while solvation dynamics occurs on a super 100 fs timescale. In a first approximation, the shift between absorption and emission spectra before solvation takes place should be equal to the Stokes shift of the same solute in a non-polar solvent such as cyclohexane [43].

With a more subtle model a better approximation can be obtained. The basic idea is that a molecule has an intrinsic spectral absorption line shape $g(\tilde{\nu})$ and an emission line-shape $f(\tilde{\nu})$. These shapes refer to the distribution of transition probabilities (cf. page 9); they are both determined by vibronic transition characteristics of the molecule. These intrinsic spectra are related to the reference spectra A_{ref} and F_{ref} for absorption and fluorescence, respectively, in a non-polar solvent by

$$g(\tilde{\nu}) \propto \tilde{\nu}^{-1} A_{\mathrm{ref}}(\tilde{\nu}) \tag{2.53}$$

and

$$f(\tilde{\nu}) \propto \tilde{\nu}^{-3} F_{\mathrm{ref}}(\tilde{\nu}). \tag{2.54}$$

Here $A(\tilde{\nu})$ is proportional to the extinction coefficient for absorption while $F(\tilde{\nu})$ is the fluorescence quantum distribution (see eq 2.18). The molecule interacts with the solvent-molecules, that are distributed around it. This distribution of solvent molecules $p(\delta)$ is assumed to be Gaussian. The solvent environment causes a broadening σ and a shift δ_0 of the spectra. These effects can be described as a convolution of the line shape function $g(\tilde{\nu})$ with the solvent distribution function $p(\delta)$. The absorption spectrum in a polar solvent is therefore written

$$A_{\mathrm{p}}(\tilde{\nu}) \propto \tilde{\nu} \int g(\tilde{\nu} - \delta) p(\delta) \mathrm{d}\delta \tag{2.55}$$

with

$$p(\delta) = \frac{1}{\sqrt{2\pi}\sigma} \exp\left\{ -\frac{1}{2} \left(\frac{\delta - \delta_0}{\sigma} \right)^2 \right\}. \tag{2.56}$$

In a similar way, the relation between the time-zero emission spectrum in a

polar solvent F_p and emission line shape $f(\tilde{\nu})$ can be expressed by

$$F_{\mathrm{p}}(\tilde{\nu}; t = 0; \tilde{\nu}_{\mathrm{ex}}) \propto \tilde{\nu}^3 \int g(\tilde{\nu}_{\mathrm{ex}} - \delta)p(\delta)f(\tilde{\nu} - \delta)\mathrm{d}\delta. \qquad (2.57)$$

Here $\tilde{\nu}_{ex}$ is the excitation frequency. The calculation of F_p requires the three functions $g(\tilde{\nu})$, $f(\tilde{\nu})$ and $p(\delta)$. $g(\tilde{\nu})$ and $f(\tilde{\nu})$ are obtained from the absorption and fluorescence spectra in a non-polar solvent. By comparison with the absorption spectra in an polar solvent, of interest, the distribution function $p(\delta)$ can be obtained [23, 43].

Chapter 3

Experimental

3.1 The setup

Femtosecond laser pulses centred at 794 nm were obtained from a Ti:Sa-oscillator-amplifier system. They were converted into pulses at 1300 and 397 nm using DFG and SHG, respectively. The 397 nm pulses were used to excite a sample in a flow cell. Spontaneous emission was collected and then focused onto a KDP crystal with astigmatism free reflective optics. Here the entire range from 435 to 610 nm was gated with a single infrared pulse using SFG without readjusting optical elements. The upconverted signal was dispersed with a grating spectrograph and detected by a CCD-camera. This was the first realization of an experimental setup for femtosecond broadband fluorescence upconversion [44, 45].

3.1.1 Oscillator and amplifier

The oscillator is a commercially available Ti:Sapphire laser (*Femtosource Pro, Femtolasers*) pumped by a solid-state diode-pumped, frequency doubled Nd:Vanadate (Nd:YVO) laser that provides single-frequency green (532 nm) output at power levels greater than 5 W (*Verdi; Coherent Inc.*). The repetition rate is 1 MHz, the pulse duration is around 10 fs and the energy of the single pulse of 4.5 nJ. The pulses are centred at 794 nm [46].

For amplification of the weak pulses a 9 pass amplifier system was used, which was constructed according to references [47] and [48]. It amplifies a 10 fs pulses of 4.5 nJ to 40 fs pulses of 600 μJ. An amplifier consists basically of 3 parts: stretcher, amplifier and compressor. The 10 fs seed pulse from the oscillator is stretched by a 5 cm block of flint glass (*Schott SF57*). After passing the block twice the pulse has a duration of approximately 10 ps. The amplifier stage consists of a focusing mirror (*R*=80 cm), a 5-mm-
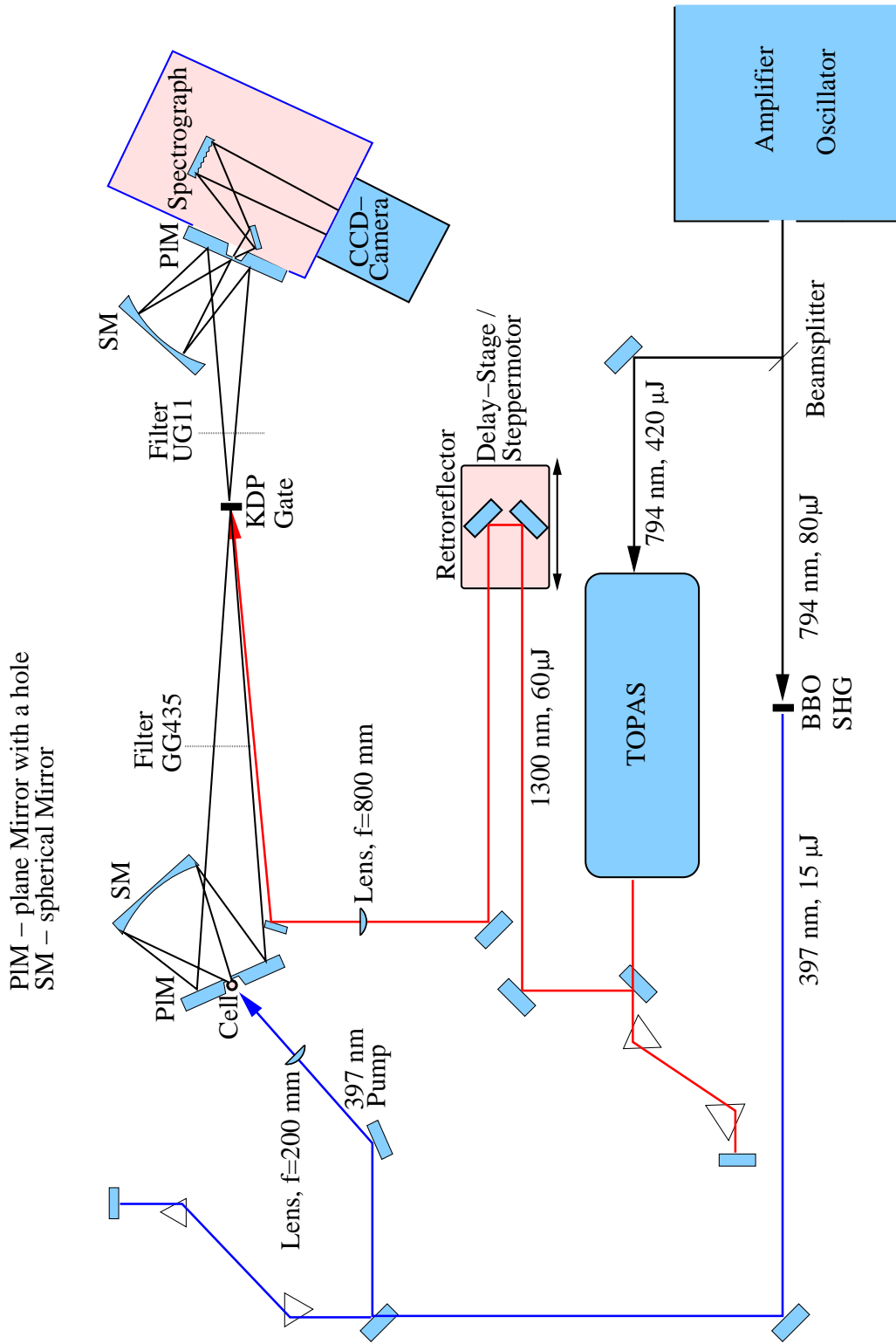
Figure 3.1: The fluorescence upconversion setup.

long Brewster-angled Ti:Sa crystal, a recollimating mirror (R=50 cm), and retroreflectors. The crystal is pumped with 9-10 mJ pulses delivered by a cw-lamp-pumped, Q-switched, intracavity frequency-doubled Nd:YLF laser (*Model 621D/2; BMI*). For suppression of amplified spontaneous emission the preamplified pulse train leaves the amplifier after four passes. It passes a pulsepicker consisting of a periscopic polarization rotator, a 1 kHz Pockels cell (*Model 5046; Lasermetrics*) and a Berek polarization compensator (*Model 5540; New Focus*). These components generate a high transmission window that is opened for 10 ns. A single pulse at the peak of the envelope of the preamplified pulsetrain can pass. This selected pulse is reinjected into the amplifier where its energy is increased to 1.4-1.6 mJ in another five passes. The compressor section consists of two sets of Brewster-angled fused-silica prisms. Additionally 16 reflections off a pair of chirped mirrors (located in the stretching section) introduce cubic and quartic dispersion to eliminate phase errors up to fourth order [49].

3.1.2 Pump and gate pulses

The pulse leaving the amplifier (794 nm, 500 μJ) is split in two fractions by a 1:5 beamsplitter. The weaker pulse fraction, 80 μJ, is converted into its second harmonic (397 nm, 15 μJ) with a β-barium borate crystal (BBO, θ=29°, d=0.2 mm). This blue pulse is compressed with a pair of fused silica prisms in order to compensate dispersion due to the BBO and a fused silica lens. With the latter (f=200 mm) the pulse was focused into the cell to excite the sample. The pulse duration was determined to be 50 fs (see page 39).

From the second fraction (420 μJ) an infrared pulse for the gating was generated with a TOPAS (*Traveling-wave Optical Parametric Amplifier of Superfluorescence; Light Conversion*). Here white light is generated by broadbanded super fluorescence. A sophisticated arrangement of nonlinear crystals, delay stages and a grating allows to select one wavelength and to amplify it [50]. Besides the desired wavelength of 1300 nm also the second and third harmonic are generated, which can be separated out in a compression stage consisting of a pair of prisms. The near infrared pulse at 1300 nm had an energy of 60 μJ and a duration of 60 fs. After passing the delay stage the pulse was focused on a KDP crystal to gate the fluorescence.

Mirrors

Before the pump and gate pulse reach the sample and the gating crystal, respectively, they are reflected nearly ten times. The loss of intensity can be minimized by applying mirrors covered with high reflectivity coatings

(*Firma Laser-Optik, Garbsen*). These are optimized for a single wavelength to maintain reflectivities greater than 99.5% at 45°. To keep the pulse shape and to avoid pulse broadening due to group velocity dispersion mirrors with single-stack coatings were used [51].

Dispersion of pulses

A short pulse is not monochromatic but extended around a central frequency ω_0. The temporal and spectral characteristics of the field are related to each other through Fourier transforms. Therefore the spectral and temporal characteristics of the intensity, bandwidth $\Delta\omega_p$ and pulse duration τ_p, cannot vary independently of each other. There is a minimum duration-bandwidth product, which is defined with respect to full width at half maximum (FWHM) of Gaussian shaped pulses as [18]:

$$\Delta\omega_p \cdot \tau_p \geq 2\pi \cdot 0.441 \tag{3.1}$$

One can apply equation 3.1 and calculate the spectral width of a 50 fs pulse centred at 400 nm. It is distributed over the spectral range from λ_{blue}=397.7 to λ_{red}=402.4 nm.

If a short pulse traverses transparent matter, e.g. a quartz lens, it will experience group velocity dispersion. Every spectral component travels at its own velocity. This phenomenon results in a temporal sweep of the frequencies, called chirp, and an associated broadening. This broadening is essentially the difference between the times that blue and red spectral components need to traverse the medium. Next, we briefly discuss broadening of Gaussian pulses by group velocity dispersion. The wavelength dependence of index of refraction is given by the dispersion relation [52]

$$n(\lambda) = \sqrt{\frac{b_1\lambda^2}{\lambda^2 - c_1} + \frac{b_2\lambda^2}{\lambda^2 - c_2} + \frac{b_3\lambda^2}{\lambda^2 - c_3} + 1}. \tag{3.2}$$

The constants for materials used in this setup are shown in Table 3.1. An unchirped pulse is assumed to have original duration τ_{p0}. After propagating a distance z through a dispersive medium the new pulse duration is [53]

$$\tau_p = \sqrt{\tau_{p0}^2 + \left(\frac{(4\ln 2)\cdot\lambda^3\cdot n_\lambda''}{\tau_{p0}\cdot 2\pi\cdot c_0^2}\right)^2}. \tag{3.3}$$

Here n_λ'' is the second derivative of the index of refraction with respect to wavelength and c_0 is the speed of light. Now it possible to estimate the dispersion due to a fused silica lens of z=2 mm thickness. If an unchirped pulse is centred at λ=400 nm and has a duration of τ_{p0}=40 fs, after propagating through the lens it will be spread to τ_p=43 fs.

29

	fused silica	sf10
b_1	0.9616630	1.6162977
b_2	0.4079426	0.2592293
b_3	0.8974794	1.0776231
c_1	0.0046791	0.0127534
c_2	0.0135120	0.0581983
c_3	97.934002	116.60768
$\lambda \; [\mu\mathrm{m}]$	.400	1.300
n_λ	1.56036	1.6974
$n_\lambda' \; [\mu\mathrm{m}^{-1}]$	-0.116021	-0.0172386
$n_\lambda'' \; [\mu\mathrm{m}^{-2}]$	0.913069	0.017461

Table 3.1: Constants for the calculation of wavelength dependent indices of refraction of different glasses using equation eq 3.2 [52].

Compression of the pulses

The broadening due to group velocity dispersion is compensated in a prism compressor. It consists of two prisms of negative dispersion. The first prism disperses the pulse in its spectral components. The second prism is rotated around 180° with respect to the first one. If it is placed properly, the blue components will only traverse the peak of the prism while the red components have to pass a longer path inside the prism. In this way the red front of the pulse train is held back. After the second prism all spectral components are parallel. The direction of the pulses is reversed by a mirror. After passing the two prisms for a second time the spectral components are recombined and the pulse is shortened in time [54].

Delay-stage

The change of temporal delay between pump and gate pulse is realized with a variable delay-stage. A linear ball screw stage (*ATS03005-N, Aerotech*) is driven by an brushless rotary servo motor (*BM75E, Aerotech*). It can be moved in steps of 0.1 μm corresponding in the time domain to a change of Δt=0.67 fs. The maximum distance that can be achieved with this delay-stage is 50 mm corresponding to a maximum time delay of 333 ps. The control unit (*BA-Intellidrive, Aerotech*) can be connected to the COM-port of a personal computer. A simple programming language allows adjustment and control of the motor velocity and positioning.

A hollow corner cube retroreflector (*OW-25-5, PLX*) [55] with an aperture

of 63 mm was mounted on the stage. It returns a beam after three reflections parallel to the incident beam with an deviation of only 5 arc sec independent of its alignment. The mirrors are coated with silver which is protected with a single dielectric layer enhancement. Its reflectivity of silver is ca. 97% at λ=1300 nm, hence the overall loss of intensity is 10%.

3.1.3 Upconversion

Sample cell and light collection

For fluorescence upconversion, the spontaneous emitted light must be collected over a large solid angle, and the light source must be imaged onto the detector. Imaging should be optimal in the following sense: it should be achromatic, different partial rays should travel the same distance to maintain time-resolution. This goal can be achieved by applying reflective instead of dispersive optics.
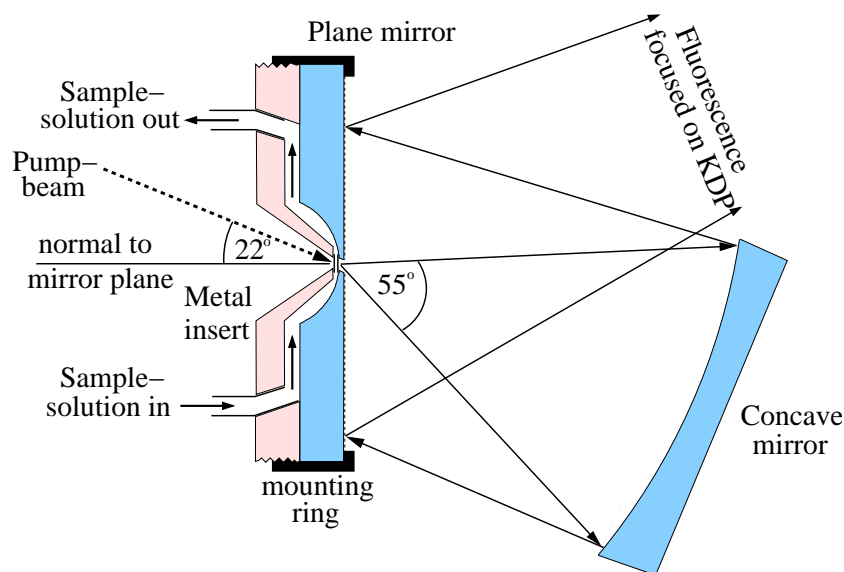

Figure 3.2: The flow cell is set into a cavity drilled into the non-reflective side of the plane mirror.

For the collection of fluorescence light and its focusing on the gating crystal a spherical mirror has been used. Auto-collinear alignment allows astigmatism-free focusing which is achieved by constructing a cell directly in the substrate of a plane mirror. Fig 3.2 shows the flow cell in the cavity in the uncoated side of a plane mirror. The cavity is a hemisphere cut into the non-reflective side of the mirror substrate leaving roughly 1 mm of glass

substrate. A hole ($\oslash$=2 mm) is drilled in the center of the mirror substrate. A fused silica window with a thickness of 0.16 mm is glued on the hole from the cavity side. Another window is glued on an steel insert that is pressed on the cavity side of the mirror. The distance between the two windows, i.e. the cell thickness, is adjustable around 0.5 mm. This insert has an inflow and an outflow for the sample solution. These lead to channels that allow the solution to be pumped through between the two windows. The insert is designed in a way that the excitation pulse can reach the cell through a conical cavity in an angle up to 30°. The insert is threaded and thus held, relative to the glass substrate, by a metal ring. Between the mirror and the insert a viton O-ring seals the cell. Between mounting ring and mirror a teflon casket protects the latter. By rotating the screw ring the thickness of the cell can be adjusted. The thickness has to be determined by measuring the absorption of a solution with known concentration and extinction coefficient.

The sample is excited with a laser beam tilted by 22° from the normal of the plane mirror. The fluorescence light is collected with a spherical concave mirror (R=150 mm, $\oslash$=76.5 mm, *UV-enhanced coating, Tafelmaier*) that reflects the excitation beam into itself. This spherical mirror is placed on a micrometer adjustable translation stage around 80 mm from the cell. The fluorescence is collected in a cone of a full angel of 55°. By moving the translation stage the focus of the collected light is adjusted to be 800 mm away. The light is reflected autocollinearly back to the plane mirror/cell-construction. The plane mirror (UV-enhanced coating) redirects the fluorescence to the crystal where it is gated with an infrared pulse.

The pump beam was focused with a fused silica lens into the cell, to a spot size of 50 μm. The aim of this part of the setup is not only to collect the light but also to magnify the spot size of fluorescence by a factor of ten (500 μm) on the gating crystal. This is necessary because focusing too hard results in continuum generation in the crystal. At the same time magnification reduces the cone angle of the light by a factor of ten from 55 to 5.5°, therefore all light will be in compliance with the angular conditions for the upconversion process.

Spherical aberration

Focusing with spherical mirrors is accompanied by spherical aberration. The approximation f=2R is only valid for rays close to the optical axis. As the angle α between the rays and the optical axis increases the picture of a point source turns into a spatial distribution (*caustic*) [56]. Due to spherical aberration there is no focus but we may think of a focal area. In our experiment it is a spot of a radius of 250 μm, in a plane normal to the optical axis and
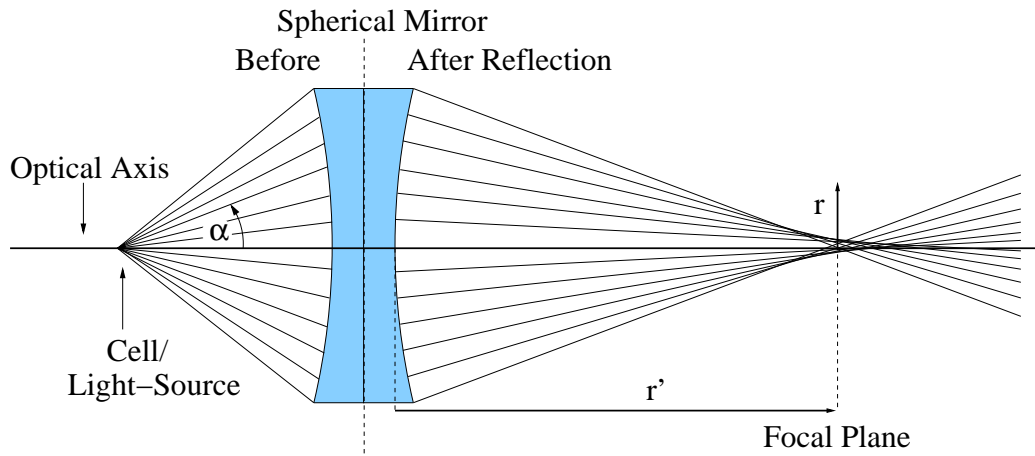
32

Figure 3.3: Spherical aberration: α is the angle between a ray leaving the point light source and the optical axis (left hand side). After reflection (right hand side) the focus is not a point but a spatial distribution (caustic) at a distance r'. r refers to the distance from the optical axis.
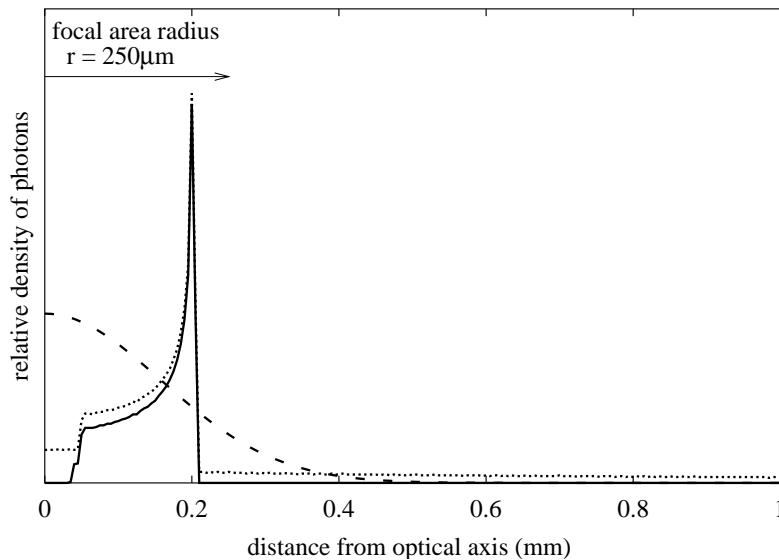

Figure 3.4: The calculated photon density profile in the focal area/plane as a function of the distance to the optical axis r. The position r' was optimized for a spot with a radius of 250 μm. The light collected over an angle $\alpha < 10°$ (—) has approximately the same profile as for $\alpha < 25°$ ($\cdots$). The additional collected light ($\alpha > 10°$) cannot be focused. A Gaussian spot profile for comparison (- - -).

$\alpha(°)$	0	5	10	12	15	20	25	30
$\Delta t(\mathrm{ps})$	0	0.002	0.023	0.047	0.116	0.378	0.969	2.127

Table 3.2: Rays with different angles α in respect to the optical axis have different path lengths between cell and caustic plane resulting in different time delays.

shifted along the optical axis to that position where it experiences maximum photon flux. Simple geometrical considerations allow to calculate the relative ray density or beam profile at a position r' along the optical axis (Fig 3.3). These relations were incorporated in a computer program in order to find the focal plane at r', for a given distance between the cell and curved mirror.

Now, we analyze the caustic beam profiles in the focal plane for two different collection angles. First for the full cone angle ($2 \cdot \alpha = 55°$, Fig 3.4, dotted line). Only 50% of the collected rays traverse the focal area; the rest is distributed uniformly over a wide area. If the light is collected over a smaller angle ($2\alpha = 20°$, solid line) all rays will traverse the focal area. Further analysis shows that only the fluorescence light collected up to $2\alpha = 24°$ can be focused with spherical mirrors into the focal area.

Another drawback of spherical optics is the difference in the pathlength between the sample and the crystal plane for central and outer rays. Table 3.2 shows the equivalent time delay between inner and outer rays as a function of the angle α between optical axis and the ray leaving the cell. Since the effective maximum angle is $2\alpha = 24°$ spherical aberration decreases the time resolution of our setup by 50 fs.

Usually in setups for fluorescence up-conversion a pair of parabolic mirrors or a Cassegrainian is used for collection of light and focusing [57]. Their advantage is that they avoid at the same time astigmatic and spherical aberrations if they are adjusted properly. In a later version of the setup a pair of off-axis parabolic mirrors was used. It was found that the adjustment is difficult, because the shape of the spot is very sensitive to position and alignment of each mirror. No improvement could be found in comparison to the spherical mirror design, neither in temporal resolution nor in intensity of the upconverted signal due to better focusing.

Nonlinear crystals

A Beta-Bariumborate (β-BaB$_2$O$_4$, BBO) crystal is used for the SHG of 794 nm. The crystal had a thickness of 200 μm. BBO is well established for this purpose because its damage threshold and its optical nonlinearity coefficient

are high. The indices of refraction can be calculated in the spectral region between 0.21 and 1.1 μm with the Sellmaier's equation for λ in μm that are given by [17, 58]:

$$n_o^2 = 2.7359 + \frac{0.01878}{\lambda^2 - 0.01822} - 0.01354\lambda^2 \tag{3.4}$$

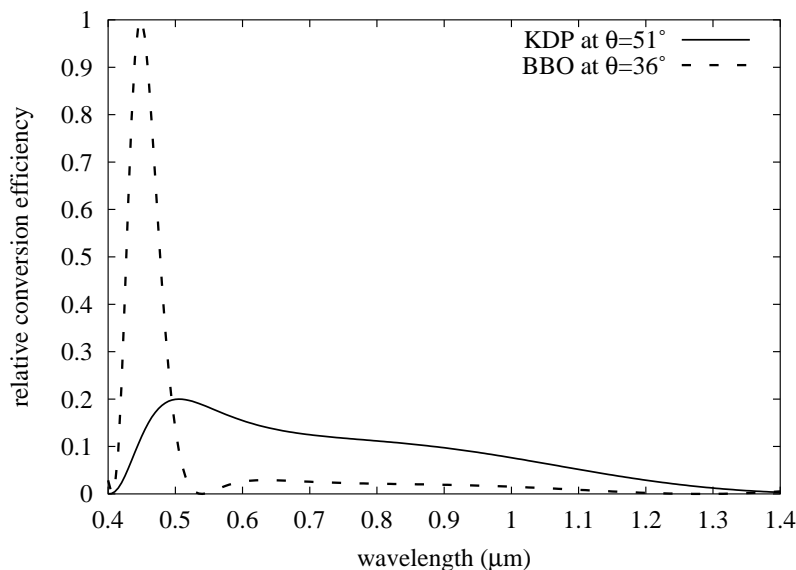$$n_e^2 = 2.3753 + \frac{0.01667}{\lambda^2 - 0.01667} - 0.01516\lambda^2 \tag{3.5}$$

Figure 3.5: The upconversion-efficiencies for two nonlinear crystals, BBO and KDP, calculated for suitable angles and experimental conditions (Type II SFG, thickness 100 μm and λ_{gate} =1300 nm). Despite its lower efficiency KDP is more suitable for broadband conversions than BBO since it covers a much wider spectral range.

The effective nonlinearity depending on θ is given by

$$d_{\text{eff}}(\theta) = 2.3(\text{pm/V}) \cdot \cos^2 \theta \tag{3.6}$$

A combination of equations 2.32, 2.40 and 2.44 allows to calculate the wavelength dependent efficiency of conversion processes (SFG and SHG) at angle θ. Consider a BBO crystal of 100 μm thickness and a gating wavelength λ_2=1.3 μm. Figure 3.5 shows the conversion efficiency (dashed line)

as function of the fluorescence at λ_1 in the spectral region between 0.4 and 1.4 μm. It is obvious that BBO is not suitable for the upconversion of the whole region at one angle θ.

For the broadband fluorescence upconversion another crystal was applied: Potassium-Dihydrogen-Phosphate (KH_2PO_4, KDP) despite the fact that it is hygroscopic and its nonlinearity coefficient is low compared to BBO [44]. But its dispersion is lower and therefore phase matching conditions are satisfied for a wider spectral range. With a 100 μm KDP it is possible to achieve SFG over the complete region between 400 and 1200 nm at only one angle θ as shown in Figure 3.5. The wavelength dependent indices of refraction for λ in μm are given by [17]

$$n_o^2 = 2.259276 + \frac{13.00522\lambda^2}{\lambda^2 - 400} - \frac{0.01008956}{\lambda^2 - (77.26408)^{-1}} \qquad (3.7)$$

$$n_e^2 = 2.132668 + \frac{3.2279924\lambda^2}{\lambda^2 - 400} - \frac{0.008637494}{\lambda^2 - (81.42631)^{-1}} \qquad (3.8)$$

and the effective nonlinearity depending on crystal angle θ for type II phase-matching is

$$d_{\text{eff}}(\theta) = 0.39(\text{pm/V}) \cdot \sin 2\theta. \qquad (3.9)$$

3.1.4 Detection

Mirrors and spectrograph

Behind the gating crystal a filter (BG3, 1 mm, *Schott*) cuts off the spectrum above 450 nm, which corresponds mainly to fluorescence itself, i.e. emitted light which was not upconverted. The upconverted light was focused onto the spectrograph input with set of mirrors that was arranged in the same manner as described above for the collection of emission. A plane mirror (UV-enhanced, $\oslash$=89 mm) with a small hole ($\oslash$=2 mm) is tilted by 24° from the central ray. It reflects the upconverted signal to a concave mirror (UV-enhanced, $\oslash$=76.5 mm, R=150 mm) which focuses it into the small hole in the center of the plane mirror. Behind this hole is placed the entrance slit (300 μm×3 mm) of a home-built Rowland-type spectrograph (Figure 3.6). The incoming light illuminates a concave standard spectrograph grating (*American Holographic 446.10*, 740 grooves/mm). The grating disperses the upconverted light into its spectral components covering the range between 250 and 550 nm. The spectrum is projected onto the flat chip of a CCD camera (see below). The spectrograph was calibrated with the light of a low pressure mercury lamp (see Figure 3.7) [59]. The effective linewidth at FWHM is 1.5 nm.
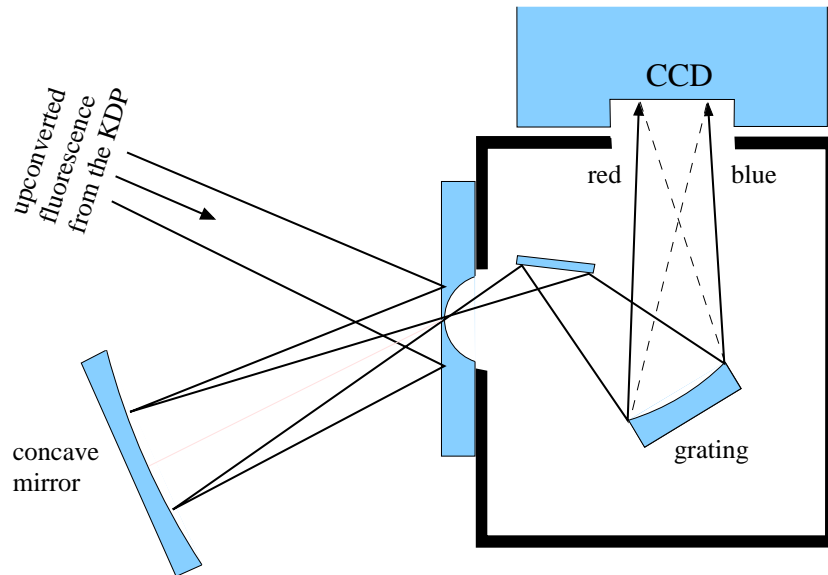
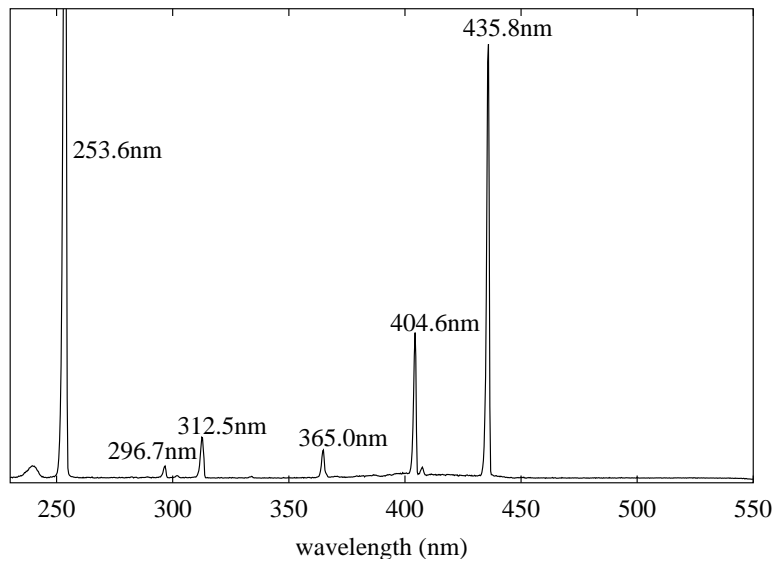**Figure 3.6:** Rowland spectrograph with spherical mirror optics for focusing.

Figure 3.7: The lines of low pressure mercury lamp were used for calibration. The FWHM of the lines is 1.5 nm.

CCD-Camera

The spectra were recorded with a CCD-camera (*Andor Technology V420-BU*). The chip of the camera is back illuminated and enhanced with an UV-anti-reflection coating. Therefore a quantum efficiency of approximately 60% is given in the region between 200 and 800 nm [60]. With thermoelectric cooling the CCD-chip can be cooled down to -60°C. In this way the dark current can be reduced to 420 counts/second in the binned mode while the noise is typically around 7 counts/second. With an array of 1024 × 256 pixels, each with 26×26 μm^2 it had an imaging area of 26.6×6.7 mm^2. The maximum number of counts per pixel is 65536.

The experiment can be controlled via an interface and a software-package delivered with the camera. The software controls cooling, wavelength calibration, graphical representation of the kinetic measurements and a simple programming language. With this language it is possible to control the camera and via the COM-ports the delay-stage, too. The script for control of the measurements is attached in appendix A.
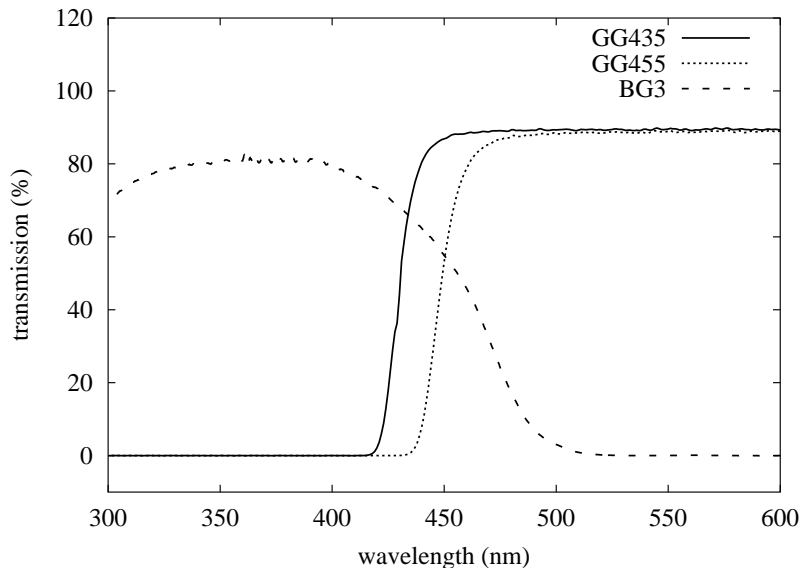
Filters

Figure 3.8: Transmission of glass filters used in the experiments (1 mm, *Schott*).

Integration of the upconverted signal over 5000 shots results in up to 1000 photons per pixel. A single 1 μm pump pulse at 400 nm corresponds to a

number of $2.5 \cdot 10^{12}$ photons. Even a small fraction of them – if scattered on the CCD-chip – would hide the signal of interest. The setup described here represents a first attempt at broadband upconversion. Here it is still necessary to use filters for removal of unwanted background light. The choice of the filter is governed by a trade-off. On the one hand the red tail of the pump pulse has to be cut off as far to the red as possible while on the other hand the early temporal spectral evolution should be observable as far to the blue as possible. A filter GG435 or GG455 (1 mm, *Schott*) is placed between the sample and the non-linear crystal. After upconversion the signal light of interest is in the spectral region between 305 and 410 nm. The stationary fluorescence signal is removed with a short-pass UV-filter (BG3, 1 mm, *Schott*) after the crystal. The transmission curves of the applied filters are shown in Figure 3.8.

3.2   Pulse characterization

Autocorrelation

The duration of short pulses cannot be determined directly but can be estimated from the intensity autocorrelation function (ACF). The autocorrelation $A(t')$ of an intensity $I(t)$ at a time t' is defined as:

$$A(t') = \int_{-\infty}^{\infty} I(t)I(t - t')dt. \tag{3.10}$$

Usually the pulse shape $I(t)$ is considered to be Gaussian.

$$I(t) = \exp\{-(t/\sigma_G)^2\}, \tag{3.11}$$

where σ_G is a parameter representing the width of the Gaussian. ACF becomes analytic solution for eq 3.10

$$\begin{aligned} A(t) &= c \cdot \exp\{-0.5(t/\sigma_G)^2\} \\ &= c \cdot \exp\{-(t/\sigma_{\mathrm{ACF}})^2\}. \end{aligned} \tag{3.12}$$

with $c = \sqrt{\sigma_G^2 \pi/2}$. The autocorrelation function of a Gaussian again results in a Gaussian. While σ_G or σ_{ACF} are fitting parameters, the parameter of interest is the pulse duration τ_p. It is defined as the full width at half maximum of the intensity $I(t)$. The relation is given by

$$\tau_p = 2\sqrt{\ln 2} \cdot \sigma_G = \sqrt{2 \ln 2} \cdot \sigma_{\mathrm{ACF}} \tag{3.13}$$
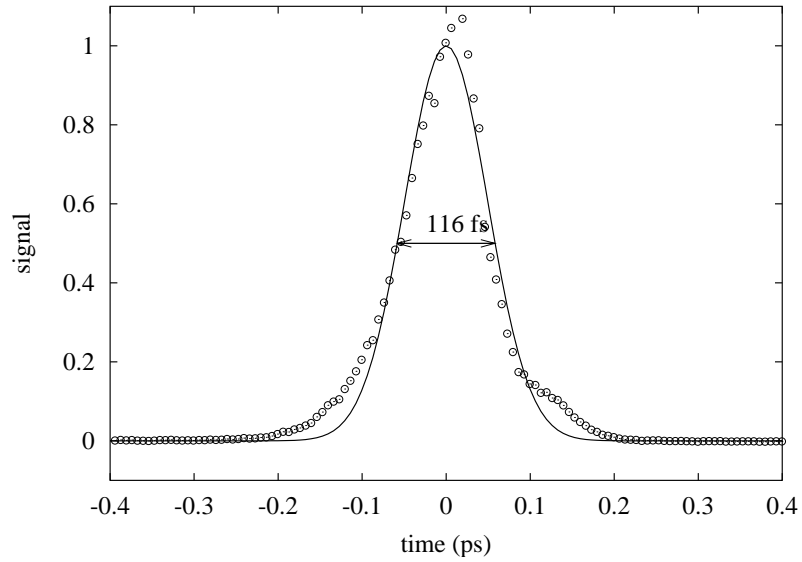
Figure 3.9: The normalized autocorrelation signal of the gate pulse integrated over all wavelength and fitted with a Gaussian.
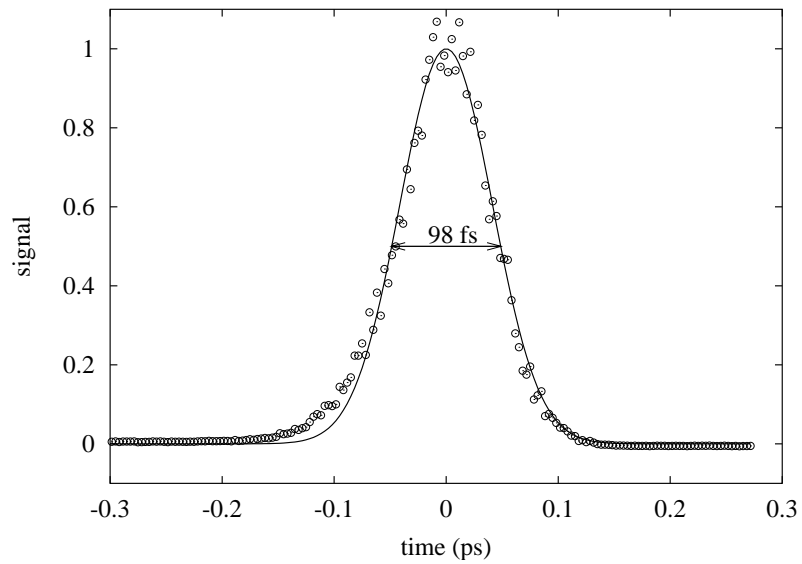

Figure 3.10: The cross correlation of the pump and gate pulse.

Cross correlation

While the autocorrelation of a pulse involves the interaction with itself, the cross correlation describes the interaction of two pulses a and b. Both are again considered to have a Gaussian line shape. The intensity cross correlation is the convolution of them. It is defined analogous to equation 3.10

$$
\begin{aligned}
C(t') &= \int_{-\infty}^{\infty} I_a(t) I_b(t - t') dt \\
&= c \cdot \exp\left\{ -\frac{t^2}{\sigma_a^2 + \sigma_b^2} \right\} = c \cdot \exp\left\{ -\frac{t^2}{\sigma_{cc}^2} \right\}, \quad\quad (3.14)
\end{aligned}
$$

with $c = \sqrt{\pi(\sigma_a^{-2} + \sigma_b^{-2})}$. If the duration of one transform-limited pulse is known the duration of the other pulse can be obtained from the width of the cross correlation.

Gate pulse

The setup was modified to measure the autocorrelation of the gate pulse. A beam splitter was inserted to split the gate pulse in two parts. While one beam was kept at fixed delay, the other beam passed the delay-stage. Both pulse were focused on the KDP crystal to undergo second harmonic generation (2/1300 nm = 1/650 nm). To detect this wavelength the grating inside the spectrograph had to be readjusted.

The autocorrelation was fitted with a Gaussian as shown in Figure 3.9. σ_{ACF} was found to be 70 fs and the duration of the gate pulse τ_{gate} 60 fs.

Pump pulse

The autocorrelation function of the pump pulse is centred at 198.5 nm and not measurable with our equipment. Hence, the pulse duration was determined from the cross correlation signal. It was measured without further changes of the setup. It is the upconverted pump pulse (397 nm+1300 nm=306 nm). Figure 3.10 shows the signal and the fit with a Gaussian. The width was determined to σ_{cc}=58 fs. To obtain the width of the pump equation 3.14 is used,

$$
\sigma_{pump} = \sqrt{\sigma_{cc}^2 - \sigma_{gate}^2} = 31 \text{ fs.} \quad\quad (3.15)
$$

And with the second term of equation 3.13 the pulse duration τ_{pump} results to be 50 fs.

3.3 Treatment of recorded spectra

3.3.1 Correction of dispersion

The index of refraction represents the ratio between the speed of light in vacuo and in medio. It is wavelength dependent, and it usually decreases with increasing wavelength. Consequently red light tends to be faster than blue light passing transparent components as cell windows, sample solution and the nonlinear crystal. This effect is called dispersion.

This effect can be measured and then corrected according to Kovalenko *et al* [9]. Focusing the pump pulse hard enough on the front window of the cell results in spectral broadening due to self phase modulation (cf. page 17) [18]. The blue pulse is turned into a white pulse covering the spectral range from ultraviolet to infrared. The white light continuum generation takes place instantaneously, e.g. 10^{-16}-10^{-15} seconds in the nonresonant case. Therefore one can consider that the undispersed, nascent white pulse has the same time duration as the parent pulse.

The exact wavelength dependence of dispersion due to all transmissive components of the setup can be measured by upconversion of the white pulse. As shown in Figure 3.11 different spectral components of the pulse are centered at different time delays due to dispersion. A correction curve is obtained by fitting Gaussians to the kinetic traces and assigning their centers to time zero. With this curve all measurements are time-corrected.

3.3.2 Correction of intensity fluctuations

Measured signal is the sum of dark current, background signal and upconverted signal. The dark current is constant and can be subtracted without further considerations. If the background signal was constant it could also be subtracted and the pure signal would be left. But the background fluctuates, therefore it has to be rescaled before subtraction.

The origin of the background is stationary fluorescence not absorbed by the filter BG3 and scattered by the grating inside the spectrograph. The spectral shape of the background is constant but its intensity is proportional to the intensity of the fluorescence. The intensity of the upconverted signal depends in the same way on the intensity of fluorescence (equation 2.44). Consequently the background and signal both have to be rescaled by the same value.

In Figure 3.12 two unprocessed spectra after subtraction of dark current are shown: one at negative delay and one at positive delay which shows the contribution of the upconverted signal around 380 nm. The region between
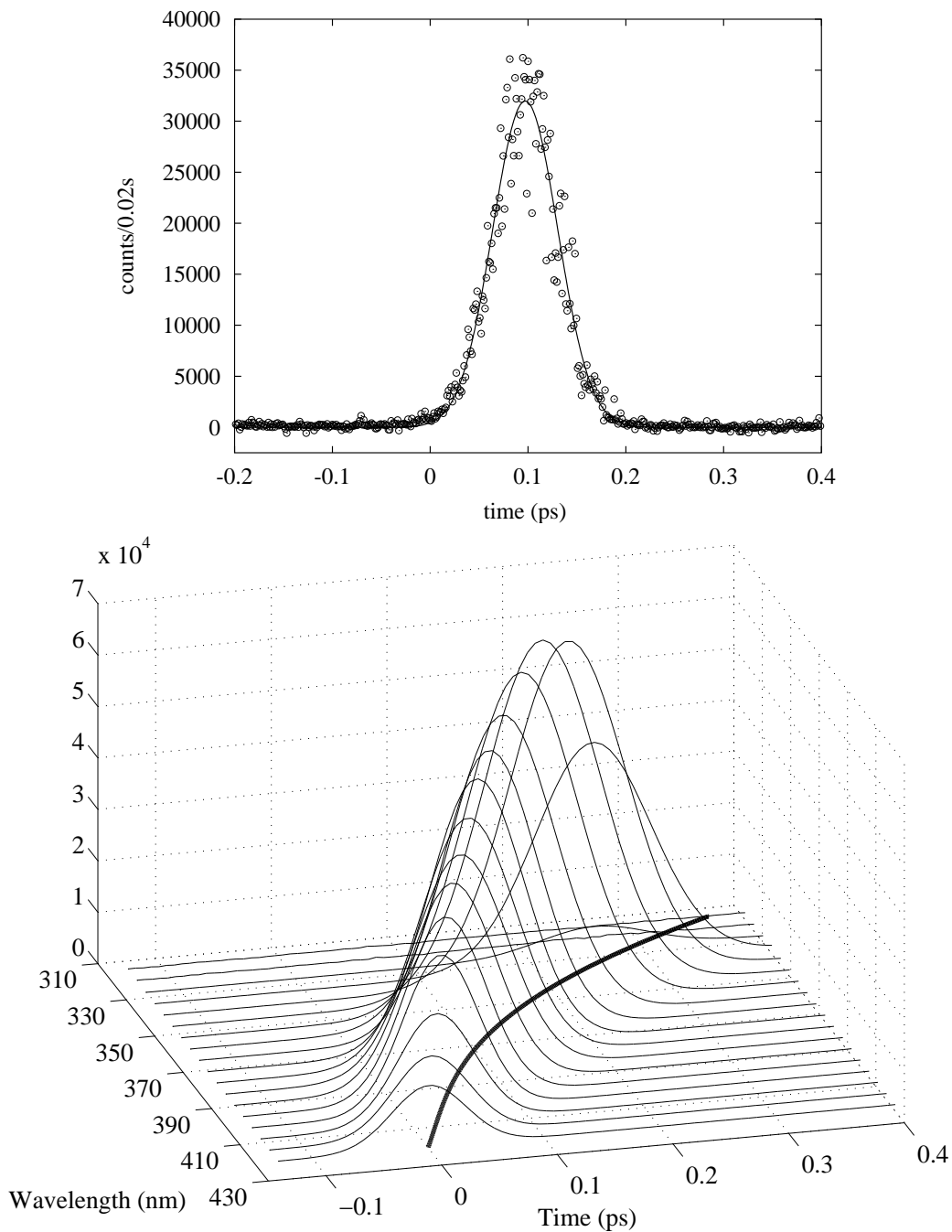
Figure 3.11: Top: Trace of the upconverted whitelight continuum at 400 nm (measurement and fit). Bottom: The full dispersive behaviour of the upconverted white light continuum. The curve on the wavelength/time-plane represents the maxima of different traces and is used for dispersion correction of the measurements.

43

225 and 300 nm shows no contribution of the signal because it is outside the spectral window for upconverted fluorescence. Therefore the sum over all counts in this region can be used for normalization of every measurement. The pure spectrum (Figure 3.12b) is obtained after subtraction of the smoothed background from the normalized signal.

Fluctuations of background signal, e.g. stationary fluorescence, are primarily due to fluctuations of the pump pulse, that we explain with instability of the pump source of the amplifier. Another source of noise are gas bubbles and density fluctuations inside the flow cell. A long time effect may be the generation of photoproducts on the cell window.

3.3.3 Fitting of the data

Spectral

To describe the evolution of the spectra in a compact way, each measured and time-corrected spectrum was fitted to the log-normal line shape function [30].

$$F(\tilde{\nu}) = h \left\{ \begin{array}{ll} \exp[-\ln(2)\{\ln(1+\alpha)/\gamma\}^2] & \alpha > -1 \\ 0 & \alpha \leq -1 \end{array} \right. \tag{3.16}$$

where

$$\alpha \equiv 2\gamma(\tilde{\nu} - \tilde{\nu}_p)\Gamma. \tag{3.17}$$

This asymmetric Gaussian can describe a structureless spectrum with four parameters only: the height h, the asymmetry parameter or skewness γ, the width parameter Γ and the peak frequency $\tilde{\nu}_p$. Of course all parameters depend on the delay time. From the temporal behaviour of $\tilde{\nu}_p$ the solvation correlation function is obtained. It is commonly used in [23, 61].

Kinetics

The true temporal behaviour of the spectra is not directly accessible. What is measured is assumed to be the true kinetics convoluted with an apparatus response function. The latter can be described with the pump/gate intensity cross correlation function. Therefore deconvolution of the measured kinetic traces from the cross-correlation function should result in the true kinetic traces. For time-resolved fluorescence the result should be a step-function multiplied by an exponential decay. The step-function $\Theta(t)$ is equal to zero at negative and equal to one at positive times. It is necessary to account for the fact there is no fluorescence before excitation of the sample at $t = t_0$.
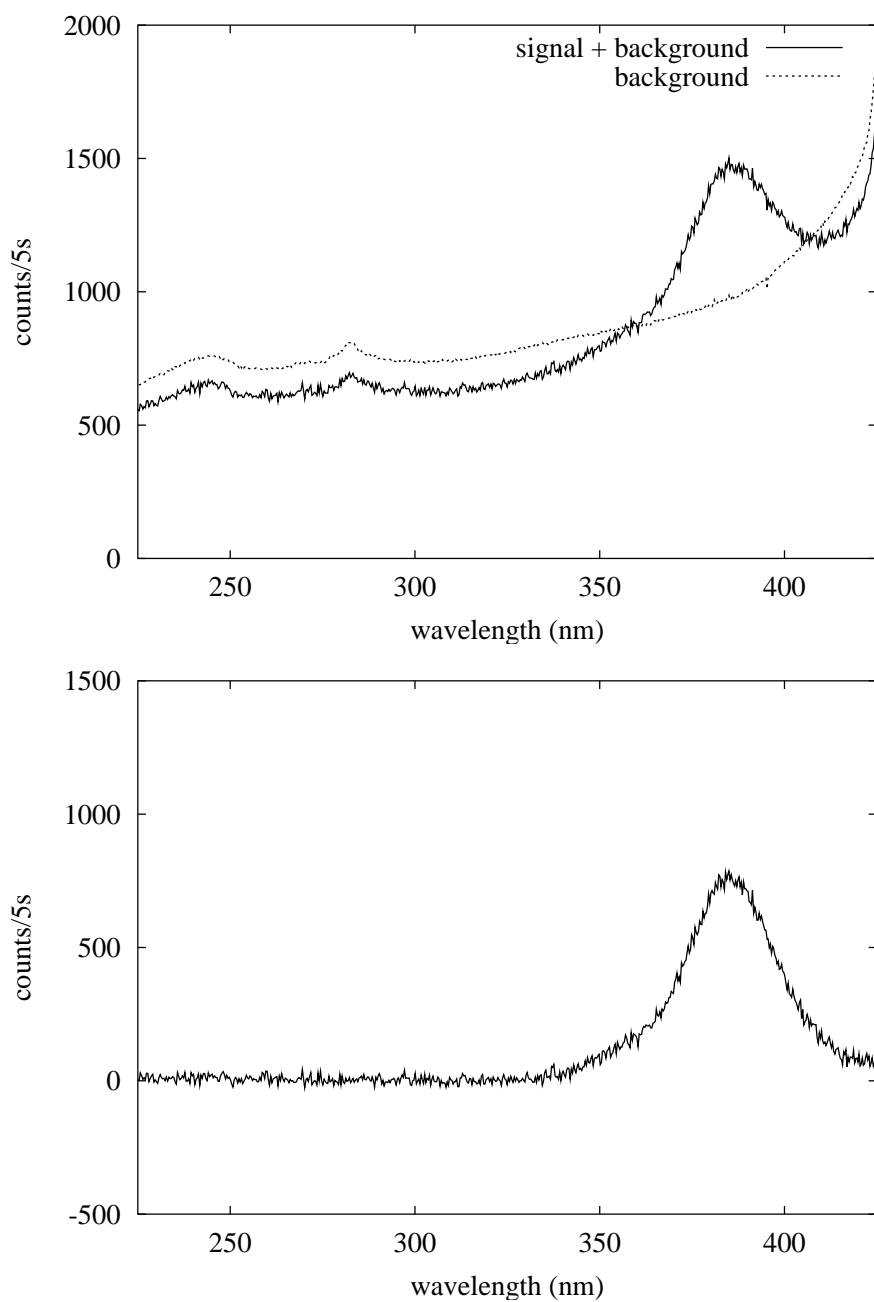
Figure 3.12: Background correction for DCS in acetonitrile (see section 4.2). The upper panel contains a measurement at negative delay (· · ·) and one at positive delay (—). The change of the background intensity is clearly visible. The lower panel shows the difference between the background and the normalized measurement: the upconverted fluorescence signal.

If one considers two functions $h(t)$ and $g(t)$ in the time domain and their Fourier transforms $H(f)$ and $G(f)$ in the frequency domain, then the convolution of $h(t)$ and $g(t)$ is equivalent to the product of their individual transforms (*convolution theorem*) [62]:

$$\int_{-\infty}^{\infty} g(t)h(t-t')dt \Longleftrightarrow G(f) \otimes H(f) \tag{3.18}$$

Therefore one deconvolution method utilizes the Fourier transforms of the measurement and the cross correlation function. Division of the measured kinetic trace by the cross correlation function in the frequency domain is equivalent to finding the true kinetic trace in the time domain. Now the algorithm for the transformation of discretely sampled data, Fast Fourier Transform (FFT), represents the transform as a sum of polynomials. But a step-function cannot be represented by a sum of polynomials well enough.

Another method of effective deconvolution is more time consuming but the representation problem of the step-function is avoided. Here the data are fitted to a sum of exponentials multiplied by the unit step-function $\theta(t)$ and convoluted analytically with a Gaussian. Now the fitting parameters can be applied to the analytically deconvoluted function to reconstruct the true kinetic traces.

The function describing the true kinetics is

$$f(t) = \theta(t) \cdot \sum_i n_i \cdot \exp\{-(t-t_0)/\tau_i\} + b \tag{3.19}$$

where $\theta(t)$ is the unit step-function, t_0 is time zero and b the background. Each exponential i is characterized by its weight n_i and decay-time τ_i. After convolution with the cross correlation function in equation 3.14 we have [63]

$$\int_{-\infty}^{\infty} f(t)C(t-t')\mathrm{d}t' =$$

$$\sum_i \frac{n_i}{2} \exp\left\{-\frac{t-t_0}{\tau_i}\right\} \exp\left\{\frac{\tau_{cc}}{2\tau_i}\right\}^2 \mathrm{erfc}\left\{\frac{t-t_0}{\tau_{cc}} - \frac{\tau_{cc}}{2\tau_i}\right\} + b \tag{3.20}$$

where τ_{cc} is the width parameter of the cross correlation function.

3.4 Steady state spectroscopy

The absorption spectra were recorded by a spectrophotometer (UV-3101PC, *Schimadzu*) at a resolution of 1 nm. Emission spectroscopy was performed

with a spectrofluorometer (Fluorolog 212, *Spex*). The photometric response of the fluorometer was calibrated with a secondary standard lamp (Optotronics). The spectrometers were wavelength-calibrated to $\pm$ 0.05 nm; all reported wavenumbers refer to measurements in air.

3.5   Chemicals

Coumarin 153 was obtained from Lambda Physik and used as received. 4-Dimethylamino-4'-cyanostilbene was synthesized at the chemistry department of the Humboldt Universität zu Berlin in the group of Professor Koert according to reference [64]. All solvents were obtained from Merck those used for the steady state and transient spectra were of spectroscopic grades *uvasol* (purity>99.9%) and *pro analysi* (purity>99.5%), respectively.

Chapter 4

Results and Discussion

4.1 Coumarin 153

First measurements with the broadband fluorescence upconversion setup were performed with coumarin 153 (C153) in acetonitrile. The spectral characteristics of this dye solution meet the requirements of the setup. The maximum of the absorption spectrum is close to the pump wavelength at 397 nm. The t_0-spectrum at 486 nm and the steady state fluorescence spectrum (t_∞) centered at 545 nm cover the spectral range of the setup. Most importantly, C153 has been already investigated extensively with the fluorescence upconversion technique (but in its conventional pointwise form) by Maroncelli and Fleming [23, 65]. Time-resolved transient absorption measurements were also performed and analyzed by Kovalenko [66]. A wealth of data is available for C153 and therefore it was chosen for testing and optimizing the present broadband setup.

C153 was investigated so extensively because it was considered an ideal molecule to probe polar solvation dynamics. It is usually assumed that its only change on optical excitation is a large change of the dipole moment. The dipole moment in the electronic ground state was determined to be 6.55 D [67] and 14.55 D in the first electronically excited state [68]. Grimme [69] showed with DFT/MR-SDCI calculations that the first excited state is well separated from the S_2 state, by 5650 cm^{-1}. According to this theoretical result the solvation dynamics of C153 can safely be discussed within a one-state model considering S_1 alone. Therefore a solvent dependence of the transition moment can be excluded [70] and the dynamic Stokes shift in acetonitrile can be ascribed to solvation dynamics alone. While in other 7-amino-coumarins electronical excitation is accompanied by geometrical changes of the amino group, in C153 they are reasonably suppressed because of the rigid juloli-
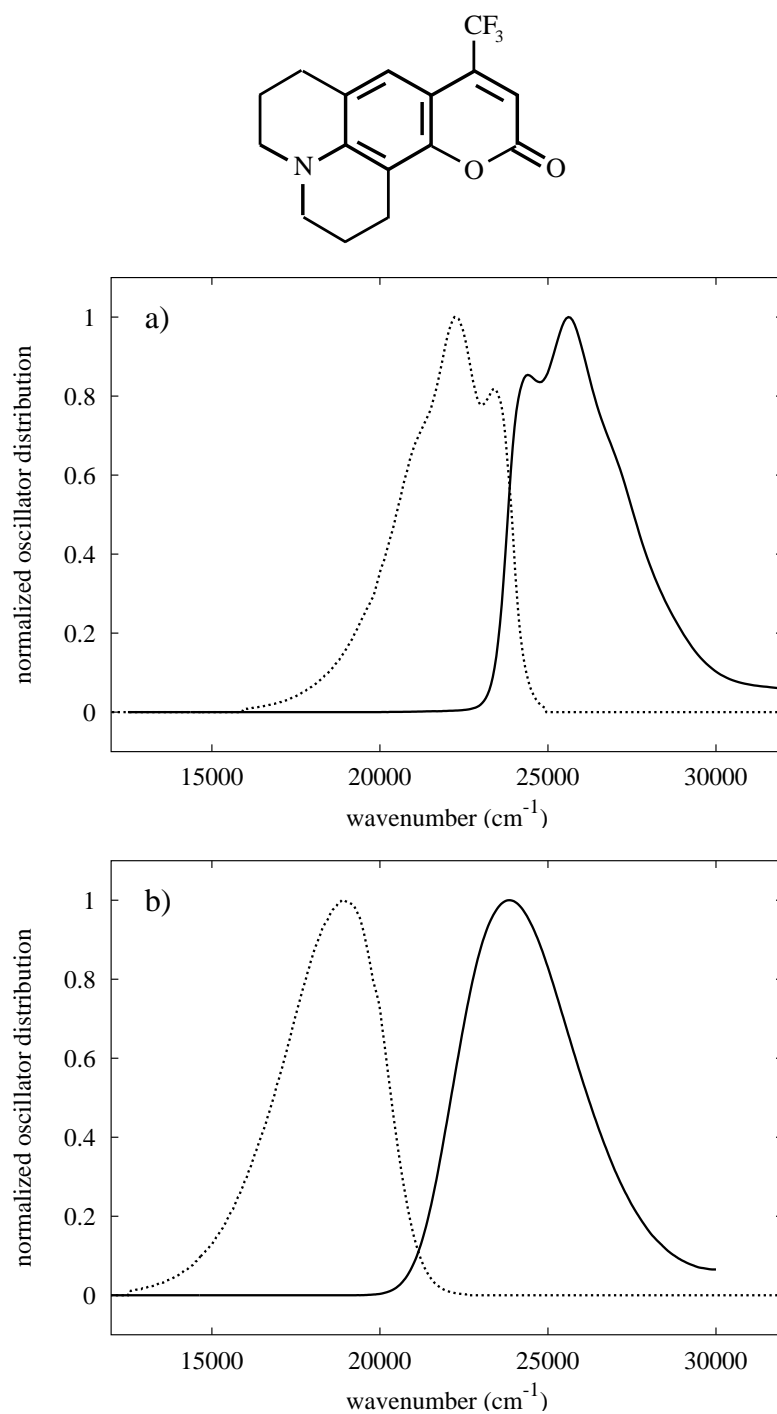
Figure 4.1: The dye molecule coumarin 153 with the rigidized amino-group. Normalized absorption (—) and emission (···) crossections in nonpolar 2-methylbutane (a) and in polar acetonitrile (b).

dine structure, i.e. the amino group is fixed with two propylene bridges to the phenyl moiety. Minor torsional rotation and planarization of the amino group are not expected to change the energy gap much [23, 69] although the shift of the band shape may be affected. Therefore the full dynamic Stokes shift may be assigned to solvation dynamics. Another important reason for the popularity of C153 are its absorption and emission properties. The maximum extinction coefficient in acetonitrile is ε_{max}=20000 mol^{-1}cm^{-1} [71], the fluorescence quantum yield ϕ_f=0.43 and the fluorescence lifetime is τ_f=5.6 ns [72].

4.1.1 Transient fluorescence measurements

The time-corrected and smoothed transient fluorescence spectra of C153 in acetonitrile at different time delays are shown in the top panel of Figure 4.2. Note, that the upconverted fluorescence signal is plotted against the original fluorescence wavelength. No transmission corrections are made at this stage. The data were fitted with log-normal functions to obtain the temporal behaviour of the peak of the band. The fitted functions for every time delay are shown in the lower panel. The purpose of the following subsection is to compare with known limiting spectra, and to gain insight into transmission function for our setup in this way.

4.1.2 Spectra at t_0 and at t_∞

The top panel of Figure 4.3 shows the upconverted emission spectrum at time-zero and its log-normal fit. The peak frequency is centered at $\tilde{\nu}_0$=20390 cm^{-1} and the spectrum has a width of Γ_0=3530 cm^{-1}. The blue edge of the earliest spectrum shown here is close to the absorption edge of the filter at 435 nm, hence we can assume that the blue side of our time-zero spectrum reaches further in the blue and cannot be measusred with our setup. Despite of this we find good agreement with Maroncelli in respect to both peak frequency already reported in [23] at $\tilde{\nu}_0$= 20580 cm^{-1} and band width Γ=3640 cm^{-1}.

Next we compare the spectrum at t_∞ with the steady state emission spectrum in Figure 4.3b. Also here the peak frequencies coincide at $\tilde{\nu}_\infty$=18800 cm^{-1}. The deviation on the red side between the two curves reflects the spectral response of the registration system, which includes crystal, filters, grating and CCD-chip. The quotient of the steady state emission and the measurement at t_∞ is caused by the effective transmission characteristics of our setup. Therefore it can be used to correct the measurements at smaller delay times.
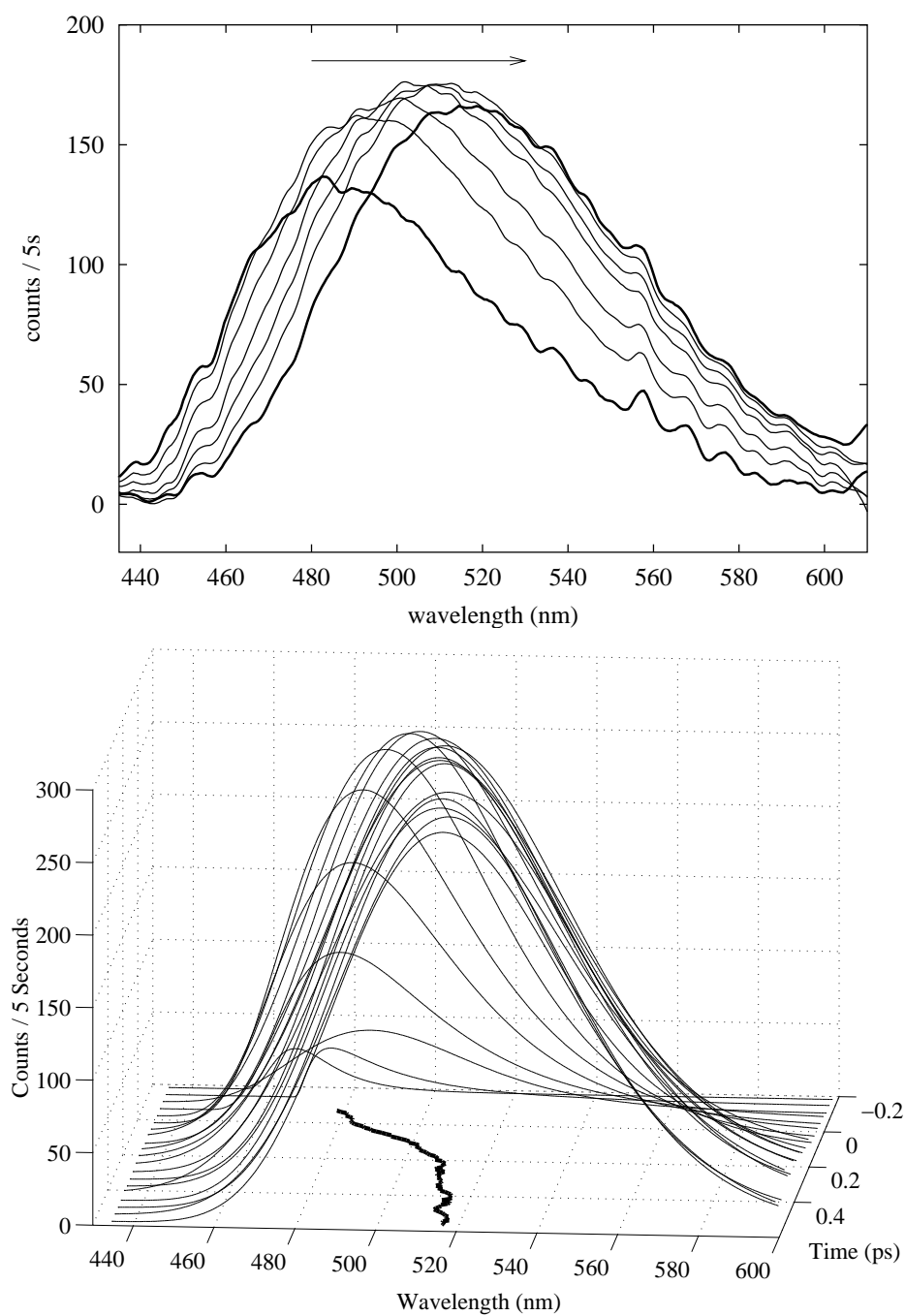
Figure 4.2: The upper panel shows transient fluorescence spectra of C153 in acetonitrile at 0, 60, 120, 200, 300, 500 and 1000 fs delay. The lower panel shows log-normal fits of the spectra. The temporal behaviour of the peak-wavelength $\lambda(t)$ is projected into the wavelength-time plane.
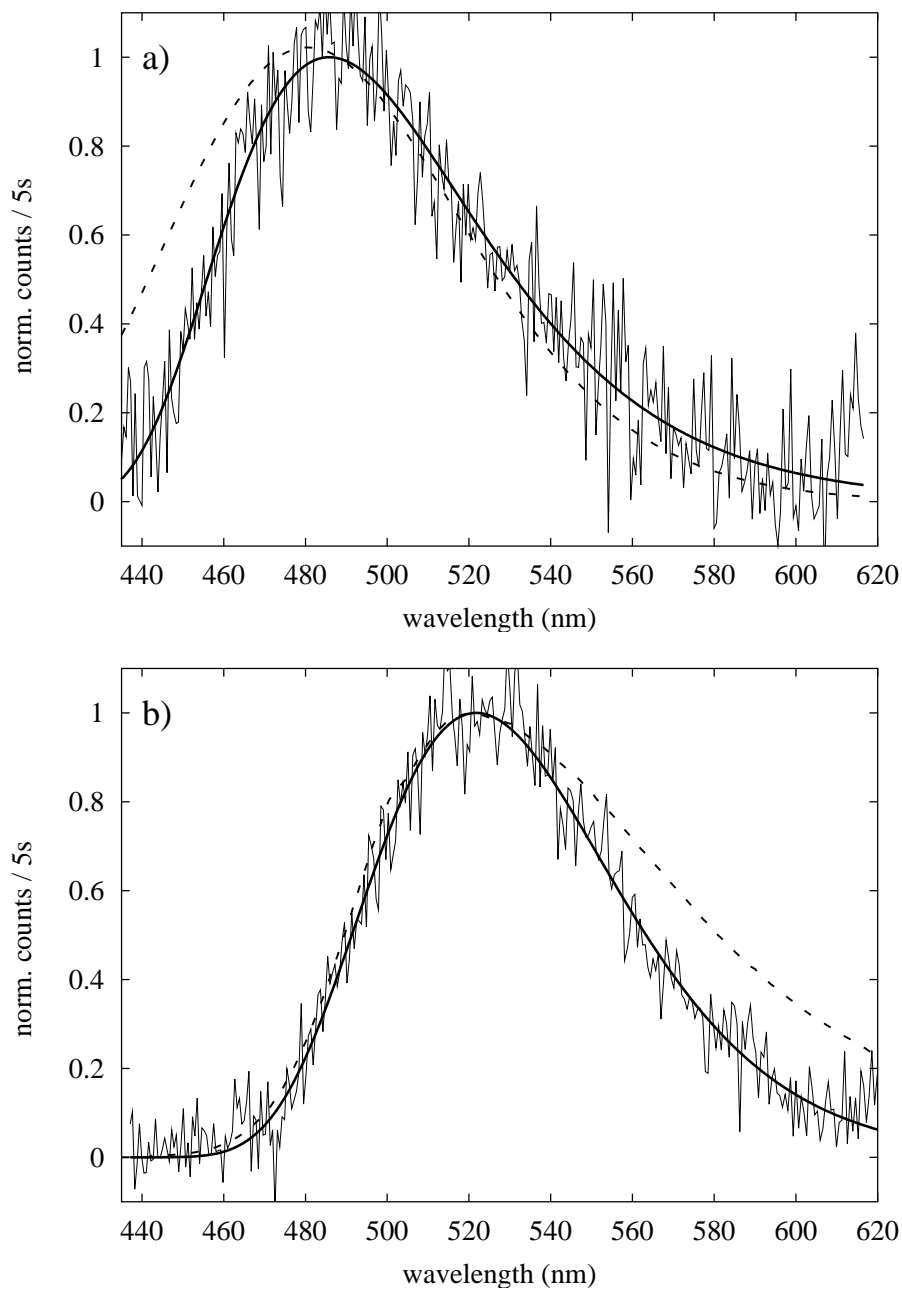
51

Figure 4.3: a) Spectrum for C153 in acetonitrile at delay t=0 as constructed from measured spectra by time correction (thin solid line) and the log-normal fit (thick solid line). The dashed line is the time-zero spectrum as reported in [23] (dotted line) for comparison with our measurement. b) The measured spectrum at t_∞ and the steady state fluorescence (dashed line).

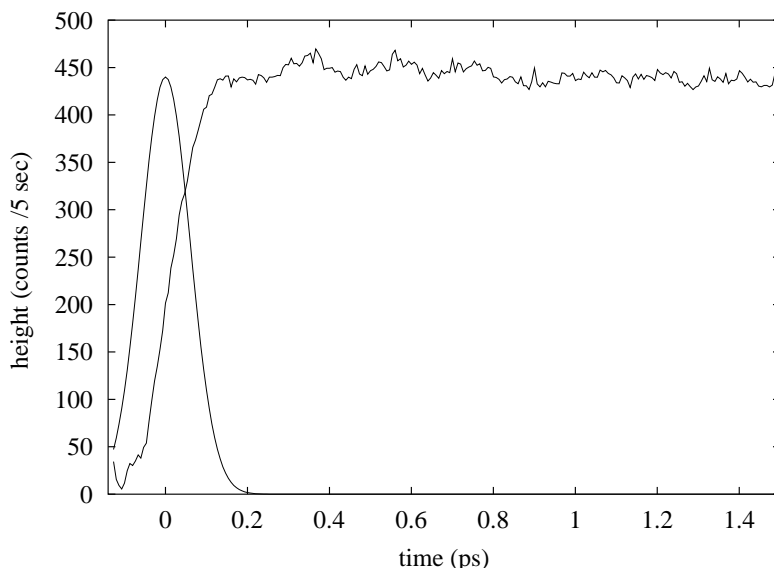### 4.1.3   Dynamics of solvation and cooling

Figure 4.4: The height $h(t)$ obtained from log-normal fits. At time-zero a Gaussian is displayed with σ=50 fs, representing the apparent function.

All spectra were multiplied by the correction quotient, converted into transition probabilities and subsequently fitted with log-normal shapes (see eq 3.16). First we look at the time dependent amplitude $h(t)$ in Figure 4.4. The rise can be compared with a step-function that is convoluted with a Gaussian of σ=50 fs, i.e. the full width at half maximum of the Gaussian is 120 fs. The pulsewidth obtained in this way is in good agreement with the autocorrelation measurement.

Solvation dynamics

Next we determine the solvation correlation function $S(t)$ from the temporal shift of the peak frequency $\tilde{\nu}(t)$ as obtained by log-normal fitting of the spectra in transition probability representation. We compare it to the theoretical function for acetonitrile assuming pure, dipolar solvation and simple continuum theory (see Fig 2.6 on page 20) [61]. In Figure 4.3 the experimental and the theoretical function are represented as solid and dashed lines, respectively. The comparison reveals a slower decay of the experimental curve due to the limited time resolution of the setup. For better comparison the exper-
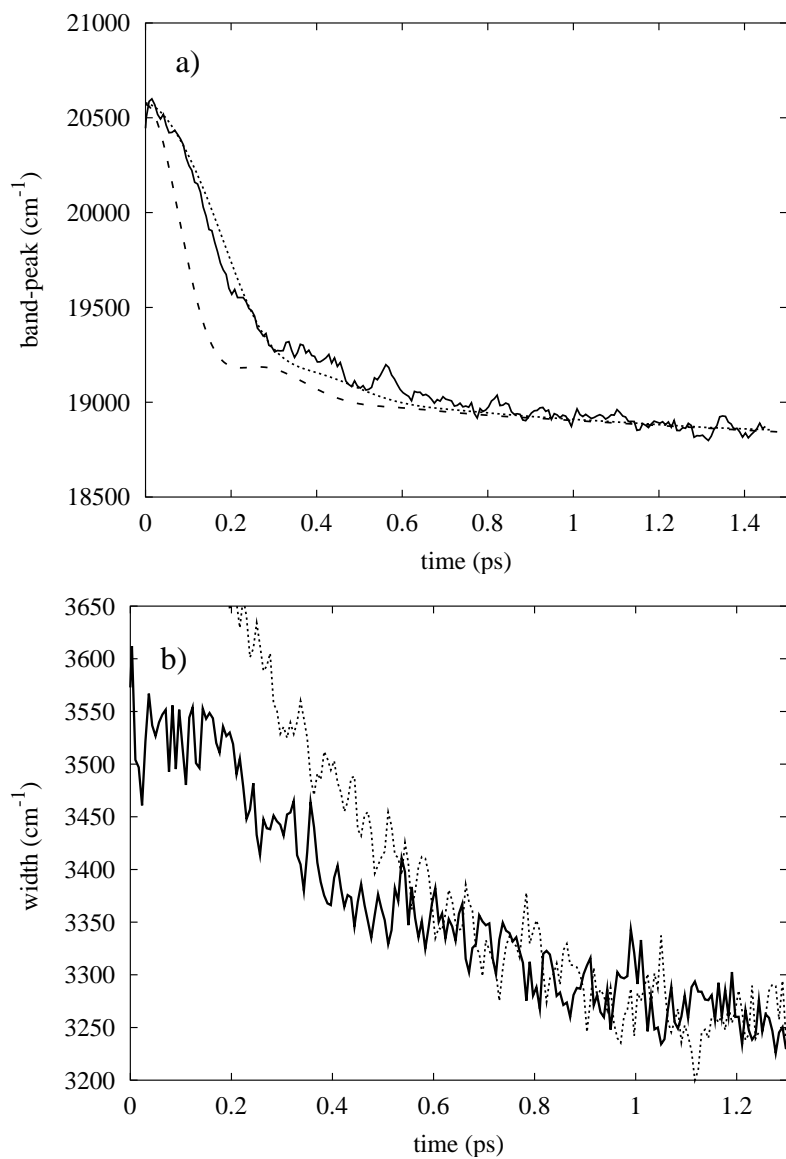
Figure 4.5: a) The temporal evolution of the peak frequency $\tilde{\nu}$ (—), of C153 in acetonitrile. On a short time scale one observes solvation dynamics. For better comparison the theoretical solvation function [61] (- - -) was broadened (···) by recalculation for $\sigma=50$ fs (see text). b) The temporal evolution of the width (—) converges after 500 fs with the slow componenet of the dynamic Stokes shift (···, shifted). We conclude that the band moves out of the spectral window; this then gives the impression a narrowing.

imental data should be deconvoluted from the pulse as described in section 3.3.3, but the signal-to-noise ratio is too low for this treatment. Instead we simulate the time-resolved emission measurement numerically taking the experimental time-resolution into account: we create a matrix, wavenumber versus time, where a band represented by a Gaussian moves in time according to the theoretical solvation correlation function from $\tilde{\nu}_0$ to $\tilde{\nu}_\infty$. The resulting kinetic traces for all wavenumbers are convoluted with the cross correlation function (eq 3.14) which is assumed to be a Gaussian of the width σ_{cc}=50 fs. From this matrix the 'broadened' solvation correlation function is then obtained by log-normal fitting. Now we find the simulated curve matching the experimental one, even the oscillation around t=400 fs may be noticed.

Another parameter obtained by log-normal fitting is the width $\Gamma(t)$ (cf. page 44). It was pointed out in section 2.2.2 that the relation between the evolution of the width and solvation dynamics as reflected by shift of the band peak is still under discussion. In Figure 4.5b both evolutions can be compared. The width is decreasing from 3550 cm^{-1} to 3250 cm^{-1}. The early evolution of width is not affected significantly by the fast component of solvation dynamics. But after 500 fs narrowing occurs exactly as the band shifts to the red. This behaviour suggests that after 500 fs the band narrows because the band shifts out of the spectral region that can be observed with the setup. Apart from this systematic error we find no correlation between narrowing and solvation therefore we conclude that our results are in accordance with the nonlinear response theory.

Cooling dynamics

After solvation dynamics is completed at 1 ps the width of the band reaches its maximum and starts thereafter to narrow exponentially with a time constant of 7.3 ps as shown in Figure 4.6b. This narrowing is commonly interpreted as vibrational thermalization independent of the solvent [32, 31, 73].

On a longer time-scale one observes the peak frequency $\tilde{\nu}(t)$ reaching its minimum $\tilde{\nu}_{min}$ and then shifting back to $\tilde{\nu}_\infty$ (see Figure 4.6a). The latter blue shift has already been observed in the case of C153 in cyclohexane after excitation with excess of vibrational energy of 3500 cm^{-1} [23]. We assign this blue-shift to cooling dynamics in the frame of the following model: after excitation the solute undergoes intramolecular vibrational redistribution thereby and establishes an initial temperature T_{ex}. The solvent environment has an ambient temperature T_a. It can be assumed that an intermolecular heat transfer takes place from the hot probe molecule to a first solvent shell. In a second step heat will flow from the shell to the bulk of solvent what results in cooling of the probe molecule. The blue-shift of 280 cm^{-1} occurs

exponentially with a time constant of 12 ps. This is the characteristic time for heat transport from the first solvent shell to the bulk solvent in acetonitrile [74].

What is the reason for this temperature dependent blue-shift? Fluorescence measurements of C153 in a supersonic jet showed that increasing excess energy changes the Franck-Condon factors of vibronic transitions. The central member (0-1) of the dominating high frequency mode acquires additional oscillator strength while the first member (0-0) decreases. This change of band-shape with increasing (decreasing) temperatures appears as a red (blue) shift of the emission band [69]. This experimental result may be explained with the anharmonicity of the effective vibronic coordinate [75]. Because anharmonicity causes a temperature dependence of the Franck-Condon pattern that affects all parameters of the band shape: position, width and skewness.

4.1.4 Conclusions

To summarize: With measurements of a well-known dye, C153, we demonstrated that the broadband fluorescence upconversion setup gives identical results (where these are known) to conventional point-by-point measurements. The spectral region between the blue filter edge at 435 nm and 600 nm on the red side can be observed in a single pump-gate scan. The temporal resolution is good enough to observe all features of solvation dynamics, although not good enough - at the moment - to reproduce the detailed results obtained with the pump super-continuum probe technique.
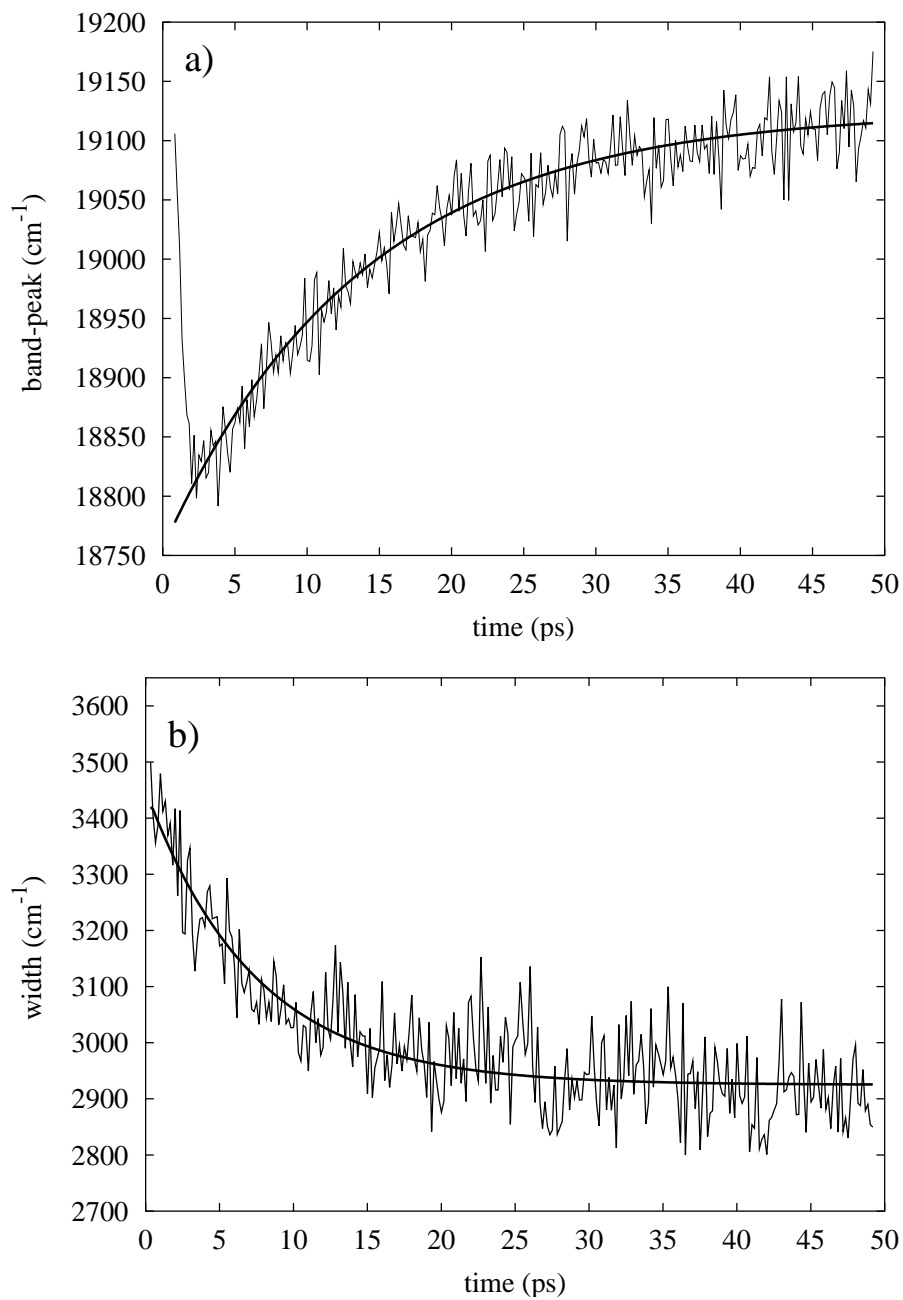
Figure 4.6: a) After 2.5 ps cooling dynamics is observed. The peak frequency shifts 280 cm^{-1} to the blue. It can be described as an exponential decay with a time constant of 12 ps which is characteristic for acetonitrile. b) The width narrows from 3500 to 2800 cm^{-1} exponentially with a time constant of 7.3 ps.

57

4.2 4-Dimethylamino-4'-cyano-stilbene

Steady state spectra

The dye 4-dimethylamino-4'-cyano-stilbene (DCS, Figure 4.7, top) is a donor-acceptor stilbene. This class of molecules was extensively used for the spectroscopical investigation of charge transfer reactions in solution [64, 76]. In DCS the dimethylanilino moiety serves as electron-donor and the benzonitrilo moiety as acceptor. The intramolecular charge transfer reaction causes an increase of the dipole moment from 7 D in the ground state to 22 D in the excited state. This large change is reflected in a solvatochromic shift of the order of 3900 cm^{-1} going from nonpolar cyclohexane to polar acetonitrile. The maximum molar extinction coefficient in n-pentane is ε_{max}=39000 mol^{-1}cm^{-1}. The fluorescence quantum yield at room-temperature in acetonitrile was found to be Φ_f=0.13 and the fluorescence lifetime is 580 ps [77].

Figure 4.7 depicts the steady state spectra of DCS in nonpolar cyclohexane and in polar acetonitrile. In cyclohexane the absorption spectrum is basically structureless and peaked at 26100 cm^{-1} while the fluorescence spectrum shows three vibronic lines and is centered at 22600 cm^{-1}. In the polar solvent acetonitrile none of the spectra is structured. The change of the solvent does not affect the position of the absorption band significantly. The fluorescence spectrum is centered at 18800 cm^{-1} [77]. A comparison of these spectra gives a rough estimate of what can be expected for a measurement of transient emission spectra in acetonitrile. The time-zero spectrum should appear roughly at the position of the fluorescence spectrum in the nonpolar solvent. This is near the blue edge of the spectral window of our setup at 435 nm, i.e. it should be possible to observe the peak but not the full width of the signal. The more elaborated time-zero analysis (see page 17) predicts an initial spectrum that can be described by the log-normal parameters $\tilde{\nu}_0$=21800 cm^{-1}, Γ_0=4680 cm^{-1}, and γ_0=-0.16. After appearance of the time-zero spectrum the emission band should shift to the position of the steady state spectrum in acetonitrile at $\tilde{\nu}(\infty)$=18800 cm^{-1} (532 nm). Hence, it should be possible to measure the complete spectral evolution of DCS in acetonitrile with femtosecond time-resolution.

Transient Spectra

Measurements of transient fluorescence spectra of DCS in acetonitrile were already reported by different scientific groups:

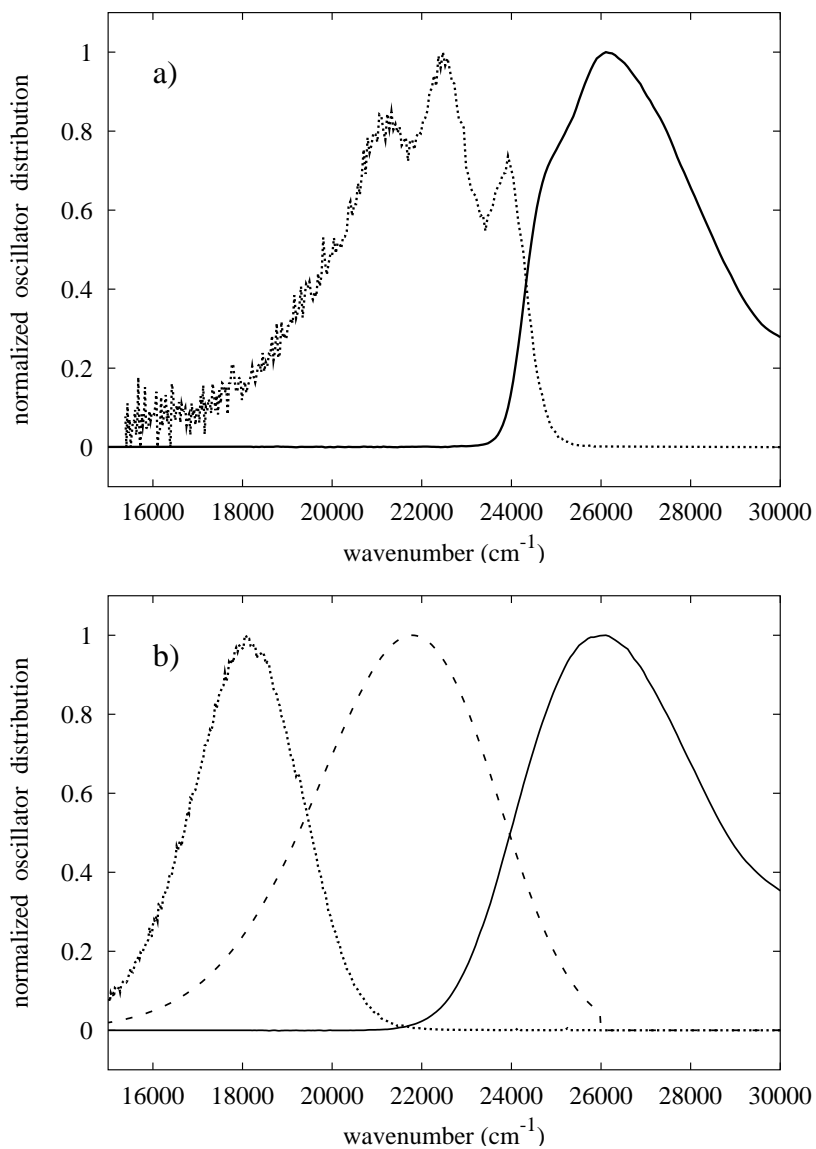- Zachariasse and coworkers [64] measured transient fluorescence of DCS

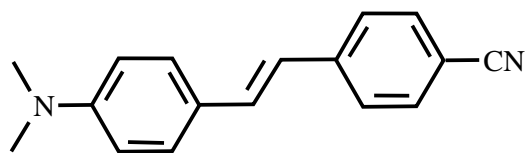**Figure 4.7:** The dye 4-Dimethyl-4'-cyano-stilbene (DCS, top). Absorption (—) and emission (· · ·) spectra of DCS in cyclohexane (a) and in acetonitrile (b). The lowest panel also includes the hypothetical emission spectrum at time-zero (- - -).

in acetonitrile at 233 K with a time-resolution of 5 ps. They observed monoexponential decay with a time constant of 1.85 ns. Solvatochromic measurements were carried out in order to investigate the dipole moments in the Franck-Condon excited state (FC) and the equilibrated S_1 (CT) state. The maxima $\tilde{\nu}$ of absorption and fluorescence bands in different solvents were plotted against solvent polarity expressed as $(\varepsilon\text{-}1)/(2\varepsilon+1)$ - $(n^2\text{-}1)/(2n^2+1)$. The resulting solvatochromic slope is related to the dipole moments by $\tilde{\nu}_{\text{abs}} \propto \mu_0 \cdot (\mu_{\text{FC}} - \mu_0)$ and $\tilde{\nu}_{\text{flu}} \propto \mu_{\text{CT}} \cdot (\mu_{\text{CT}} - \mu_{\text{FC}})$. The resulting dipole moments suggest the following model for the excited state evolution of DCS: excitation from the ground state (μ_0=7 D) to the Franck-Condon excited state (μ_{FC}=13 D) is followed by relaxation to the equilibrated charge transfer state (μ_{CT}=21 D). The authors could not observe dual fluorescence and concluded that state-to-state relaxation FC→CT takes place on a time scale clearly shorter than 5 ps, or that the increase in dipole moment already occurs during light absorption.

- Eilers-König *et. al.* measured emission of DCS in acetonitrile with fluorescence upconversion at different wavelengths in order to investigate the spectral evolution with time resolution better than 200 fs [76]. They have observed two bands: the first band establishes immediately after excitation at 20000 cm^{-1} and decays after 150 fs while at the same time a second band is rising at 18500 cm^{-1}. In between they noted an isosbestic point at 19200 cm^{-1}. The authors assigned the first band to a locally excited Franck-Condon-state ($S_{1,FC}$) and the second band to a charge-transfer state ($S_{1,CT}$). This reasonable interpretation is in agreement with the model elaborated by Zachariasse.

- Rulliere and coworkers also measured the transient emission in acetonitrile after excitation with pulses centred at 300 nm [78, 79]. Their time-resolution of 15 ps did not allow to observe the emission around time-zero; nevertheless an interesting observation was made. There is a square dependence of peak position and band-shape on both concentration and excitation-power indicating a two photon process. The authors proposed the existence of an excited state dimer called 'bicimer'. This bicimer was determined to emit at $\tilde{\nu}$=18600 cm^{-1} – a little red shifted compared to the single-molecule species at $\tilde{\nu}$=19000 cm^{-1} with a fluorescence life time of 170 ps.
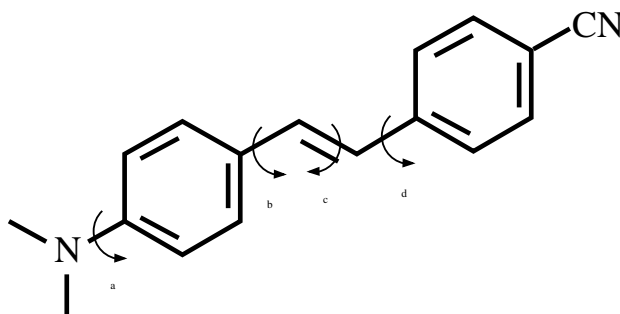
Figure 4.8: The excited DCS has four rotational degrees of freedom.

Considerations of intramolecular twisting

DCS has four bonds around which rotation could take place upon excitation in the S_1 state and which could influence its transient spectral behaviour (Fig 4.8). Until now only the existence of cis/trans-isomerisation is proven. Zachariasse determined the time constant for this process to be 0.7 ns [80]; therefore it should not affect measurements on a femtosecond time scale[1]. A twist of the dimethylamino-group as in dimethylamino-benzonitrile was excluded by Görner who compared the absorption and emission spectra of DCS to those of a derivative with the amino-group incorporated in a stiff dihydroindole ring and found no significant difference [77]. Suitable model compounds for DCS in which only the twist of the benzonitrilo moiety is locked are not reported so far. But quantum mechanical calculations show a rise of the potential energy surface towards the torsional coordinate that allows to exclude the twist of the benzonitrilo moiety in the S_1 state [81, 82].

It is reasonable to consider the existence of a twist of the anilino moiety. Rulliere and Rettig have investigated DCS and rigidized derivatives at 200 K in solution [83]. They measured fluorescence spectra of DCS-B24 in several solvents. In this molecule the single bonds between the benzonitrilo and dimethylanilino moieties to the ethylenic group were locked. The authors observed a dramatic decrease of the fluorescence quantum yield. Their conclusion was that excitation of DCS must be followed by a rotation of the dimethylanilino group leading to a twisted intramolecular charge transfer complex (TICT) [84]. On the other hand in jet-cooled spectra a difference between DCS and DCS-B24 became evident: the barrier for cis/trans-isomerisation is decreased from 790 cm^{-1} to 50 cm^{-1}, respectively. Therefore - at least in the gas phase - DCS-B24 is not a suitable model compound for

---

[1]Over several measurements the concentration of the cis-isomere decreases.

DCS [85]. The discussion whether TICT occurs in DCS or not should be considered still unresolved.

4.2.1 Transient measurements

Fluorescence

Transient fluorescence measurements of DCS in acetonitrile were performed. The measured spectra were corrected for dispersion and shifted by the gating frequency. The excitation energy was kept at 1 μJ. At first, using high concentrations ($1.8 \cdot 10^{-3}$ M) dual emission was observed as reported by Eilers-König [76]: a first band appears around 470 nm until after 200 fs it vanishes while simultaneously a second band is rising centred at 540 nm (Fig 4.9a). Then the concentration was decreased in two steps. The amplitudes of both bands vanished as the concentration of the sample was decreased to $2.2 \cdot 10^{-4}$ M (Fig 4.9b). At a concentration as low as $1.1 \cdot 10^{-4}$ M the dual behaviour completely disappeared (Fig 4.9c), and instead, only a single band is observed rising around 470 nm and shifting during the first picosecond to 540 nm. In a another series of measurements the excitation energy was decreased from 1 to 0.2 μJ resulting also in a decrease of the dual emission behaviour (Fig 4.10). A dependence of the emission of DCS on the concentration and excitation energy was already reported by Rulliere and co-workers. They explained these dependences with an intermolecular process, the formation of a dimer [64].

In transient absorption spectra (Fig 4.12) as well as in semi-empirical calculations (Tab. 4.1, p. 71) we noted a strong absorption band from the S_1 to a higher excited state exactly in the spectral region where the dip appears at high concentration and excitation energy. Therefore we considered transient excited state reabsorption to be the true origin of the dependence on concentration and excitation energies. This encouraged us to make additional measurements to prove our hypothesis. The concentration and the excitation energy were kept constant at $4.4 \cdot 10^{-4}$ M and 1 μJ, respectively, and instead the thickness of the sample was decreased. The thickness was then determined from absorption spectra of the sample cell measured with a commercial spectrophotometer (cf. section 3.4) and appropriate application of the Lambert-Beer law (cf. eq 2.17). The spectra of transient emission at different time delays are depicted in Figure 4.11. By decreasing the thickness of the cell from 0.6 mm, over 0.35 mm to finally 0.05 mm the dual emission behaviour is diminished. This observation allows us to exclude any kind of intermolecular interaction as origin of the strong spectral sensitivity of DCS in respect to concentration and excitation energy. The discussion will be
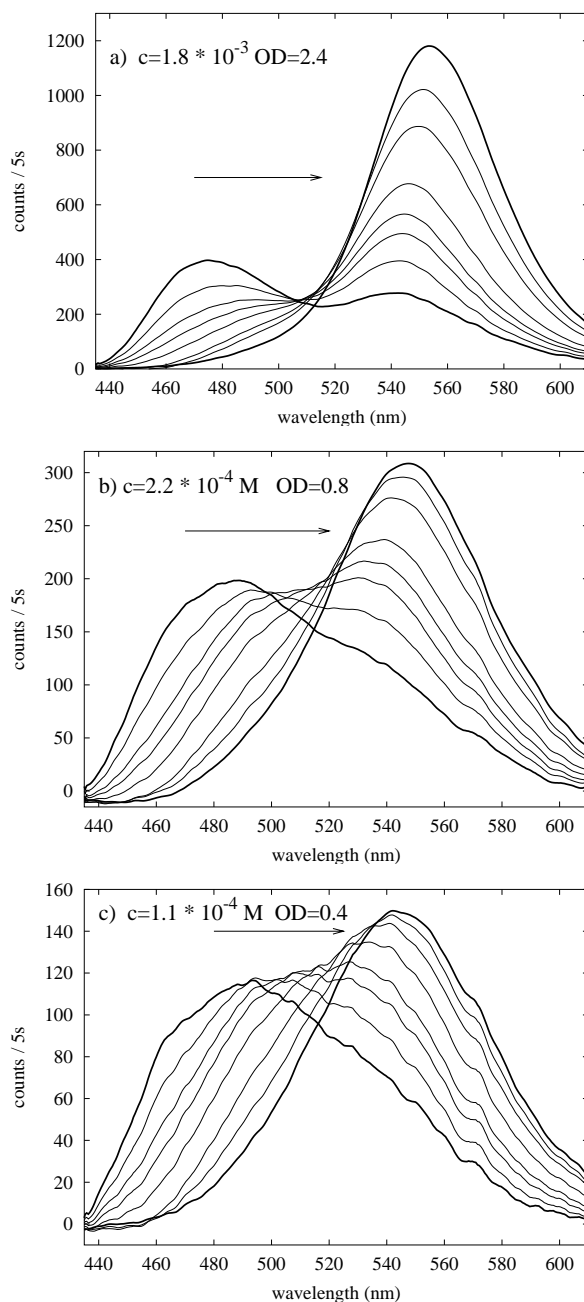
Figure 4.9: Time-resolved fluorescence measurements of DCS in acetonitrile at different time delays (t = 80, 120, 160, 200, 300, 600 fs, 1, 5 ps) shifting from the blue to the red. The dual emission behaviour vanishes as the *concentration* is decreased. The pulse excitation energy and the cell thickness were kept constant at 1 μJ and 0.6 mm, respectively.

Figure 4.10: Time-resolved emission of DCS at different time delays (t = 80, 120, 160, 200, 300, 500 fs, 1, 5 ps) shifting from the blue to the red. Here decrease of the *excitation energy* leads changes in the spectral behaviour. In both panels the optical density is 1.5, the concentration $4.4 \cdot 10^{-4}$ M and the thickness of the cell 0.6 mm.
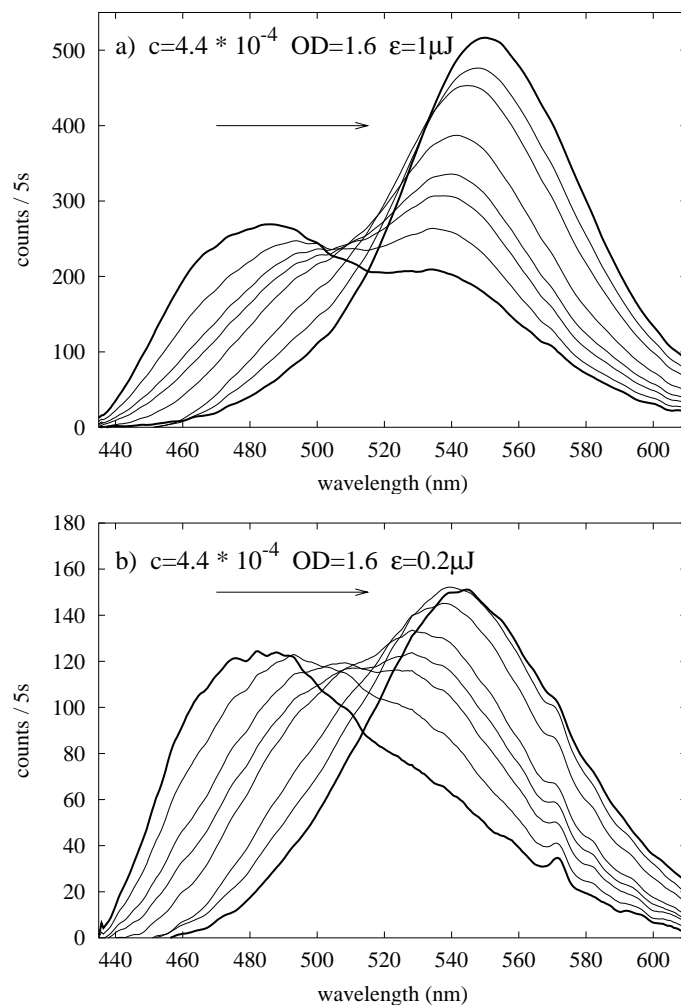
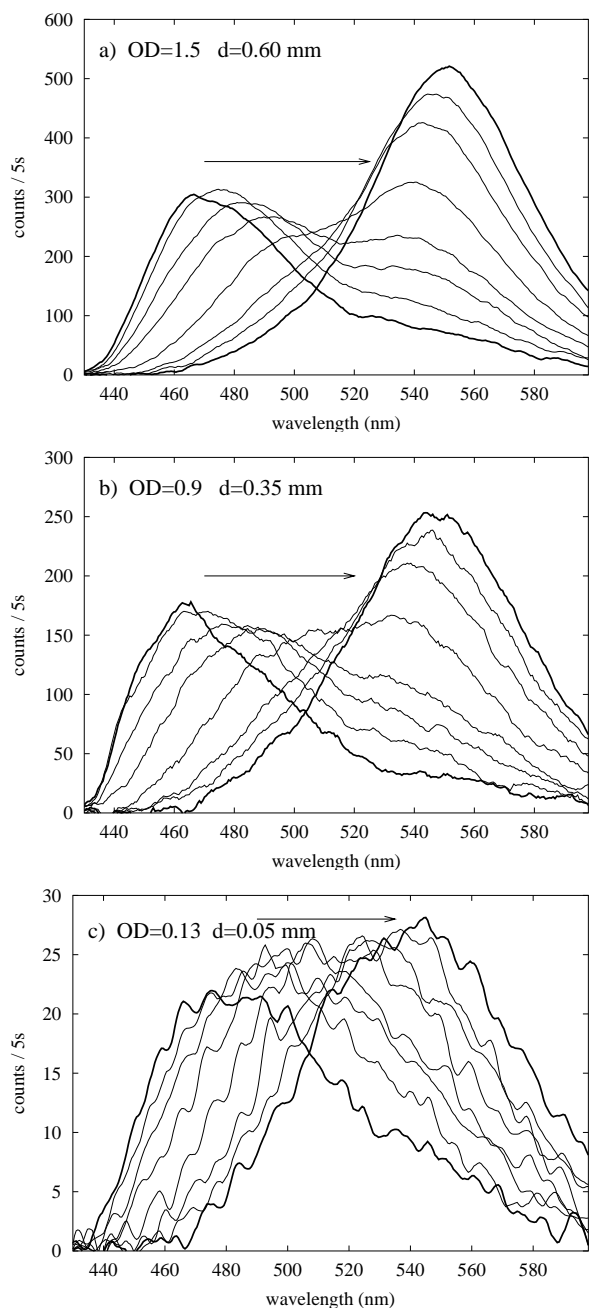**Figure 4.11:** Time-resolved emission of DCS at different time delays(t = 80, 120, 160, 200, 300, 500 fs, 1, 5 ps) shifting from the blue to the red. In contrast to Fig 4.9 here the *cell thickness* is decreased. Optical densities at the absorption peak and cell thicknesses are indicated. The pulse excitation energy was 1 μJ and the concentration $4.4 \cdot 10^{-4}$ M.

continued after a brief analysis of transient absorption spectra in the next subsection.
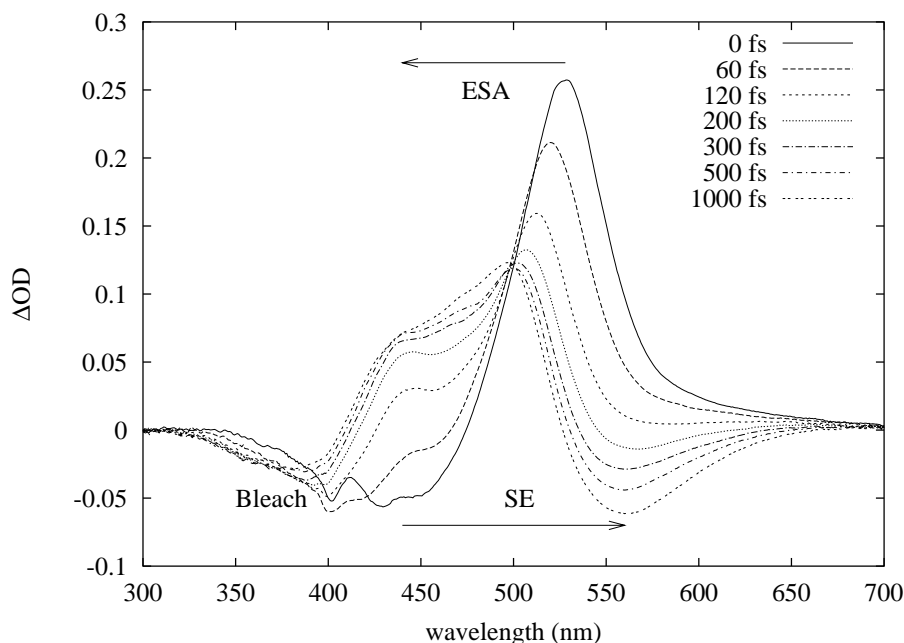

Figure 4.12: Transient absorption measurements on DCS in acetonitrile are dominated by a strong excited state absorption band (ESA) shifting to the blue and establishing after 200 fs around 500 nm; where the dip in transient fluorescence measurements (see Figures 4.9a, 4.10a, and 4.11a appears.

Absorption

A reasonable interpretation of the dependence on cell thickness, laser intensity and concentration is difficult without analysis of transient absorption spectra which were measured by Kovalenko [45]. The setup is described in detail in reference [9]. The sample solution in the cell had an optical density of 0.6. The excitation wavelength and the pump energy were 397 nm and 0.2 μJ, respectively. The transient spectra shown in Figure 4.12 are dispersion corrected. Negative ΔOD corresponds to bleach and stimulated emission (SE), positive ΔOD corresponds to excited state absorption (ESA).

Around time-zero the bleach is not completely established at 380 nm and SE is visible at 430 nm overlapping with a strong ESA band at 530 nm. During the first 200 fs the SE disappears at 430 nm and reappears at 550

nm. Synchronously the ESA band shifts to the blue and establishes two peaks at 400 and 520 nm. After 1 ps the spectral evolution is complete.

If the measurements of transient absorption are compared to those of transient emission it may be noted that the strong ESA band is placed in the spectral region where the dip separates the two emission bands in the emission spectra in Figures 4.9a, 4.10a and 4.11a. It is consistent with our observations that this dip scales with concentration, excitation energy and path length to assign it to excited state re-absorption. In this case the true governing parameter is the number of excited dye molecules that reabsorb the fluorescence light in the spectral region around 500 nm. This then gives the impression of two emission bands. The latter may therefore be assessed as an artifact which appears at high optical density. There is not dual fluorescence.

4.2.2 Spectra at t_0 and at t_∞

The following analysis is limited to the samples of low optical density. Figure 4.13a depicts the experimental and theoretical spectra at zero delay. While on the red side they match, the hypothetical spectrum obtained from time zero analysis (cf. p.24) reaches further into the blue than the one obtained by experiment. After multiplication of the hypothetical spectrum by the transmission of the filter GG435 we find good agreement with the experimental spectrum. The full spectrum at zero delay can not be observed with our setup. This raises the question whether the observed maximum at 442 nm is due to the nature of the early emission band or of the filter. In agreement with earlier discussion of steady state spectra (see page 58) we assume that we are able to determine the peak frequency of the emission band around zero delay directly from our measurements. In Figure 4.13b the upconverted and spectrally corrected signal at time infinity is shown. Comparison with the steady state fluorescence shows good agreement, except for a slight deviation in the region around 480 nm. We conclude that our measurements allow us to determine the evolution of the dynamic Stokes shift correctly but that we are not able to investigate the temporal behaviour of width and skewness of the fluorescence.

4.2.3 Dynamics

After dispersion correction and conversion to wavenumber scale and transition probabilities the time-dependent peak-frequencies can be extracted from a log-normal fit. The dynamic Stokes shift is compared to the broadened solvation correlation function (see section 4.1.3, p. 53) in Figure 4.14. Both curves match. It can be safely concluded that the only process governing the
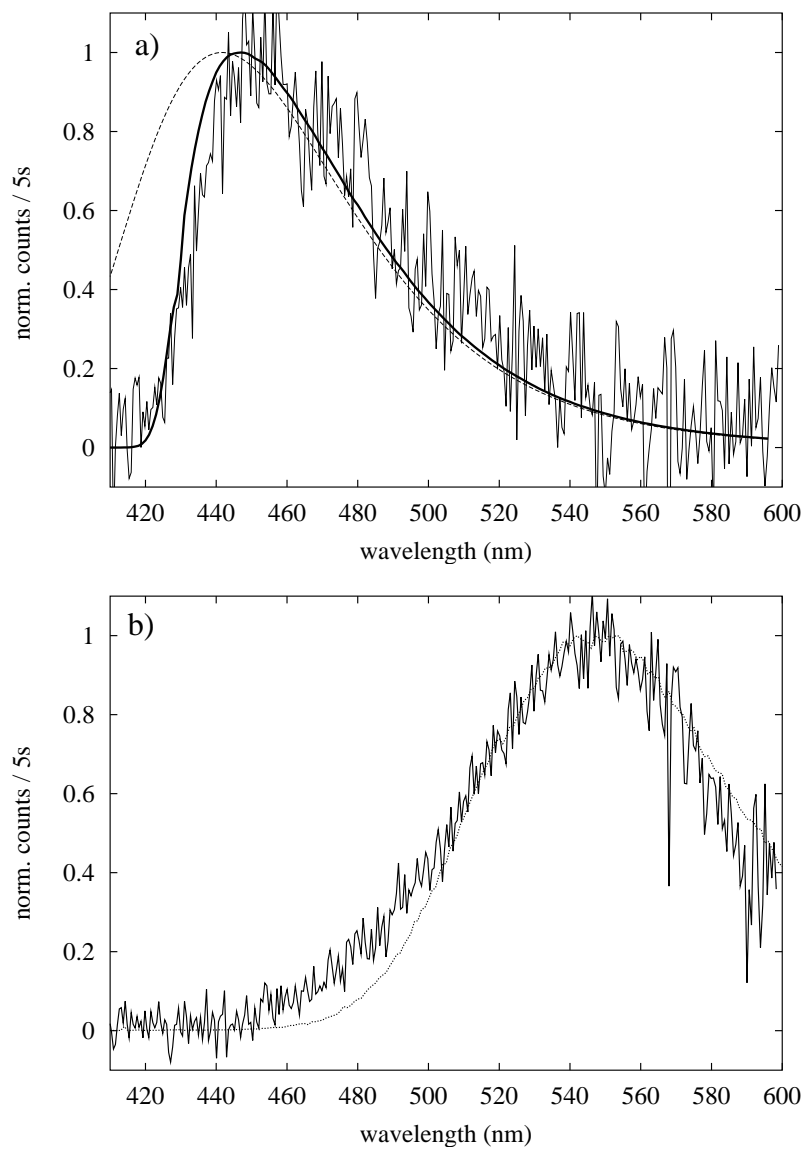
Figure 4.13: a) The spectrum of DCS in acetonitrile at t_0 (thin solid line). For comparison the time-zero spectrum (dotted line) multiplied by the transmission of GG435 is also shown (thick solid line). b) The spectrum at t_∞ spectrally corrected, and the steady state emission spectrum $(\cdots)$.
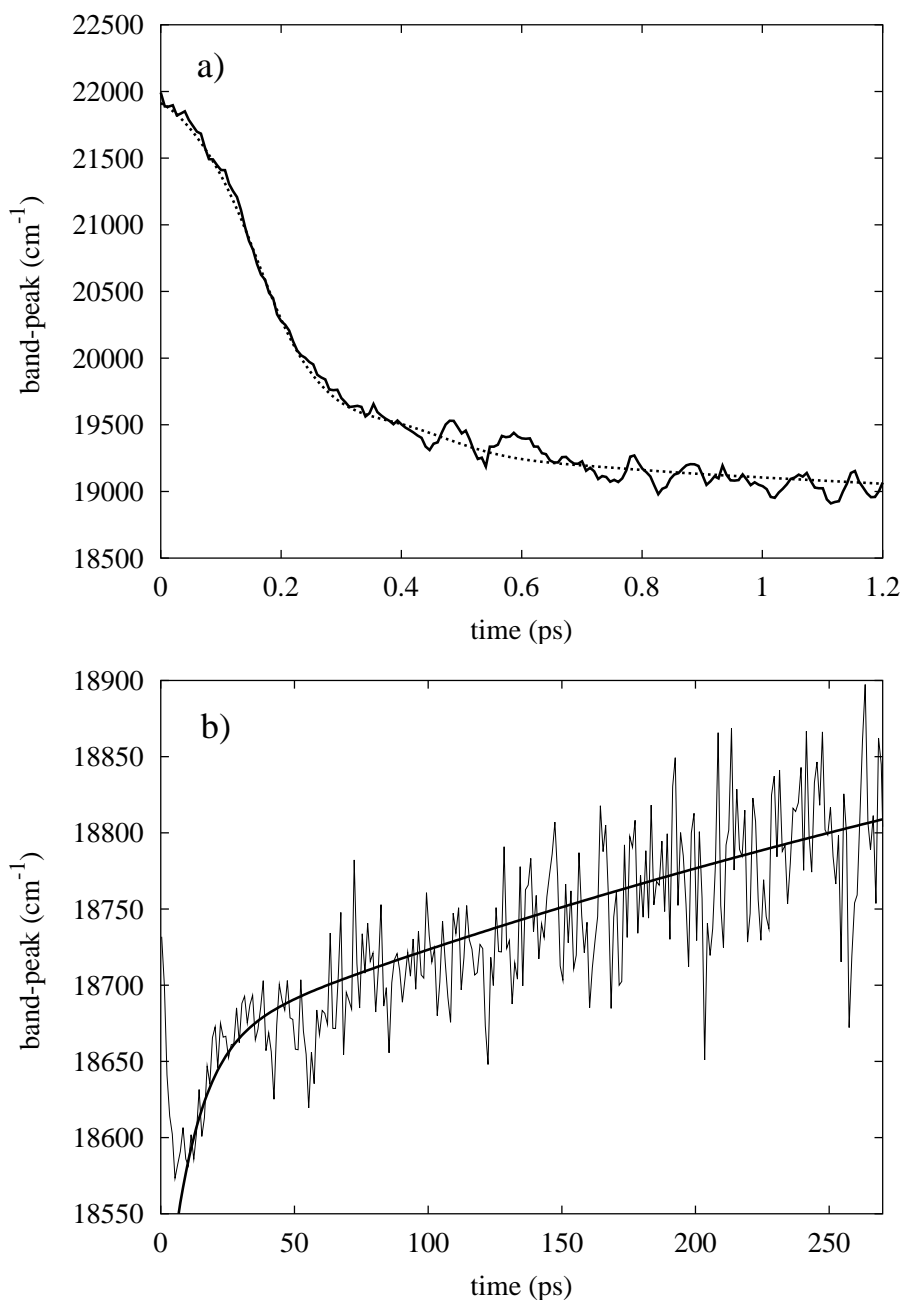
Figure 4.14: a) The dynamic Stokes shift of DCS in acetonitrile matches with the solvation correlation function modified for a 50 fs Gaussian pulses (see page 53). b) At later times the peak frequency $\tilde{\nu}$ shifts to the blue. The fast component τ=12 ps between 2.5 and 20 ps reflects cooling dynamics in acetonitrile. The slow component is due to the decay of DCS (τ=580 ps) and the concurring decrease of excited state reabsorption.

spectral evolution of the first picosecond is solvation. We do not find any indication for another process occurring on this time scale [45].

After solvation dynamics is complete a blue-shift is observed. It can be described biexponentially $\tilde{\nu}(t) = 19060 - a_1 \exp(-t/\tau_1) - a_2 \exp(-t/\tau_2)$. The fast component $\tau_1 = 12$ ps reflects cooling dynamics as already discussed for C153 in acetonitrile on page 55. The slow-component $\tau_2 = 580$ ps is equal to the fluorescence life time. As the excited molecules return back to the ground state the filter effect due to excited state reabsorption also decreases. This gives the impression of a blue-shift.

4.2.4 Semi-empirical calculations

To support interpretation of our measurements semi-empirical calculations were performed with the Ampac 6.55 program package (*Semichem*) using the SAM1 Hamiltonian (Semi-Ab initio-Model 1) [86]. In the case of para-nitroaniline this Hamiltonian has been most suitable among the semi-empirical Hamiltonians tested. It has shown good agreement between calculated and experimental data [87]. To obtain reasonable excited state properties and transition energies the number of molecular orbitals taken into account for configuration interaction was 16.

The properties of the polar solvent acetonitrile were considered applying the conductor-like screening model (COSMO) developed by Klamt [88, 89]. Here the solvent is represented as charges distributed over the van-der-Waals surface of the solute. While the dielectric properties of the solute are represented as point charges and dipoles centered in every solute atom. Now solute-solvent-interaction energy is nothing but Coulomb interaction between charges inside the atoms and on the surface. This energy is scaled with $(\varepsilon - 1)/(\varepsilon + 1/2)$, where ε is the dielectric constant of the solvent. This rescaled interaction is included in the Hamiltonian. Hence solvation is considered in the course of geometry optimization automatically. The transition frequencies of UV-spectra can also be calculated in frame of the COSMO-model.

Spectral properties of the S_1-state

In order to understand transient absorption and stimulated emission spectra after photo excitation into the S_1-state a first set of semi-empirical calculations was performed. The calculated transition energies, dipole moments and permanent dipole moments are summarized in Table 4.1. Here subscripts 'opt' and 'fc' denote the optimized and the Franck-Condon-state, respectively.

transition	transition energy	dipole moment	osc. strength
$S_{0,opt}$		9.0D	
$S_{0,opt} \rightarrow S_{1,fc}$	3.61eV/342 nm	35.3D	1.09
$S_{0,opt} \rightarrow S_{2,fc}$	4.18eV/296 nm	40.0D	0.03
$S_{1,fc} \rightarrow S_{0,opt}$	-2.05eV/-603 nm		0.90
$S_{1,fc} \rightarrow S_{7,fc}$	2.61eV/ 474 nm	28.0D	0.93
$S_{1,fc} \rightarrow S_{8,fc}$	2.71eV/ 456 nm	27.0D	0.63
$S_{1,opt}$		37.2D	
$S_{1,opt} \rightarrow S_{0,fc}$	-1.73eV/-712nm	10.0D	0.98
$S_{1,opt} \rightarrow S_{7,fc}$	2.75eV /451nm	26.7D	1.36
$S_{1,opt} \rightarrow S_{8,fc}$	2.78eV /445nm	30.1D	0.14

Table 4.1: Results from semi-empirical calculations of DCS. The dielectric solvent effects of acetonitrile were taken into account by COSMO-model (see text).

The S_1-state is energetically isolated, i.e. the energy gap to the next higher state is larger than 0.5 eV. The dipole moment of the Franck-Condon-state ($S_{1,fc}$) is 35 D. After relaxation, i.e. in the optimized excited state ($S_{1,opt}$), the dipole moment is increased by only 2 D. This suggests that the electronic structure does not change much during relaxation of the Franck-Condon state. Only minor geometrical changes are predicted and there are no indications for a twist around the double bond or of the amino-group. Therefore the relaxation of 0.2 eV can be assigned to intramolecular vibrational relaxation along other modes.

Next we examine optical transitions from the S_1 state. Two strong nearby ESA transitions are calculated at 2.61 eV and 2.71 eV. They can be assigned to transitions $S_1 \rightarrow S_7$ and $S_1 \rightarrow S_8$. In the Franck-Condon state the oscillator strengths are 0.9 and 0.6. During optimization they disproportionate to 1.36 and 0.14. The sum of oscillator strengths stays constant around 1.5. Since calculations suffer from systematic error as excitation energy increases, it is impossible to discuss numbers here. But the calculation of two ESA-bands may be in agreement with transient absorption measurements. In Figure 4.12 we find some structure in ESA at later times.

Twist of the dimethylanilino group

Another set of calculations concerns the possibility of a twist of the dimethyl-anilino group. The potentials of S_0 and S_1 were calculated along the twisting angle θ between the dimethylanilino and the para-cyanostyryl moiety. For
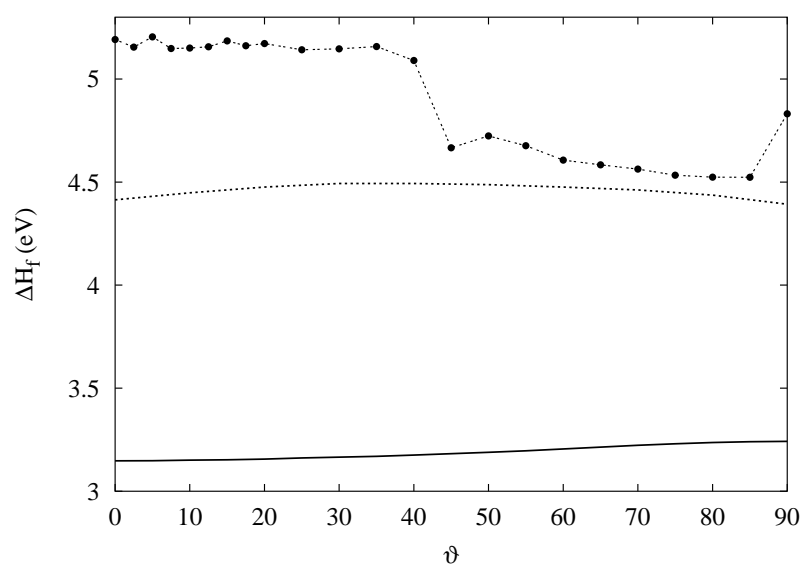
Figure 4.15: Potential of the twist of the anilino group in acetonitrile.The ground (—) and excited (–●–) state potentials were calculated semi-empirically. The excited state potential as calculated with ab-initio methods by Amatatsu (· · ·) [82]. The potential curves in ground and excited state run rather parallel so that twist would not influence the emission spectra.

every single calculation θ was kept fixed while all other modes were optimized. The result is shown in Figure 4.15. The ground state potential is flat. The difference between the minimum at $0°$ and the maximum at $90°$ is only 0.1 eV. The first excited state is also flat, at least in the region $0° < \theta < 40°$. The precision of these excited state calculations does not allow to decide whether there are local minima around $0°$ and $10°$ or not. From 40 to $45°$ the potential decreases by 0.5 eV, indicating that the character of the S_1 state changes dramatically or that the SAM1 Hamiltonian is not applicable for these geometries.

It seems reasonable to use for further considerations the potential energy curve reported by Amatatsu [82] who performed extensive ab initio calculations, namely complete active space self-consistent field (CASSCF) and second order perturbation (MRMP2) calculations. The solvent was taken into account by applying the polarizable continuum model. This S_1 potential energy curve is essentially flat with a small barrier around $45°$, of 0.085 eV. Therefore the excited molecule initially experiences no driving force towards its TICT state and the evolution may be characterized as torsional diffusion over a low barrier. The ground state energy as seen from that barrier, of 0.039 eV, may reliably be taken from our semiempirical calculations. Hence the S_0 and S_1 potential energy curves run rather parallel up to $45°$ so that conformational evolution in that range should not influence the spectral evolution of fluorescence.

4.2.5 Conclusion

The result of this study may be summarized as follows. The electronic structure and transitions of DCS in solution are characterized by a strong overlap of fluorescence and excited state absorption bands. Reabsorption of emission in transient fluorescence experiments distorts the spectral evolution and may lead to wrong conclusions. But if the change of optical density is kept low then the true evolution of transient fluorescence for DCS in acetonitrile can be observed as shown in Figures 4.9c, 4.10c, and 4.11c. The spectral dynamics of DCS in acetonitrile is characterized by a transient Stokes shift that reflects pure solvation dynamics [45].

Chapter 5

Outlook

In this work the first realization of a broadband fluorescence upconversion setup with femtosecond time-resolution is presented. But of course it may be further improved with regard to signal intensity and temporal resolution. Optical losses can be reduced by substituting the grating in the polychromator by prisms. A great part of noise is due to fluctuation of the gate-pulse energies as produced in the TOPAS. Instead one could directly generate femtosecond-pulses of 100 μJ at 1250 nm in a Cr:Forsterite amplifier [90]. In total one can expect an improvement of the signal/noise by a factor of 50 in this way.

The time resolution could be improved by replacement of our optics for collection, magnification and focusing of fluorescence light by a Cassegrainian in which spherical aberrations are mostly compensated. If the signal to noise ratio is increased, then one could afford decreasing the thickness of the cell, thereby reducing a dispersion of travel times and improving time resolution.

The upconversion efficiency may be increased by using crystals of higher effective non-linearity than KDP. In a non-collinear arrangement also BBO should allow upconversion of light beetween 400 and 1400 nm. This can be calculated with equation 2.44 for an angle between fluorescence and gate pulse of 16°, type II phase matching, a crystal length of 100 μm and a phase matching angle of 42.5° (Fig 5.1). The disadvantage of this approach would be a loss of time resolution — unless the pulse front is tilted. Another crucial point is that with only minor modifications the proposed scheme may also cover the UV-range. This can be achieved with the same crystal but with difference frequency conversion of the UV fluorescence.

Furthermore it would be interesting to investigate model systems that are related to biological problems. For instance, light-harvesting systems containing chlorophyll and carotenoids are not completely understood yet [91, 92]. Interesting results could be achieved from studying rhodopsin with our
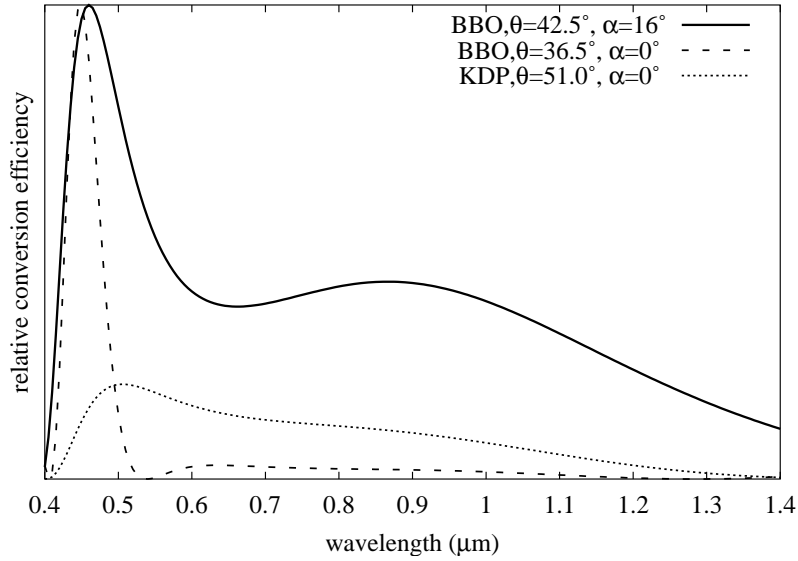
Figure 5.1: The calculated upconversion efficiency for a collinear arrangement ($\alpha=0°$) and a non-collinear one ($\alpha=16°$).

technique. Previous femtosecond transient absorption experiments revealed a strong excited state absorption band overlapping with the fluorescence band known from steady state measurements [93, 94]. Hence femtosecond spontaneous emission measurements might bring new insight into the first key step of vision. Finally, another promising direction of research is the investigation of conformational changes of peptides. If a photochromic group such as azobenzene is incorporated in the backbone of a monocyclic peptide ring then a conformational change can be induced by a femtosecond pulse and monitored by measuring the transient absorption [95]. It would be interesting to obtain additional information by utilizing the azobenzene chromophore also as fluorescence probe by measuring its spontaneous emission [96].

Appendix A

Program

A.1 A program for measurement control

This code is written in *Andor*-Basic. It controls the CCD-camera and the stepper motor.

```
rem chr$(2)  = $<$ctrl-A$>$ toggle local $<$-$>$ remote
rem chr$(5)  = $<$ctrl-D$>$ RESET
rem chr$(10) = $<$line feed$>$
rem chr$(13) = $<$cr$>$
rem 1 Step = 0.1 mikron  =$>$ Step = 0.66 fs
rem #100 is the measure matrix
rem IIN Steps FSpeed
steps=3000       :rem full number of steps, one step is 0.66 fs.
negative=600     :rem negative  delay
measures=300     :rem number of measurements
mtime  =5        :rem exposure time in seconds
onestep=-steps/measures :rem this deltat, time between
 ... two measurements
%
start$="IIN  "+str$(negative)+" F5000"+chr$(13)
home$="IIN 0 F5000"+chr$(13)
%
setacquisitiontype(0)  :rem 0=signal, 1=background, 2=reference
setacquisitionmode(1)  :rem 1=Single scan mode, 2=accumulate,
... 3=kinetics
setreadoutmode(0)      :rem Full Vertically Binned (FVB) spectra
setdatatype(1)         :rem 1=counts, 2=counts(background
corrected),
```

```
... 3=absorbance ... setexposuretime(5)
%
load(#88,"c:$\backslash$andor$\backslash$hg.sif")  :rem load  wavelengthscale
minimizewindow(#88)
%
create(#99,1024,1,1):copyxcal(#88,#99):minimizewindow(#99)
create(#100,1024,1,measures)     :rem create a matrix
... with 1024 x 1 x 500
copyxcal(#88,#100)
maximizewindow(#100)
%
handshake(1,0) :rem settings com1.
baud(1,9600)
terminator(0x0a) :rem termination character is linefeed
%
rr$="RR5"+chr$(13) :rem 2=status, 3=position feedback
:rem 4=velocity feedback, 5= position command
:rem 6=position error, 7=current command
%
comwrite(1,rr$)
delay(100)
comread(1,a$)
print "time zero position: ";a$
%
comwrite(1,start$) :rem move steppermotor to negative delay
delay(2000)

comwrite(1,rr$)
delay(100)
comread(1,a$)
print "startposition: ";a$
setexposuretime(0.021)
    run()
setexposuretime(mtime)
    run()
    #0[1]=0
    #99=#0  :rem #99 will be the background
    counter=1
while counter <= measures    :rem go in 10 steps forward

position=negative+(counter-1)*onestep
```

```
go$="IIN  "+str$(position)+" F5000"+chr$(13)
comwrite(1,go$)
delay(500) :rem wait 1 seconds

comwrite(1,rr$)
delay(100)
comread(1,a$)
print(counter;" of ";measures,"     ";back$;" at  position ";a$;
..." = ";-0.000667*position;"  ps" )
infotext(#100," at  position ";a$;" = ";
...-0.000667*position;"ps" )

setexposuretime(0.021)
run() :rem run() acquires a scan
setexposuretime(mtime)
run() :rem run() acquires a scan

#0[1]=-0.000667*position      :rem introduce time
#100{counter} = #0-#99       :rem signal-background
activekineticposition(#100,counter)
counter=counter+1
wend
comwrite(1,home$):rem move stepper back.
delay(2000)

closewindow(#88)

comwrite(1,rr$)
delay(100)
comread(1,a$)
print "end position: ";a$
```

78

Bibliography

[1] J. Shah. Ultrafast luminescence spectroscopy using sum frequency generation. *IEEE J. Quant. Electr.*, 24(2):276–288, 1988.

[2] Joseph R. Lakowicz. *Principles of Fluorescence Spectroscopy*. Kluwer Academic/Plenum Publischers, New York, 2nd edition, 1999.

[3] M. Hirsch and D.Mahr. An optical up-conversion light gate with picosecond resolution. *Opt. Comm.*, 13:96–99, 1975.

[4] T.C. Damen and J. Shah. Femtosecond luminescence spectroscopy with 60 fs compressed pulses. *Appl. Phys. Lett.*, 52:1291, 1988.

[5] A. Mokhtari, A. Chebira, and J. Chesnoy. Subpicosecond fluorescence dynamics of dye molecules. *J. Opt. Soc. Am. B*, 7(8):1551–1557, 1990.

[6] M. Maroncelli and G.R. Fleming. Picosecond solvation dynamics of coumarin 153: The importance of moelcular aspects of solvation. *J. Chem. Phys.*, 86(1):6221–6239, 1987.

[7] P.F. Barbara and W. Jarzeba. Ultrafast photochemical intramolecular charge and excited state solvation. In D.H. Volman, G.S. Hammond, and K.Gollnick, editors, *Advances in Photochemistry*, volume 15, pages 1–68. John Wiley & Sons, Inc. New York, 1990.

[8] D. Bingemann and N.P. Ernsting. Femtosecond solvation dynamics determining the band shape of stimulated emission from a polar styryl dye. *J. Chem. Phys.*, 102(7):2691–2700, 1995.

[9] S.A. Kovalenko, A.L. Dobryakov, J. Ruthmann, and N.P. Ernsting. Femtosecond spectroscopy of condensed phases with chirped supercontinuum probing. *Phys. Rev. A*, 59:2369–2384, 1999.

[10] Y. Kanematsu, H. Ozawa, I. Tanaka, and S. Kinoshita. Femtosecond optical kerr-gate measurement of fluorescence spectra of dye solutions. *J. Lumin.*, 87-89:917–919, 2000.

[11] J.M. Hollas. *Modern Spectroscopy*. John Wiley & Sons, 2nd edition, 1992.

[12] H.-H. Perkampus. *Encyclopedia of Spectroscopy*. VCH, 1995.

[13] Theodor Förster. *Fluoreszenz Organischer Verbindungen*. Vandenhoeck & Ruprecht in Göttingen, 1951.

[14] Noboru Mataga and Tanekazu Kubota. *Molecular Interactions and Electronic Spectra*. Marcel Dekker, Inc., 1970.

[15] Alan Hinchliffe and Robert W. Munn. *Molecular Electromagnetism*. John Wiley & Sons Ltd., 1985.

[16] Frits Zernike and John E. Midwinter. *Applied Nonlinear Optics*. John Wiley & Sons, Inc., 1973.

[17] V.G. Dmitriev, G.G. Gurzadyan, and D.N. Nikogosyan. *Handbook of Nonlinear Optical Crystals*. Springer, 2nd edition, 1997.

[18] J.-C. Diels and W. Rudolph. *Ultrashort Laser Pulse Phenomena*. Academic Press, 1995.

[19] R.R. Alfano and S.L. Shapiro. Observation of self-phase modulation and small-scale filaments in crystals and glasses. *Phys. Rev. Lett.*, 24(11):592–594, 1970.

[20] R.L. Fork, C.V. Shah, C. Hirlimann, R. Yen, and W.J. Tomlinson. Femtosecond white-light continuum pulses. *Opt. Lett.*, 8(1):1–3, 1983.

[21] E.G. McRae. Theory of solvent effects on molecular electronic spectra. frequency shifts. *J. Phys. Chem.*, 61:562, 1957.

[22] G. Van der Zwan and J.T. Hynes. Time-dependent fluorescence solvent shifts, dielectric friction, and nonequilibrium solvation in polar solvents. *J. Phys. Chem. B*, 89:4181–4188, 1985.

[23] M.L. Horng, J.A. Gardecki, A. Papazyan, and M. Maroncelli. Subpicosecond measurements of polar solvation dynamics: Coumarin 153 revisited. *J. Phys. Chem.*, 99(48):17311–17337, 1995.

[24] E.W. Castner and M. Maroncelli. Solvent dynamics derived from optical kerr effect, dielectric dispersion, and time-resolved stokes shift measurements: An empirical comparison. *J. Mol. Liquids*, 77:1–36, 1998.

[25] M. Maroncelli. The dynamics of solvation in polar liquids. *J. Mol. Liquids*, 57:1–37, 1993.

[26] J.D. Simon. Time-resolved studies of solvation in polar media. *Acc. Chem. Res.*, 11:128–134, 1988.

[27] M. Maroncelli and G.R. Fleming. Comparison of time-resolved fluorescence stokes shift measurements to a molecular theory of solvation dynamics. *J. Chem. Phys.*, 89(2):875–881, 1988.

[28] C.-P. Hsu, X. Song, and R.A. Marcus. Time-dependent stokes shift and its calculation from solvent dieelectric dispersion data. *J. Phys. Chem. B*, 101:2546–2551, 1997.

[29] S.A. Kovalenko. private communication.

[30] D.B. Siano and D.E. Metzler. Band shapes of the electronic spectra of complex molecules. *J. Chem. Phys.*, 51(5):1856–1861, 1969.

[31] T. Elsaesser and W. Kaiser. Vibrational and vibronic relaxation of large polyatomic molecules in liquids. *Annu. Rev. Phys. Chem.*, 42:83–107, 1991.

[32] A. Mokhtari, J. Chesnoy, and A. Laubereau. Femtosecond time- and frequency-resolved fluorescence spectroscopy of a dye molecule. *Chem. Phys. Lett.*, 155(6):593–597, 1989.

[33] R.F. Loring, Y.Y. Yan, and S. Mukamel. Time- and frequency resolved fluorescence line shapes as a probe of solvation dynamics. *Chem. Phys. Lett.*, 135(1,2):23–29, 1987.

[34] Y.J. Yan and S. Mukamel. Femtosecond pump-probe spectroscopy of polyatomic molecules in condensed phase. *Phys. Rev. A*, 41(11):6485–6504, 1990.

[35] S. Kinoshita, H. Itoh, H. Murakami, H. Miyasaka, T. Okada, and N. Mataga. Solvent relaxation effect on transient hole-burning spectra of organic dyes. *Chem. Phys. Lett.*, 166(2):123–127, 1989.

[36] S. Kinoshita, N. Nishi, and T. Kushida. Stochastic behavior of the dynamic stokes shift in rhodamine 6g. *Chem. Phys. Lett.*, 134(6):605–609, 1986.

[37] K. Nishiyama and T. Okada. Relaxation of inhomogeneous spectral band width of dye molecules in polar solvents studied by time-resolved hole and fluorescence spectroscopy. *J. Phys. Chem. A*, 101(32):5729–5735, 1997.

[38] T. Kakitani and N. Mataga. On the possibility of dielectric saturation in molecular systems. *Chem. Phys. Lett.*, 124(5), 1986.

[39] E.A. Carter and J.T. Hynes. Solvation dynamics for an ion pair in a polar solvent: Time-dependent fluorescence and photochemical charge transfer. *J. Chem. Phys.*, 94(9):5961–5979, 1991.

[40] D. V. Matyushov. Time-resolved fluorescence of polarizable chromophores. *J. Chem. Phys.*, 115(19):8933–8941, 2001.

[41] P. van der Meulen, A.M. Jonkman, and M. Glasbeek. Simulations of solvation dynamics using a nonlinear response approach. *J. Phys. Chem. A*, 102:1906–1911, 1998.

[42] N.A. Smith, S.R. Meech, I.V. Rubtsov, and K. Yoshihara. Lds-750 as a probe of solvation dynamics: a femtosecond time-resolved fluorescence study in liquid aniline. *Chem. Phys. Lett.*, 303:209–217, 1999.

[43] R.S. Fee and M. Maroncelli. Estimating the time-zero spectrum in time-resolved emission mearsurements of solvation dynamics. *Chem. Phys.*, 183:235–247, 1994.

[44] R. Schanz, S.A. Kovalenko, V. Kharlanov, and N.P. Ernsting. Broadband fluorescence upconversion for femtosecond spectroscopy. *Appl. Phys. Lett.*, 73(5):566–568, 2001.

[45] S.A. Kovalenko, R. Schanz, T.A. Senyushkina, and N.P. Ernsting. Femtosecond spectroscopy of p-dimethylaminocyanostilbene in solution — no evidence for dual fluorescence. *Accepted by Phys. Chem. Chem. Phys.*, 2002.

[46] A. Stingl, M. Lenzner, Ch. Spielmann, R. Szipöcs, and F. Krausz. Sub-10-fs mirror-dipersion-controlled ti:sapphire laser. *Opt. Lett.*, 20:602, 1994.

[47] S. Sartania, Z. Cheng, M. Lenzner, G. Tempea, Ch. Spielmann, F. Krausz, and K. Ferencz. Generation of 0.1-tw 5-fs optical pulses at a 1-khz repetition rate. *Opt. Lett.*, 22:1562, 1997.

[48] Ch. Spielmann, M. Lenzner, F. Krausz, and A.J. Schmidt. Compact, high-throughput expansion-compression scheme for chirped pulse amplification in the 10 fs range. *Opt. Comm.*, 120:321, 1995.

[49] R. Szipöcs, K. Ferencz, Ch. Spielmann, and F. Krausz. Chirped multilayer coatings for broadband dispersion control in femtosecond lasers. *Opt. Lett.*, 19:200, 1994.

[50] Light Conversion Ltd., P/O Box 1485, LT-2040 Vilnius, Lithuania. *Traveling-wave Optical Parametric Amplifier of Superfluorescence - User's Manual*, 1998.

[51] W.H. Knox, N.M. Pearson, K.D. Li, and C.A. Hirlimann. Interferometric measurements of femtosecond group delay in optical components. *Opt. Lett.*, 13:574–576, 1988.

[52] Schott optical glass catalogue, 1996.

[53] Anthony E. Siegmann. *Lasers*. University Science Books, 1986.

[54] Zs. Bor and B. Racs. Group velocity dispersion in prisms and its application to pulse compression and travelling-wave excitation. *Opt. Comm.*, 9(5):165–170, 1985.

[55] PLX inc., 40 West Jefryn Blvd. Deer Park, NY 11729, USA. *Characteristics of Mirror Coatings*, 2000.

[56] Bergmann Schaefer. *Lehrbuch der Experimentalphysik*, volume Optik. Walter de Gruyter, 9. auflage edition, 1993.

[57] T. Gustavsson, L. Cassara, V. Gulbinas, G. Gurzadyan, J.-C. Mialocq, S. Pommeret, M. Sorgius, and P. van der Meulen. Femtosecond spectroscopic study of relaxation processes of three amino-substituted coumarin dyes in methanol and dimethyl sulfoxide. *J. Phys. Chem. A*, 102:4229–4245, 1995.

[58] H. Schmidt and R. Wallenstein. Beta-bariumborat: Ein neues optisch nichtlineares material. *Laser unt Optoelektronik*, page 302, 1987.

[59] J.C. Scaiano. *Handbook of Organic Photochemistry*, volume 1. CRC Press, Inc., 1989.

[60] Marconi Applied Technologies. *Data-Sheet: CCD30-11 Back Illuminated High Performance CCD Sensor*.

[61] S.A. Kovalenko, J. Ruthmann, N.P. Ernsting, and D. Ouw. Femtosecond relaxation of 2-amino-7-nitro-fluorene in acetonitrile: Observation of the oscillatory contribution to the solvent response. *J. Chem. Phys.*, 109(13):5466–5468, 1998.

[62] W.H. Press, S.A. Teukolsky, W.T. Vetterling, and B.P. Flannery. *Numerical Recipies in FORTRAN: the art of scientific computing*. Cambridge University Press, 2nd edition, 1992.

[63] V.M. Farztdinov. private communication, 2000.

[64] Y.V. Il'ichev, W. Kühnle, and K.A. Zachariasse. Photophysics of 4-dimethylamino-4'-cyanostilbene and 4-azetidinyl-4'-cyanostilbene. time-resolved fluorescence and trans-cis photoisomerisation. *Chem. Phys.*, 211:441–453, 1996.

[65] S.J. Rosenthal, X. Xie, M. Du, and G.R. Fleming. Femtosecond solvation dynamics in acetonitrile: Observation of the inertial contribution to the solvent response. *J.Chem. Phys*, 95(6):4715–4718, 1991.

[66] S.A. Kovalenko, J. Ruthmann, and N.P. Ernsting. Ultrafast stokes shift and excited-state transient absorption of coumarin 153 in solution. *Chem. Phys. Lett.*, 271:5466–5468, 1997.

[67] C.R. Moylan. Molecular hyperpolarizabilities of coumarin dyes. *J. Phys. Chem.*, 98:13513–13516, 1994.

[68] K. Rechthaler and G. Köhler. Excited state properties and deactivation pathways of 7-aminocoumarins. *Chem. Phys.*, 189:99–116, 1994.

[69] A. Mühlpfordt, R. Schanz, N.P.Ernsting, V. Farztdinov, and S. Grimme. Coumarin 153 in the phase: optical spectra and quantum chemical calculations. *Phys. Chem. Chem. Phys.*, 1:3209–3218, 1999.

[70] J.E. Lewis and M. Maroncelli. On the (uninteresting) dependence of absorption and emission transition moments of coumarin 153 on solvent. *Chem. Phys. Lett.*, 282:197–203, 1998.

[71] G.A. Reynolds and K.H. Drexhage. New coumarin dyes with rigidized structure for flashlamp-pumped dye lasers. *Opt. Comm.*, 13(3):222–225, 1975.

[72] G. Jones II, W.R. Jackson, C. Choi, and W.R. Bergmark. Solvent effects on emission yield and lifetime for coumarin laser dyes. requirements fo a rotary decay mechanism. *J. Phys. Chem.*, 89:294–300, 1985.

[73] T. Gustavsson, G. Baldacchino, J.-C. Mialocq, and S. Pommeret. A femtosecond fluorescence up-conversion study of the dynamic stokes shift of the dcm dye molecule in polar and non-polar solvents. *Chem. Phys. Lett.*, 236:587–594, 1995.

[74] S.A. Kovalenko, R. Schanz, H. Hennig, and N.P. Ernsting. Cooling dynamics of an optically excited molecular probe in solution from femtosecond broadband transient absorption spectroscopy. *J. Chem. Phys.*, 323(7):3256–3275, 2001.

[75] K. Ohta, T.J. Kang, K. Tominaga, and K. Yoshihara. Ultrafast relaxation process from a higher excited electronic state of a dye molecule in solution: a femtosecond time-resolved fluorescence study. *Chem. Phys.*, 242:103–114, 1999.

[76] N. Eilers-König, T. Kühne, D. Schwarzer, P. Vöhringer, and J. Schröder. Femtosecond dynamics of intramolecular charge transfer in 4-dimethylamino-4'-cyanostilbene in polar solvents. *Chem. Phys. Lett.*, 253:69–76, 1996.

[77] H. Gruen and H. Görner. Fluorescence of trans-4-cyano-4'-dimethylaminostilbene; no evidence for a tict state. *Z. Naturforsch.*, 38a:928–936, 1983.

[78] E. Abraham, J. Oberle, G. Jonusauskas, R. Lapouyade, and C. Rulliere. Picosecond time-resolved dual fluorescence, transient absorption and reorientation time measurements of push-pull diphenyl-polyenes: evidence for 'loose' complex and 'bicimer' species. *Chem. Phys.*, 219:73–89, 1997.

[79] E. Abraham, J. Oberle, G. Jonusauskas, R. Lapouyade, and C. Rulliere. Photophysics of 4-dimethylamino-4'-cyanostilbene and model compounds: dual excited states revealed by sub-picosecond transient absorption and kerr ellipsometry. *Chem. Phys.*, 211:441–453, 1996.

[80] Y.V. Il'ichev and K.A. Zachariasse. Intramolecular charge transfer, photoisomerisation and rotational reorientation of trans-4-dimethylamino-4'-cyanostilbene in liquid solution. *Ber. Busenges. Phys. Chem.*, 101:625–635, 1997.

[81] R. Lapouyade, A. Kuhn, J.-F. Letard, and W. Rettig. Multiple relaxation pathways in photoexcited dimethylaminonitro- and dimethylaminocyano-stilbenes. *Chem. Phys. Lett.*, 208(1-2):48–58, 1993.

[82] Y. Amatatsu. Ab initio study on the photochemical behavior of 4-dimethylamino,4'-cyanostilbene. *Chem. Phys.*, 274:87–98, 2001.

[83] R. Lapouyade, K. Czeschka, W. Majenz, W. Rettig, E. Gilabert, and C. Rulliere. Photophysics of donor-acceptor substituted stilbenes. a time-resolved fluorescence study using selectively bridged dimethyl-amino cyano model compounds. *J. Phys. Chem.*, 96:9643–9650, 1992.

[84] Z.R. Grabowski and J. Dobkowski. Twisted intramolecular charge transfer (tict) excited states: energy and molecular structure. *Pure & Appl. Chem.*, 55(2):245–252, 1983.

[85] C. Monte. *Die Photophysik donor-akzeptor-substituierter Stilbene, Laserspektroskopische Untersuchungen im Molekularstrahl.* PhD thesis, Technical University Berlin, 1996.

[86] M.J.S. Dewar, C. Jie, and J. Yu. Sam1: The first of a new series of general purpose quantum mechanical molecular models. *Tetrahedron*, 48(23):5003–5038, 1993.

[87] V. M. Farztdinov, R. Schanz, S.A. Kovalenko, and N.P. Ernsting. Relaxation of optically excited p-nitroaniline: Semiempirical quantum-chemical calculations compared to femtosecond experimental results. *J. Phys. Chem. A*, 104:11486–11496, 2000.

[88] A. Klamt and G. Schüürmann. Cosmo: A new approach to dielectric screening in solvents with explicit expressions for the screening energy and its gradient. *J. Chem. Soc., Perkin. Trans. 2*, pages 799–805, 1993.

[89] A. Klamt. Calculation of uv/vis spectra in solution. *J. Phys. Chem.*, 100:3349–3253, 1996.

[90] V. Shcheslacskiy, V. Petrov, F. Noack, and N.Zhavoronkov. An all-solid state laser system for generation of 100 μj femtosecond pulses near 625 nm at 1khz. *Appl. Phys. B*, 69:167–169, 1999.

[91] P.J. Walla, J. Yom, B.P. Krueger, and G.R. Fleming. Two-photon excitation spectrum of light-harvesting complex ii and fluorescence upconversion after one- and two-photon excitation of the carotenoids. *J.Chem. Phys. B*, 104(19):4799–4806, 2000.

[92] T. Polivka, D. Zigmantas, V. Sundström, E. Formaggio, G. Cinque, and R. Bassi. Carotenoid s_1 state in a recombinant light-harvesting complex of photosystem ii. *Biochemistry*, 41(2):439–450, 2002.

[93] L.A. Peteanu, R.W. Schoenlein, Q. Wang, R.A. Mathies, and C.V. Shank. The first step in vision occurs in femtoseconds: Complete blue and red spectral studies. *Proc. Natl. Acad. Sci. USA*, 1993.

[94] G.G. Kochendoerfer and R.A. Mathies. Spontaneous emission study of the femtosecond isomerization dynamics of rhodopsin. *J. Phys. Chem.*, 1996.

[95] C. Renner, R. Behrendt, S. Spörlein, J. Wachtveitl, and L. Moroder. Photomodulation of conformational states. i. mono- and bicyclic peptides with (4-amino)phenylazobenzoic acid as backbone constituent. *Biopolymeres*, 54(7):489–500, 2000.

[96] N. Tamai and H. Miyasaka. Ultrafast dynamics of photochromic systems. *Chem. Rev.*, 100:1875–1890, 2000.

Lebenslauf

Am 15. Juni 1971 wurde ich, Hans Roland Schanz, als Kind von Dr. med. Hans Michael Schanz und Brigitte Schanz, geb. Mayer, in Freiburg im Breisgau geboren. Von 1978 bis 1982 besuchte ich die Markus-Grundschule in Berlin. Im August 1982 wechselte ich auf das Gymnasium Steglitz in Berlin und erwarb dort am 8. Juni 1991 das Zeugnis der Allgemeinen Hochschulreife mit Graecum und Latinum.

Zum Wintersemester 1991/92 immatrikulierte ich mich an der Albert-Ludwig-Universität in Freiburg im Breisgau für den Diplomstudiengang Chemie und bestand im August 1993 die Diplomchemiker Vorprüfung. Im September 1993 immatrikulierte ich mich im Rahmen eines Erasmus Programmes an der University of Manchester Institute of Science (UMIST) für den "Honours Degree Course" in Chemie und erwarb im Juli 1994 den Grad des "Bachelor of Science" (BSc).

Zum Wintersemester 1994/95 immatrikulierte ich mich an der Technischen Universität Berlin für den Diplomstudiengang Chemie. Im Wintersemester 1995/1996 wechselte ich an die Humboldt-Universität zu Berlin. Im Oktober 1997 begann ich unter der Leitung von Herrn Prof. Dr. Ernsting am Institut für Theoretische und Physikalische Chemie meine Diplomarbeit mit dem Thema "Coumarin 153 in der Gasphase" welche ich im August 1998 mit dem Diplom abschloß.

Anschließend beschäftigte ich mich als wissenschaftlicher Mitarbeiter im gleichen Arbeitskreis zunächst mit der Messung und Analyse breitbandiger transienter Absorptionsspektren. Später konzentrierte ich mich auf den Aufbau einer Anlage zur Messung breitbandiger transienter Fluoreszenzspektren. Daraus entstand die vorliegende Dissertation.

Acknowledgement

This thesis would not have been the same without

- Prof Ernsting who committed this wonderful topic to me. He supplied this project generously not only with brilliant ideas.

- Dr Kovalenko who iniated me into the realm of ultrafast spectroscopy. His wisdom and experience as well as his restlessness harmonized perfectly with my design and preparations; it took us four weeks from placing the first mirror until final analysis of the first measurement.

- A bunch of alchemists sitting in dark workshops in Berlin and Göttingen. Master Waterstradt, Master Lück and Master Zillmann turned steel into gold while Master Sauermann found an elegant way to do the same with glass and mirrors.

- My dear collegues Dr Dobryakov, Dr Hennig, Dr Perez, Dr Photiadis, Dr Saroya, Dr Senyushkina, Mrs Steingräber and Mrs Unger.

- Dr Farztdinov who performed breathtaking convolutions with a pencil.

- Dr Steinel who leads my life in a parallel world and shares the cv.

- Miss Strothotte who is specialized in fireworks and has ignited my heart.

- All my parents. Maybe the thesis would have been the same without you but certainly not I. Thank you!

Hiermit versichere ich, Roland Schanz, die vorliegende Arbeit selbständig und ohne unerlaubte Hilfe angefertigt zu haben.